UNIVERSITÉ DU QUÉBEC

THÈSE PRÉSENTÉE À
L'UNIVERSITÉ DU QUÉBEC À CHICOUTIMI
COMME EXIGENCE PARTIELLE
DU DOCTORAT EN INGÉNIÉRIE

par
Vinay Kumar Jaiswal

FINITE ELEMENT MODELING OF ELECTRIC FIELD DISTRIBUTIONS AROUND A RESISTIVE GLAZED POST STATION INSULATOR COVERED WITH ICE

MODÉLISATION PAR ÉLÉMENTS FINIS DE LA DISTRIBUTION DU CHAMP ÉLECTRIQUE AUTOUR D'UN ISOLATEUR DE POSTE AVEC UNE COUCHE SEMI-CONDUCTRICE RECOUVERT DE GLACE

JUILLET 2005

Bibliothèque
Paul-Émile-Boulet

UQAC
Université du Québec
à Chicoutimi

Mise en garde/Advice

Afin de rendre accessible au plus grand nombre le résultat des travaux de recherche menés par ses étudiants gradués et dans l'esprit des règles qui régissent le dépôt et la diffusion des mémoires et thèses produits dans cette Institution, **l'Université du Québec à Chicoutimi (UQAC)** est fière de rendre accessible une version complète et gratuite de cette œuvre.

Motivated by a desire to make the results of its graduate students' research accessible to all, and in accordance with the rules governing the acceptation and diffusion of dissertations and theses in this Institution, the **Université du Québec à Chicoutimi (UQAC)** is proud to make a complete version of this work available at no cost to the reader.

L'auteur conserve néanmoins la propriété du droit d'auteur qui protège ce mémoire ou cette thèse. Ni le mémoire ou la thèse ni des extraits substantiels de ceux-ci ne peuvent être imprimés ou autrement reproduits sans son autorisation.

The author retains ownership of the copyright of this dissertation or thesis. Neither the dissertation or thesis, nor substantial extracts from it, may be printed or otherwise reproduced without the author's permission.

Abstract

The main objective of this research is to study the potential and electric field distributions around a semi-conducting glazed standard post insulator for power frequency operation, in the presence of lightning impulse (LI) and switching impulse (SI) voltages under icing conditions. Those distributions are computed numerically using the finite element method (FEM). The thicknesses and conductivities of the semi-conducting glaze, the ice layer and the water film are varied and their effects are studied for the purpose of improving the electrical performance of the insulator under icing conditions. The thin semi-conducting glaze requires a very large number of elements for the FEM because of the open boundary around the insulator. To reduce the number of elements, the open boundary is simulated using a form of Kelvin transformation. The computation time is compared with that of using an artificial boundary. It is found that this time is considerably reduced by applying the Kelvin transformation to a wet ice-covered semi-conducting glazed insulator.

Simulation results are confirmed by laboratory experiments, and it is found that the switching impulse is the limiting factor in the design of a semi-conducting glazed insulator under icing conditions contrary to clean ones, i.e. ice-free conditions where the lightning impulse is the limiting factor. Any wet ice, accumulated on the insulator, has very little effect on the electric field distribution for a lightning impulse voltage, but has a major effect on the electric field distribution and hence, on the flashover performance of the insulator, for a switching impulse voltage. For the time instant of breakdown, the flashover occurs after the peak voltage for the clean as well as the wet ice-covered insulator under the lightning impulse voltage, and before the peak voltage for the clean insulator and after the peak voltage for the wet ice-covered insulator under the switching impulse voltage.

Résumé

L'objectif principal de cette recherche est d'étudier la distribution du potentiel et du champ électrique autour d'un isolateur de poste standard recouvert d'une couche semi-conductrice à fréquence industrielle, en présence de chocs de foudre et de manoeuvre sous des conditions givrantes. Les distributions sont calculées numériquement en utilisant la méthode des éléments finis (FEM). L'influence des épaisseurs et de la conductivité de la couche semi-conductrice, de la couche de glace et du film d'eau a été étudiée afin d'améliorer la performance électrique des isolateurs recouverts de glace. La minceur de la couche semi-conductrice exige un très grand nombre de mailles en raison de la frontière ouverte autour de l'isolateur. Pour réduire le nombre d'éléments, la frontière ouverte est simulée en utilisant une forme de la transformation de Kelvin. Le temps de calcul est comparé à celui avec la frontière artificielle. On observe une économie considérable de temps dans le cas de la transformation de Kelvin appliquée à un isolateur avec couche semi-conductrice recouvert de glace humide.

Les résultats de simulation ont été confirmés par des expériences de laboratoire, et on a trouvé que le choc de manœuvre est le facteur limite dans la conception des isolateurs de couche semi-conductrice pour des conditions de glace, contrairement à des conditions propres (sans la présence de glace sur les isolateurs et où le facteur limite est le choc de foudre). La glace humide accumulée sur l'isolateur a très peu d'effet sur la distribution du champ électrique quand cet isolateur est soumis aux chocs de foudre. Toutefois, s'il est soumis aux chocs de manœuvre, la glace accumulée a un effet important sur la distribution du champ électrique et, par conséquent, sur le comportement diélectrique de l'isolateur. Sous chocs de foudre, l'instant du contournement se produit après la crête de l'onde de tension aussi bien pour un isolateur propre que pour un isolateur recouvert de glace humide; sous chocs de manœuvre. Par contre, cet instant se produit avant la crête de l'onde de tension pour un isolateur propre, et après celle-ci pour un isolateur recouvert de glace.

Acknowledgements

This work was carried out within the framework of the NSERC/Hydro-Quebec/UQAC Industrial Chair on Atmospheric Icing of Power Network Equipment (CIGELE) and Canada Research Chair on Engineering of Power Network Atmospheric Icing (INGIVRE) at the University of Quebec at Chicoutimi in collaboration with McGill University, Montreal, Canada. I would like to thank all the sponsors of the project.

I would like to take this opportunity to express my deep sense of gratitude and great pleasure to Prof. Masoud Farzaneh, the director of my studies, for his financial support, guidance, suggestions, criticism and encouragement. It has been a great experience to work with him and I enjoyed my stay at the institute.

I am very grateful to Prof. David A. Lowther, the co-director of my studies, for his availability, supervision, suggestions, criticism and encouragement.

I would like to thank all the CIGELE and INGIVRE researchers, technicians, secretaries, and my friends, for their co-operation, moral as well as technical support, and encouragement.

And finally, most respectfully, I remember my parents, brothers and sister, who were, are and will be my greatest source of inspiration.

Table of Contents

List of Symbols and Abbreviations

BEM	Boundary Element Method
BIL	Basic Lightning Impulse insulation level
BSL	Basic Switching Impulse insulation level
CIGELE	NSERC/Hydro-Quebec/UQAC Industrial Chair on Atmospheric Icing of Power Network Equipment
CSM	Charge Simulation Method
DC	Direct Current
FDM	Finite Difference Method
FEM	Finite Element Method
GND	Ground
HV	High Voltage
INGIVRE	Canada Research Chair on Engineering of Power Network Atmospheric Icing
LI	Lightning Impulse
RG	Resistive Glazed
SI	Switching Impulse
UQAC	University of Quebec at Chicoutimi

E	Complex electric field strength vector
F_{eq}	Equivalent Frequency
g	A driving function in the Helmholtz equation
H	Complex magnetic field strength vector

k^2 A constant in the Helmholtz equation

p, q Material properties

t_r Rise time of the impulse

ρ Volume charge density

ω Angular frequency

ε Absolute permittivity

σ Conductivity

μ Permeability

∇U Potential gradient

List of Tables

List of Figures

CHAPTER 1

INTRODUCTION

1.1 Overview

The energized high voltage (HV) line conductor in a transmission system, has to be physically attached to the support structure, but electrically isolated from it because it is at ground potential. The insulator performs the dual functions of support and electrical insulation. Insulators are recognized by the dielectric material used to construct them. There are three main types of dielectrics used for outdoor HV insulator construction i.e. porcelain, glass and polymer. These materials form the basis for the well-known nomenclature of porcelain, glass and polymeric insulators. Porcelain insulators are also known as ceramic insulators and include station post, suspension, distribution line post and pin type insulators. Station post insulators are used for the substations. Polymeric insulators are also commonly known by other names, such as, composite and non-ceramic insulators and, in polluted conditions, a special type of porcelain insulator is used to improve the electrical performance; this insulator has a semi-conducting glaze instead of the insulating glaze used on normal porcelain insulators. Such insulators are called semi-conducting or resistive glazed (RG) insulators. The power dissipated in the glaze raises the surface temperature several degrees above the ambient to prevent wetting by condensation. In this way a sufficient dry band is maintained and protected from condensation during fog. The leakage current in the semi-conducting glaze makes the potential distribution

almost linear along the insulator. In this work, the thickness and conductivity of the semi-conducting glaze are varied and their effects on the potential and electric field distributions have been studied in order to improve the electrical performance of the insulator under icing conditions.

Electrical stresses on the insulator include the steady state stress caused by the power frequency nominal operating voltage. Voltage surges generated by lightning or switching operations impose a high and transient stress on the insulator. During flashover, an insulator is subjected to a large fault current (several kA) at power frequency, in the form of an arc called a "power arc". This persists until the protection isolates the fault.

Whether an insulator fails by surface flashover or puncture depends on the magnitude and duration of the electric stress applied, insulator dimensions, and defects in the material. Puncture breakdown occurs at the point where the voltage-time curve of surface flashover intersects that of internal breakdown. Breakdown requires the formation of an ionized channel, and this channel needs to be established within the duration of the applied voltage. If the insulator is defective (i.e., has large voids or impurities), puncture can be caused by extremely short duration, large magnitude pulses. Lightning surges, which have a rise time in the microsecond range, do not cause puncture if the insulator is sound. Similarly, switching surges normally do not cause puncture. Both lightning and switching surges can cause flashover if they have adequate magnitude, even under dry conditions. Longer duration stresses, such as those imposed by the power frequency voltage, do not result in a puncture. A flashover is possible, however, in a wet and contaminated environment.

Voltage surges produced by the lightning and/or switching operations are major factors to be considered in the electrical design of the insulator. Insulators should be designed such that they do not fail at surge voltage magnitudes that are lower than the value for which the power system apparatus has been designed. For higher magnitude surges, the insulator should flashover. The determining values of these surges are defined by the Basic Lightning Impulse insulation level (BIL) and Basic Switching Impulse insulation level (BSL).

In many cases, the insulators function in an outdoor environment. In such applications in cold climate regions, the HV insulator surfaces are exposed to atmospheric pollution and also to the accretion of snow or ice of different natures. The performance of a HV insulator under an ice-free condition is quite different from those under ice-covered conditions. This is because, for a wet ice-covered insulator, the field distribution is capacitive-resistive depending upon the severity of the ice, while for a clean ice-free insulator the field is purely capacitive. Therefore, it is very important to know the changes in the field distribution around an insulator caused by different severities of the ice-accretion.

1.2 An Ice-covered Insulator

There are many parameters which control the type of the ice accumulated on the insulator. The main parameters include the temperature of the insulator surface, the ambient air temperature, liquid water content (LWC), the size & temperature of the water droplets as well as the wind velocity.

Figure 1.1 shows a laboratory model of an insulator covered with a glaze ice. This insulator has been simulated in this work.

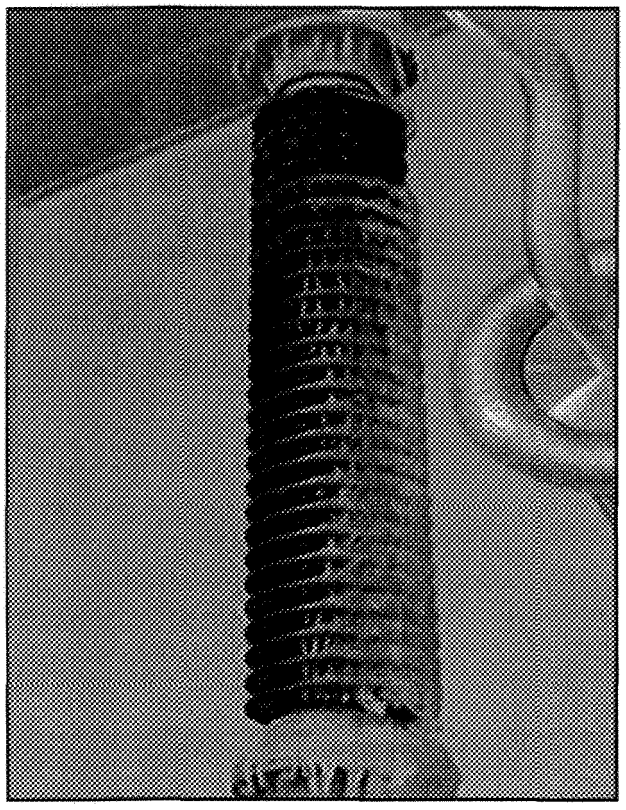

Figure 1.1: An insulator covered with a glaze ice (laboratory model).

Flashover phenomena on ice-covered insulators have been reported from a large number of cold climate countries, including Canada [1]-[4], China [5], [6], the former Czechoslovakia [7], England [8], Finland [9], Japan [10]-[13], Norway [14], [15], Switzerland [16], Sweden [17], [18], the U.S. [19]-[21], and the former Yugoslavia [22]. Flashover on the ice-covered insulator is a complex phenomenon as it involves many

processes and mechanisms [23]. Studies of flashover characteristics of insulators are necessary to determine suitable insulator profiles for a particular application [24]-[27]. Flashover performance can be studied by computing the potential and electric field distributions around the insulator.

The flashover voltage depends on the electric field distribution that is mainly distorted by the presence of a water film and air gaps i.e. ice-free areas formed along the ice-covered insulators. In the absence of a water film, the electric field distribution is also distorted by the surface charge density within the dielectric material. The surface charge density along the dielectric surface produces an electric field with two components, i.e. the component acting inside the dielectric and that in the air surrounding the material. The magnitudes of the field components depend on the surface charge density and the polarization in the dielectric material. This surface charge dependent field distorts the externally applied field and can lead to a flashover. The distribution of the surface charge and hence the variation of the field along a given insulator surface is, to some extent, dependent on the profile of the insulator surface. It is possible to study the flashover voltage on the basis of surface field or charge distribution evaluations.

Theoretical models that compute the flashover voltage of ice-covered insulators are useful for two main purposes: (i) for better understanding of the physical processes responsible for the flashover, and (ii) if the model can be shown to be well correlated with field or laboratory experiences, this could be used for the prediction of flashover voltages over a wide range of field conditions; thus reducing the number of costly laboratory experiments in the design of better insulators.

1.3 Numerical Techniques for Field Computations

The field distribution can be evaluated using numerical techniques, such as, the boundary element method (BEM) [28], the charge simulation method (CSM) [29, 30], the finite difference method (FDM) [31], and the finite element method (FEM) [32].

1.3.1 Boundary Element Method

The BEM offers advantage in that the dimensionality of the problem is reduced from three to two, but this method is not very good for field problems with non-linear materials. A hybrid solution employing BEM for the linear exterior source free region and the FEM for the non-linear and source region holds promise as an economical technique.

1.3.2 Charge Simulation Method

Programming of the CSM is easy with highly attained precision. However, it is not suitable for the considerably complicated fields. This method is applicable to fields containing unbounded region, but it is not good for fields with many dielectrics or complex electrode configuration, and for specific fields containing space charges or leakage resistance.

1.3.3 Finite Difference Method

The FDM requires the domain to be discretized by grids at finite and equal distances. It requires considerable memory and computation time for the complex geometries. Hence, it is not used for complex geometries.

1.3.4 Finite Element Method

The FEM is most convenient for a field with many dielectrics, inhomogeneous and nonlinear materials, complex fields and a field containing the distributed space charges and singular points. FEM is one of the most successful numerical methods for solving electrostatics field problems because it involves discretization of the domain according to the anticipated value of field distributions, i.e. fine mesh generation at critical regions and course mesh generation at non critical regions, thus saving considerable memory and computing time for the complex geometries. At the same time, a suitable discretization mesh for the field domain is needed at the beginning of the calculation, which is not only a discouraging preliminary step for the non expert, but also a cumbersome job for the expert. Such mesh generation plays an important role in the finite element modeling and analysis process because the quality of the computed results depends strongly upon the choice of the meshes. The expense of generating a suitable mesh is often much more than that of solving the equation system.

1.4 Objectives of the Thesis

The objectives of the thesis are:

1. To find out the effects of surface glaze (Semiconductor) coatings on the potential distributions around the ice-covered insulators for the power frequency voltage.
2. To study the effects of Lightning Impulse (LI) and Switching Impulse (SI) voltages on the potential and electric field distributions around the insulators under clean and icing condition.
3. To compute the potential and electrical field distributions around an ice-covered insulator i.e. an open boundary problem using a Finite Element Method based approach, and compare the computation times required using an artificial boundary around an ice-covered insulator and the open boundary around the insulator simulated by a form of the Kelvin transformation.
4. To study the effects of semi-conducting glaze conductivity & thickness, water film conductivity & thickness, and ice layer thickness on the electrical performance of the insulator.
5. To study the flashover performances based on the potential and electric field distributions around the ice-covered normal glazed and semi-conducting glazed insulators under various conditions. This will aid in the better design of insulators under various conditions for the power transmission lines, and reduce the number of costly laboratory experiments.

1.5 Statement of Originality

From the review of the literature presented in the next chapter, it is found that several studies have been carried out for the flashover voltage and low frequency electric field distributions around insulators under icing conditions, but none of them has considered the effects of the glaze coatings on insulators. A thin layer of the semi-conducting glaze coating on the insulator has major effects on the electric field distribution around the insulator and this, in turn, affects the flashover performance of the insulator considerably. In this work, effects of semi-conducting glaze coatings on the insulators, has been studied in detail under various conditions.

1.6 Structure of the Thesis

The following is the summary of the contents of various chapters presented in this thesis:

Chapter 2 deals in detail with the literature available regarding the ice and the field computations around the insulators under various conditions and the studies conducted so far by the various researchers in this field and the relevant discussions on them.

Chapter 3 presents the open boundary approximations applied to an ice-covered insulator with a water film in the presence of an icicle and an air gap.

Chapter 4 discusses the proposed method for the computation of the electric field distributions under the transient voltages around the clean and ice-covered insulators using the Finite Element Method, and flashover performances of the insulators based on the electric field distributions.

Chapter 5 presents the laboratory experiments done to validate the proposed model.

Chapter 6 discusses the proposed method for the computation of the potential distributions under the sinusoidal voltages along the clean and ice-covered insulators using the Finite Element Method, and flashover performances of the insulators based on the electric field distributions.

Chapter 7 presents the important conclusions arising out of this work as well as topics for the future research.

The next chapter presents a review of the literature on the studies conducted by various researchers in the area of electric field computations around the ice-covered insulators.

CHAPTER 2

LITERATURE REVIEW

The literature review is divided in five parts as follows:

1. Types of Ice,
2. Laboratory Model of an Ice-Covered Insulator,
3. Properties of Ice,
4. An Open Boundary around an Insulator,
5. Flashover Model of an Insulator.

2.1 Types of Ice

An ice accumulated on the insulator is divided into two categories, dry and wet. The dry ice, of a relatively low density, whether hard rime or soft rime gets formed at a low droplet size and with the ambient temperature below zero degrees centigrade. The wet ice or glaze, which is the most dangerous type of ice for the electrical performance of the insulator, grows in the presence of a surface water film. The density of the glaze is relatively high, about 0.9 g/cm^3. Table 2.1 and Table 2.2 show the names of different types of ice and the atmospheric conditions favorable for the formation of each type of ice [33, 25].

Table 2.1: Characteristics of the ice-formation on structures

Type of Ice	Density (g/cm^3)	Appearance	Shape
Glaze	0.8 to 0.9	Transparent and clear	Cylindrical icicles
Hard Rime	0.6 to 0.8	Opaque	Eccentric pennants into the wind
Soft Rime	< 0.6	White and opaque	Feathery and granular

Table 2.2: Atmospheric parameters for the formation of various types of ice

Type of Ice	Air Temperature (°C)	Wind Speed (m/s)
Glaze	0 to -3	1 to 20
Hard Rime	-3 to -15	5 to 20
Soft Rime	-5 to -25	5 to 20

2.2 Laboratory Model of an Ice-Covered Insulator

Ice in the laboratory can be produced under both wet and dry regimes [25]. In a dry regime, ice is produced as a result of a small water-droplet (15 μm) spray that freezes immediately upon impact on the surface. A surface temperature below 0°C will ensure the instant thermal equilibrium between ice deposits and the ambient air, where the heat disturbance is because of the impact of water droplets and forced convection. When dry ice is produced, it has a low density of about 0.4 to 0.6 g/cm^3 similar to natural light ice and it is opaque in appearance [26].

Wet grown ice is produced by water droplets (50 to 80 μm), which are bigger than those observed during the formation of low-density ice. These water droplets are not in a frozen state before impacting the surface of the insulator in air and they reach the insulator

in a supercooled liquid form. As a result, the ice will get accreted between the skirts of the insulator in the form of icicles. The density of this type of ice is approximately 0.9 g/cm^3 for the icicles and approximately 0.87 g/cm^3 for the ice deposit on the surface of the insulator. The color and transparency of the ice in this regime depend on the presence of air bubbles in the ice.

Farzaneh et al. [26] studied an ice-covered insulator model in the laboratory. The insulator was covered with a glaze ice for the experimental validation of the theoretical results. Artificial ice was accreted on a station post insulator in a climate room at CIGELE. The air temperature in the climate room was controlled with a precision of about ± 0.2°C. A mesh-grid ceiling placed on the climate room facilitated quick exchanges of temperatures and minimized the temperature gradient inside the climate room. De-ionized water was used to spray the insulator that was placed vertically in the center of the climate room. The electrical conductivity of the water was adjusted by adding sodium chloride.

The spray system had 4 air atomizing nozzles that were mounted on an oscillating support parallel to the axis of the insulator. The oscillating movement helped to keep the mean liquid water content approximately constant along the vertical axis of the insulator, thus forming ice with a uniform thickness along the insulator string.

A uniform wind in the climate room was generated by a system of eight fans. The fans were installed to generate the wind up to a speed of 50 km/h along the axis of the insulator.

The density of ice accumulated on the insulator was determined by weight and volume measurements. The volume was calculated by immersing an ice sample in light

mineral oil. In order to prevent the penetration of oil into the pores of the ice, the sample was covered with a thin film of Formvar, the volume of that was subtracted from the total buoyancy measured.

The thickness of the ice accumulated on the insulator was found out by measuring the thickness of the ice accumulated on a monitoring cylinder, 3.8 cm in diameter and rotating at 1 rpm [26].

2.3 Properties of Ice

The water molecule has an electric dipole moment, and therefore if the water molecules in ice can orient themselves when an electric field is applied, ice can have quite a large electric permittivity. This fact is responsible for the most straightforward electric properties of ice. However, unlike the situation in liquid water, the molecules are not free to rotate in the field, and the mechanism by which they turn around introduces complications. In addition to this dielectric effect, ice can also conduct a direct current of electricity, and shows thermoelectric effects and other more complex electrical effects. Much work has been done on these phenomena and some are relatively well understood, while others are still the subject of controversy and study [34]. Many of the effects are profoundly affected by small amounts of dissolved impurities in the ice. Surface effects have also confused the situation, so care should be taken in using numerical data, especially if the ice type or size of sample is very different from those to which the data apply.

When an electric field is applied to a specimen of ice three distinct processes occur:

1. The individual molecules are polarized by the field. This involves displacements of the electrons relative to the nuclei and small distortions of the molecules under the restoring forces. These are the forces which occur in any material. The response to a change in field is very rapid, so that the effects are independent of frequency up to microwave frequencies [34].

2. The ice is polarized by the reorientation of molecules or bonds. The energies of some of the proton configurations that are compatible with the ice rules are lowered relative to others, so that in thermal equilibrium there is a net polarization of the ice. The achievement of this equilibrium is a comparatively slow process, requiring thermal activation and local violations of the ice rules [34].

3. With suitable electrodes a steady current flows in accordance with Ohm's law. There is no detectable electronic conduction in ice and the observed current arises from a flow of protons. Because the conduction process has features in common with electronic conduction in semiconductors ice is sometimes referred to as a 'protonic semiconductor', but the protons do not share the quantum mechanical properties that are an essential feature of the band theory of electrons in solids [34].

2.3.1 Complex Relative Permittivity of Ice

The complex relative permittivity of the glaze ice, ε_r^*, can be expressed in terms of the volume conductivity of ice, σ_v, and the real relative permittivity of ice, ε_r, as follows [45],

$$\varepsilon_r^* = \varepsilon_r - j\frac{\sigma_v}{\omega\varepsilon_0}, \tag{2.1}$$

where ε_0 is the permittivity of free space, and ω is the angular frequency.

In this work, due to high conductivity of the semi-conducting glaze and the water film, conductivity of the ice is neglected assuming that all the leakage current flows in the semi-conducting glaze and the water film.

Hence the complex relative permittivity of ice,

$$\varepsilon_r^* \approx \varepsilon_r, \tag{2.2}$$

is approximately equal to the real relative permittivity of ice.

2.3.2 Real Relative Permittivity of Ice with Frequency

The real relative permittivity of the ice, ε_r, depends on the frequency of the applied voltage, according to the following expression [35],

$$\varepsilon_r = \varepsilon_\infty + \frac{\varepsilon_s - \varepsilon_\infty}{1 + \omega^2 \tau^2}\ , \qquad (2.3)$$

where,

ε_r is the real relative permittivity of the ice,

ε_∞ is the real relative permittivity of the ice at very high frequency,

ε_s is the static permittivity of the ice,

ω is the angular frequency, and

τ is the relaxation constant.

The relaxation constant, τ, is given by the following expression [35],

$$\tau = C_\tau \exp\left(\frac{E_\tau}{KT}\right), \qquad (2.4)$$

where,

C_τ is a constant of value 7.7×10^{-16} s,

E_τ is the activation energy of value 9.29×10^{-20} joules,

T is the temperature (°K), and

K is the Boltzmann constant.

2.3.3 High Frequency Permittivity, ε_∞, of Pure Ice

The origin of the permittivity, ε_∞, is the polarization of the molecules by displacements of the electronic charge distribution and distortion of the molecules in the electric field.

The limiting permittivity at frequencies above the Debye relaxation has been determined in the course of normal dielectric measurements over the temperature range 200-230 °K by Johari and Jones [36], but for higher temperatures it was necessary to use special measurements in the range 1-100 MHz [37]. A typical value is $\varepsilon_\infty = 3.16 \pm 0.02$ at 253 °K, falling to 3.14 at 200 °K. Measurements by Gough [38] show a continual decrease down to 3.093 ± 0.003 at 2 °K. Using a microwave resonator at 39 GHz Matsuoka et al. [39] found that ε_∞ is anisotropic, which is equivalent to the ice being birefringent. At 252 °K they obtained values of 3.1734 ± 0.0055 and 3.1396 ± 0.0049 for electric fields parallel and perpendicular to the *c*-axis respectively. They also made measurements with a parallel plate capacitor at 1 MHz. The anisotropy was independent of frequency and temperature, but their 1 MHz values were higher (by about 0.044) than their values at 39 GHz.

2.3.4 Static Permittivity, ε_s, of Ice

The static value of the permittivity, i.e. the value for zero frequency, depends on the crystal orientation, being quite markedly larger if the electric field is parallel to, rather than perpendicular to, the *c*-axis (axis of symmetry in the hexagonal ice cell). The static value also varies with temperature, increases as the temperature decreases.

Johari et al. [40] measured the static permittivity, ε_S, of the pure polycrystalline ice, and found out its values as a function of temperature, T, as shown in Figure 2.1.

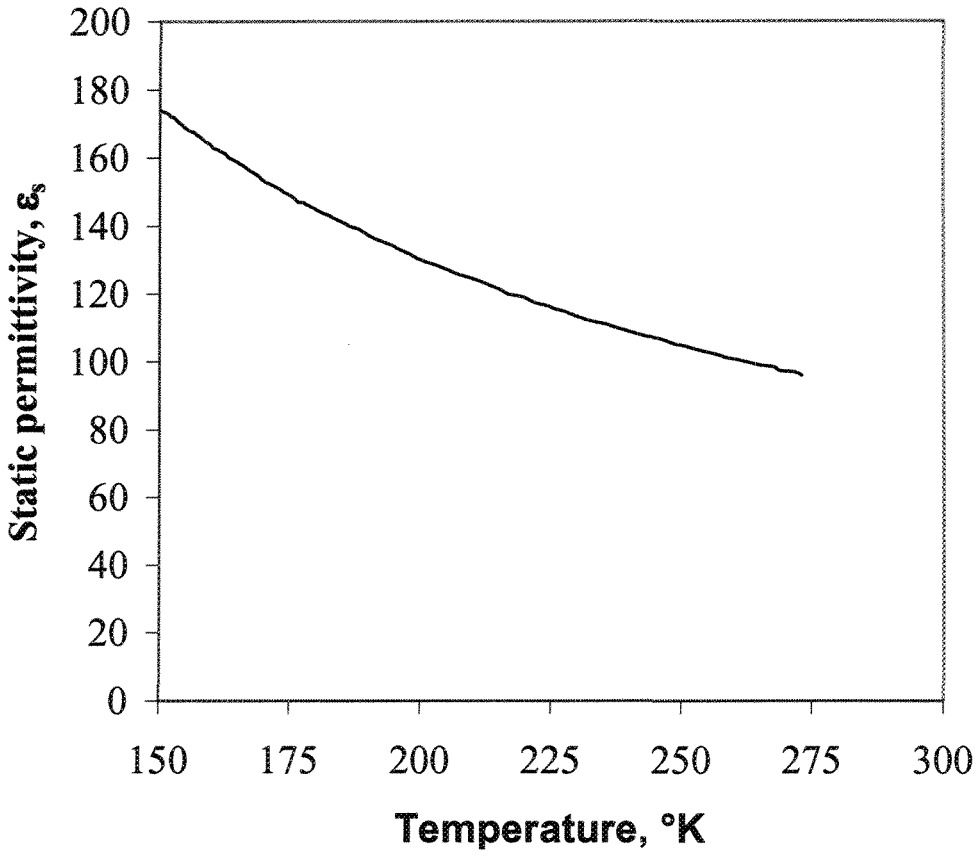

Figure 2.1: Static permittivity, ε_S, of pure polycrystalline ice as a function of the temperature, T.

2.4 An Open Boundary around an Insulator

The ice-covered insulator is an open boundary problem, and hence for studying the effects of a semi-conducting glaze coating on the electrical performance by computing potential and electric field distributions around the insulator using a finite element based approach, an artificial boundary, far away from the device where electric fields are effectively zero, is to be defined when the mesh is generated [41]. At this boundary, it is assumed that the electric fields fall off to zero. The position of the artificial boundary is important because the entire interior region up to the boundary must be discretized, and this increases the size of the problem without adding any useful information to the desired solution. This approach may result in considerable memory and computation time for the computation of the potential and electric field distributions along the semi-conducting glazed insulator under icing conditions.

An ice-covered insulator problem may be solved without approximation by several techniques, all having in common the idea that the open (infinitely extending) region is subdivided into two portions,

- The interior portion,
- The exterior portion,

so that the interior part contains the structures and fields of principle interest. An artificial, more or less arbitrary, boundary Γ is placed around the interior region Ω_i, separating it from the rest of space, the outer region Ω_o.

As in finite regions, the essence of the finite element method is still to render stationary a functional, typically,

$$\Im(U) = \int_{\Omega} \left(\nabla U . \nabla U - k^2 U^2 - gU\right) d\Omega , \qquad (2.5)$$

where,

∇U is the potential gradient,

k^2 is a constant in the Helmholtz equation, and

g is a driving function, assumed to be given,

the integral being taken over all space. The integral divides naturally into integrals over the two regions Ω_i and Ω_o.

$$\Im(U) = \int_{\Omega_i} \left(\nabla U . \nabla U - k^2 U^2 - gU\right) d\Omega + \int_{\Omega_o} \left(\nabla U . \nabla U - k^2 U^2 - gU\right) d\Omega . \qquad (2.6)$$

The inner region is amenable to treatment by standard finite element techniques. The exterior region must adhere to the same general principles as the interior ones, but applied to an infinite geometric extent. Thus, it must possess suitable approximating functions, able to model the function behavior in the exterior adequately. At the exterior-interior interface Γ, the principal continuity conditions must be satisfied. In an ice-covered insulator problem, this means the potential function U must be continuous across Γ.

Three distinct techniques are available for constructing approximating functions for the exterior region as follows:

1. Recursive growth (Ballooning),
2. Geometric transformation,
3. Implicit construction.

2.4.1 Recursive Growth Process

The family of recursive growth methods for modeling infinite regions, often also called "balloon" algorithms [42], forgoes reaching true infinity and settles for a very large though finite region instead. It uses standard finite elements as its fundamental building blocks and it effectively constructs a huge mesh without writing down the corresponding huge matrices.

Consider that a finite element model is to be built for the region of principal interest $\Omega^{(p)}$. The problem is to construct a valid representation of the outside region, an infinite element, whose interior edge will match both the shape and the type of approximating functions of the interior model, making the complete geometric model seamless and the potential continuous across Γ_0. The steps for the ballooning algorithm are shown in Figure 2.2.

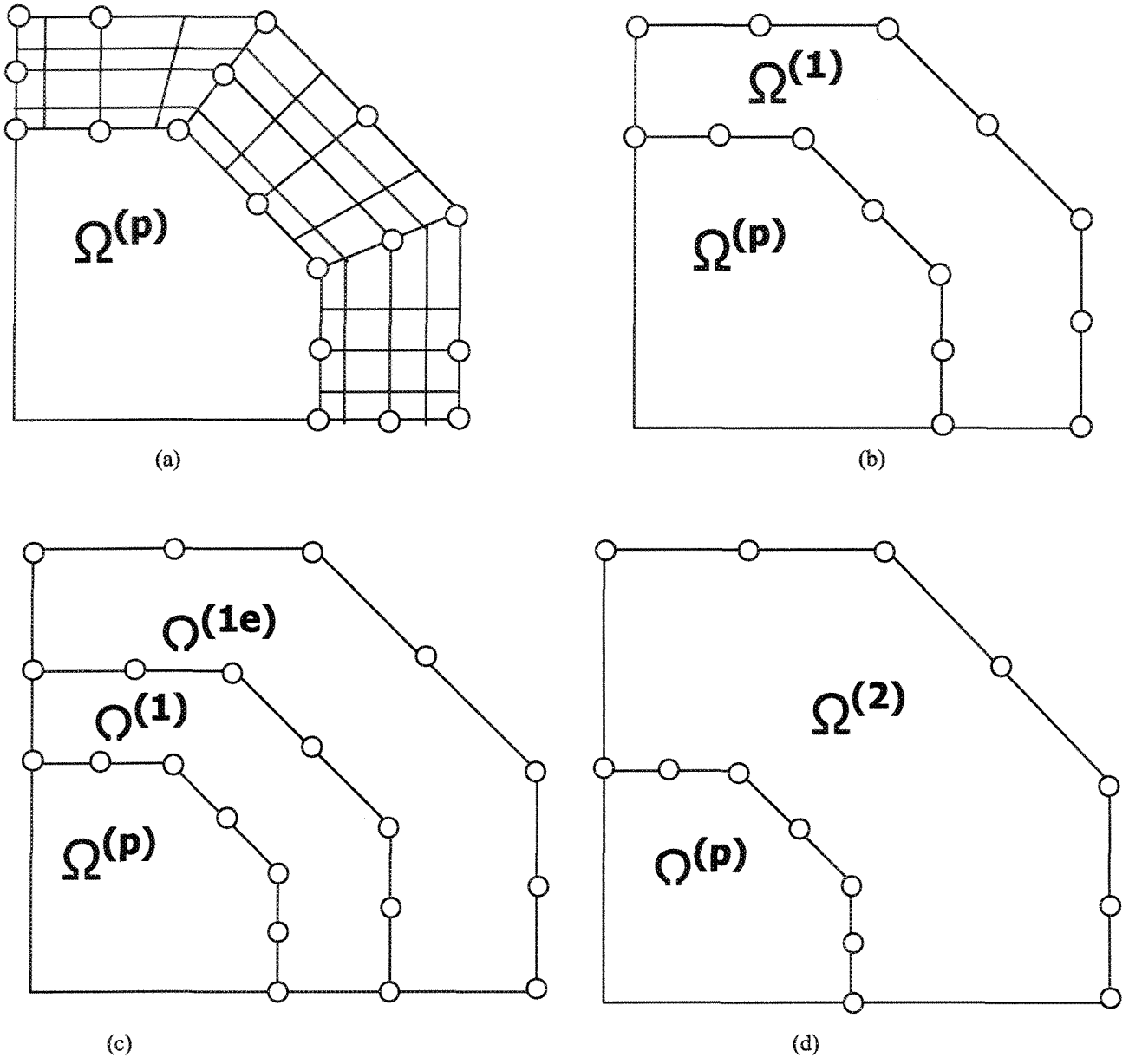

Figure 2.2: The ballooning algorithm. (a) The region of principal interest $\Omega^{(p)}$ is augmented by a border of elements. (b) Bordering elements are condensed to form a single superelement $\Omega^{(1)}$. (c) The superelement is scaled and attached to itself. (d) Condensation produces an enlarged superelement $\Omega^{(2)}$.

For the Helmholtz equation in the plane, two matrices are generated:

$$T_{ij} = \int_{\Omega^{(1e)}} \alpha_i \alpha_j d\Omega, \tag{2.7}$$

and,

$$S_{ij} = \int_{\Omega^{(1e)}} \nabla\alpha_i . \nabla\alpha_j d\Omega, \tag{2.8}$$

where the region of integration $\Omega^{(1e)}$ is the enlarged superelement. It is a proportional enlargement of $\Omega^{(1)}$, all linear dimensions [42] being multiplied by some scale factor ρ,

$$\int_{\Omega^{(1e)}} \alpha_i \alpha_j d\Omega = \frac{|\Omega^{(1e)}|}{|\Omega^{(1)}|} \int_{\Omega^{(1)}} \alpha_i \alpha_j d\Omega . \tag{2.9}$$

In two-dimensional problems, $\boldsymbol{T}$ thus scales by ρ^2,

$$T_{ij}\,|_{\Omega^{(1e)}} = \rho^2 T_{ij}\,|_{\Omega^{(1)}}, \tag{2.10}$$

while in three dimensions, the scaling factor is ρ^3,

$$T_{ij}\,|_{\Omega^{(1e)}} = \rho^3 T_{ij}\,|_{\Omega^{(1)}} . \tag{2.11}$$

The matrix $\boldsymbol{S}$ in two dimensions is invariant [42],

$$S_{ij}\,|_{\Omega^{(1e)}} = S_{ij}\,|_{\Omega^{(1)}}, \tag{2.12}$$

but in three-dimensional problems it scales with length,

$$S_{ij}\,|_{\Omega^{(1e)}} = \rho S_{ij}\,|_{\Omega^{(1)}} \ . \qquad (2.13)$$

In summary, the matrices T and S for the enlarged superelement are obtained by a simple scalar multiplication [42].

2.4.2 Geometric Transformations (Exterior Mappings)

Geometric transformations turn the exterior infinite region into a finite region. The functional $\Im(U)$ is transformed in this process, so the construction of element matrices for the infinite region is replaced by the construction of element matrices for the transformed functional, but over a finite region. The transformed region can be treated by a standard or nearly standard finite element method.

There are two types of exterior mappings as follows:

1. Coordinate and functional transformation,
2. Kelvin transformation.

2.4.2.1 Coordinate and Functional Transformation

In this transformation, a coordinate transformation $\Im$ is to be found that maps the exterior region Ω_o into a finite transformed region Ω_t, subject to the requirement that the separating boundary Γ must map into itself: $\Im\ \Gamma = \Gamma$. This transformation is shown in Figure 2.3.

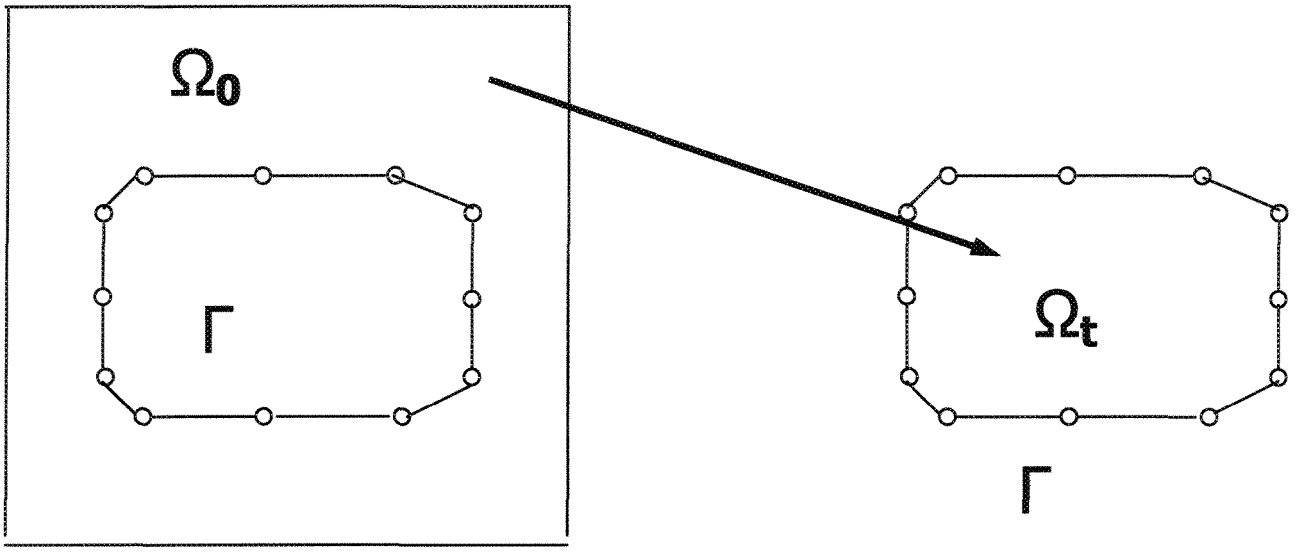

Figure 2.3: Coordinate transformation $\Im$ maps the outer region Ω_o into a finite region Ω while preserving the separating boundary Γ.

The finite element functional is written as the sum of two integrals, over the inner and outer regions. Thus,

$$\Im(U) = \Im_i(U) + \Im_o(U),$$
$$\Im_o(U) = \int_{\Omega_o} (\nabla U.\nabla U + k^2U^2 - gU)d\Omega. \qquad (2.14)$$

The integral for outer region $\Im_o(U)$, is transformed to an integral over Ω_t under the coordinate transformation T which carries the original coordinates x, y into new coordinates x', y'.

The derivatives in ∇U must be written in the transformed coordinates x', y' as follows,

$$\begin{bmatrix} \frac{\partial U}{\partial x} \\ \frac{\partial U}{\partial y} \end{bmatrix} = \begin{bmatrix} \frac{\partial x'}{\partial x} & \frac{\partial y'}{\partial x} \\ \frac{\partial x'}{\partial y} & \frac{\partial y'}{\partial y} \end{bmatrix} \begin{bmatrix} \frac{\partial U}{\partial x'} \\ \frac{\partial U}{\partial y'} \end{bmatrix} = J \begin{bmatrix} \frac{\partial U}{\partial x'} \\ \frac{\partial U}{\partial y'} \end{bmatrix}, \tag{2.15}$$

where J denotes the Jacobian of the transformation.
The surface (or volume) integral transforms,

$$d\Omega = dxdy = |J| dx'dy' = |J| d\Omega'. \tag{2.16}$$

Hence,

$$\nabla U.\nabla U = \left(J \begin{bmatrix} \frac{\partial U}{\partial x'} \\ \frac{\partial U}{\partial y'} \end{bmatrix} \right)^T \left(J \begin{bmatrix} \frac{\partial U}{\partial x'} \\ \frac{\partial U}{\partial y'} \end{bmatrix} \right), \tag{2.17}$$

$$= \begin{bmatrix} \frac{\partial U}{\partial x'} & \frac{\partial U}{\partial y'} \end{bmatrix} J^T J \begin{bmatrix} \frac{\partial U}{\partial x'} \\ \frac{\partial U}{\partial y'} \end{bmatrix}. \qquad (2.18)$$

The energy density W is given by,

$$W = \frac{1}{2} E \,.D = \frac{1}{2} E \,.(\overline{\overline{\varepsilon}} E),$$

$$W = \frac{1}{2} \nabla \phi \,.(\overline{\overline{\varepsilon}} \nabla \phi),$$

$$\nabla U \,.\nabla U = \nabla' U \,.(\overline{\overline{p}} \nabla' U) |J| \qquad (2.19)$$

where $\overline{\overline{p}}$ represents the apparent tensor material property in x', y' coordinates,

$$\overline{\overline{p}} = \frac{J^T J}{|J|}. \qquad (2.20)$$

Thus,

$$\Im_o(U) = \int_{\Omega_o} (\nabla' U \,.\overline{\overline{p}} \nabla' U + \frac{k^2}{|J|} U^2 - \frac{g}{|J|} U) |J| d\Omega \,, \qquad (2.21)$$

where the primes indicate that differentiation is to be carried out with respect to the primed coordinates.

Expressing $\Im_o(U)$ as an integral over the transformed region,

$$\Im_o(U) = \int_{\Omega_t} (\nabla' U . \overline{\overline{p}} \nabla' U + \frac{k^2}{|J|} U^2 - \frac{g}{|J|} U) d\Omega \,. \qquad (2.22)$$

This integral is easy to treat numerically, because it covers the finite (transformed) region of integration Ω_t.

2.4.2.2 Kelvin Transformation

The Kelvin transformation [42] transforms the exterior of a circle into its interior, as shown in Figure 2.4.

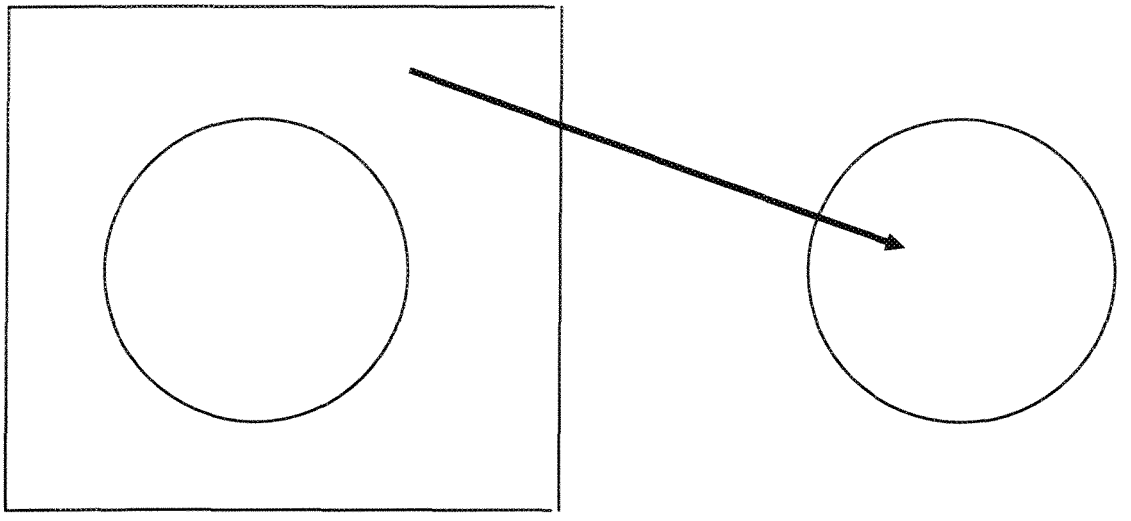

Figure 2.4: The Kelvin transformation maps the exterior of a circle onto the interior of another circle of the same radius.

Using the Kelvin transformation, the entire *x*-*y* plane can be transformed onto the two faces of a circular disk: the circular interior region onto one face, the exterior of this circle onto the other.

In polar coordinates, coordinate transformation from r, θ into r', θ',

$$r' = \frac{R^2}{r}$$
$$\theta' = -\theta \qquad (2.23)$$

In polar coordinates, the gradient is given by:

$$\nabla U = 1_r \frac{\partial U}{\partial r} + \frac{1_\theta}{r} \frac{\partial U}{\partial \theta}. \qquad (2.24)$$

The Jacobian relates the incremental distances in the two coordinate systems. The Jacobian of the Kelvin transformation is given by:

$$\begin{bmatrix} dr' \\ r'd\theta' \end{bmatrix} = J \begin{bmatrix} dr \\ rd\theta \end{bmatrix} = \begin{bmatrix} \frac{\partial r'}{\partial r} & \frac{1}{r}\frac{\partial r'}{\partial \theta} \\ r'\frac{\partial \theta'}{\partial r} & \frac{r'}{r}\frac{\partial \theta'}{\partial \theta} \end{bmatrix} \begin{bmatrix} dr \\ rd\theta \end{bmatrix}$$

$$J = \begin{bmatrix} -\frac{R^2}{r^2} & 0 \\ 0 & -\frac{R^2}{r^2} \end{bmatrix} = -\frac{R^2}{r^2} \begin{bmatrix} 1 & 0 \\ 0 & 1 \end{bmatrix}. \qquad (2.25)$$

The Jacobian matrix equals the unit matrix with a multiplier. This property simplifies both the mathematical development and computation. The important point is that the Kelvin transformation makes the fictitious anisotropic material property $\overline{\overline{p}}$ turn into,

$$\overline{\overline{p}} = \frac{J^T J}{|J|} = \begin{bmatrix} 1 & 0 \\ 0 & 1 \end{bmatrix}, \qquad (2.26)$$

the identity matrix.

The transformed exterior functional $\Im_o(U)$ therefore becomes,

$$\Im_0(U) = \int_{\Omega_t} \left\{ \nabla' U . \nabla' U + k^2 (\frac{r'}{R})^2 U^2 - g(\frac{r'}{R})^2 U \right\} d\Omega. \qquad (2.27)$$

In this work, to reduce the computation time and memory, a form of Kelvin transformation has been used to simulate the open boundary around the ice-covered insulators.

2.4.3 Implicit Construction of the Exterior Region

Implicit modeling methods are sometimes called hybrid methods. The differential equation boundary-value problem in the outer region is reformulated as an integral equation problem, so that integral-operator finite elements are used in the exterior. The approximating functions used in the exterior are not explicitly known, except for their values on the boundary Γ itself [42].

2.5 Flashover Model of an Insulator

In general, researchers have focused on the computation of electric fields and potential distributions along normal glazed (conductivity 0) insulators for power frequency voltages under various conditions. Contributions in low frequency field computations for pure as well as lossy dielectrics are as follows:

Asenjo et al. [31] proposed a method to solve low frequency complex fields in polluted insulators in which σ (the conductivity) is of the same order of magnitude as $\omega\varepsilon$ (angular frequency × permittivity) by using the finite difference method. The approach was based on a quasi-static approximation obtained by neglecting the electric field induced by the magnetic field. The problem was reduced to finding a solution to Laplace's equation that satisfies the usual boundary conditions.

Later Asenjo et al. [32] proposed an alternate scheme to compute the low frequency complex electric field in the polluted insulators using the finite element method. The method was based on a quasi-static approximation which permits the decoupling of Maxwell's equations.

Sundararajan et al. [43] developed a dynamic model that computes the flashover voltages of polluted insulators energized with a dc voltage. The salient feature of this model was that it took into account the configuration of the insulator profile at every instant, which plays an important role in the flashover process of dc polluted insulators.

Farzaneh et al. [26] studied the natural ice accretion on HV insulators as well as performing a laboratory investigation of the ac flashover performance of various types of insulators covered with artificial ice. A method based on the standard IEC 507 methods, was developed for measuring the maximum withstand voltage of ice-covered insulators. They studied the effect of thickness and uniformity of the ice, as well as the arcing distance of the insulators, and the conductivity of the freezing water.

El-Kishky et al. [29] used a modified charge simulation method for computing the electric potential and field distributions along ac HV outdoor insulators. They modeled non-ceramic and ceramic suspension insulators of various voltage ratings under clean and dry surface conditions.

Chakravorti et al. [30] computed the capacitive-resistive field distribution around a polluted insulator using the charge simulation method. They computed the electric field for the power frequency voltage and also for the lightning and switching impulse voltages.

Guerrero [44] studied experimentally the flashover performance of a normal glazed ice-covered insulator under impulse voltages. She considered the effects of the polarity of the applied impulse voltage on the flashover performance of an ice-covered normal glazed insulator and also how accumulation of the ice on the insulator affects the flashover voltage of the normal glazed insulator under lightning and switching impulse voltages.

Volat [45] computed the potential and electric field distributions along normal glazed ice-covered insulators for the power frequency voltage using the Boundary Element Method. He studied the effects of the number, size and position of the air-gaps formed on the electric field distributions along an ice-covered insulator.

Farzaneh et al. [46] developed a model for predicting the flashover voltage of ice-covered insulators energized with an ac voltage. The model takes into account the variation of ice surface conductivity as a function of the freezing water conductivity. They also determined the effects of the length of the arc on its own characteristics, as well as an ac arc reignition condition, in a laboratory investigation using the triangular ice samples.

The next chapter discusses the two open boundary approximations applied to an ice-covered insulator with a water film in the presence of an icicle and an air gap and also the comparison of computation times and results using both the approximations.

CHAPTER 3

SIMULATION OF AN OPEN BOUNDARY AROUND AN INSULATOR FOR FIELD COMPUTATIONS

An actual ice-covered station post insulator, shown in Figure 1.1, has been simulated in this work. It is assumed that the ice is accumulated uniformly on the insulator. The potential and electric field distributions have been computed on a vertical plane cutting the insulator into four symmetrical parts [45].

3.1 Low Frequency Fields around the Insulators

The general solution for the low frequency electromagnetic fields in insulating systems can be obtained by solving Maxwell's equations, but this would be a formidable task due to the coupling between the electric and magnetic fields.

However, Maxwell's field equations,

$$\nabla \times E = -j\omega\mu H \qquad (3.1)$$

$$\nabla . \varepsilon E = \rho \qquad (3.2)$$

$$\nabla \times H = \sigma E + j\omega\varepsilon E \qquad (3.3)$$

$$\nabla . \mu H = 0 \qquad (3.4)$$

Where,

E = Complex electric field strength vector,

H = Complex magnetic field strength vector,

ρ = Volume charge density,

ω = Angular frequency,

ε = Permittivity,

σ = Conductivity,

μ = Permeability.

can be decoupled in the following situations:

a) When the frequency is low and $\sigma >> \omega\varepsilon$, it is possible to approximate the time-varying field by a dc field $(\omega = 0)$. In this case, Maxwell's equations are reduced to the static approximation. In the proposed work, the water film and semi-conducting glaze come in this category.

b) When $\omega\varepsilon >> \sigma$, the field is solved as in the electrostatic case. This implies neglecting σ relative to $\omega\varepsilon$ in (3.3), and also assuming $\omega\mu H = 0$ in (3.1), which results in de-coupled fields. Since the term proportional to ω is neglected only in the second member of (3.1) and not in equation (3.3), this solution could be called a quasi-static approximation. In the proposed work, dielectric and ice come in this category.

c) In some high voltage heterogeneous dielectric systems $\sigma \approx \omega\varepsilon$, the decoupling is obtained by assuming $\omega\mu H = 0$ in (3.1).

To apply the finite element method, a functional based on the system energy is defined that can be applied for the stated problem. Minimization of the system energy, leads to a system of algebraic equations, whose solution, under the application of the corresponding boundary conditions (Dirichlet, Neuman or mixed), supplies the required node potentials, and then in turn electric field strengths can be calculated by the numerical differentiation of the potential with respect to the distance at any point. Since numerical differentiation can introduce a large error, in some cases, potential distributions along the insulators have been computed in this work. By visible inspection of the potential distributions, flashover performances have been studied.

3.2 Simulation Parameters

Table 3.1 shows the set of parameters used in the simulation work. The conductivities of the ice and the porcelain are neglected assuming that all the leakage current flows in the water film [45]. All the computations have been done using a commercially available program based on the FEM by Infolytica Corporation, Montreal, Quebec, Canada.

Table 3.1: Simulation parameters

	Porcelain	Ice-layer	Water film
Relative Permittivity (ε_r)	6.0	75.0 for 60 Hz	81.0
Conductivity (S/m)	0	0	0.030
Thickness (mm)	-	25	3.0

3.3 An Open Boundary around an Insulator

Since an ice-covered insulator is an open boundary problem. There are two methods considered in this work to compute the potential and electric field distributions around the insulator.

1. An Artificial boundary
2. The Open Boundary Simulated by the Kelvin Transformation

3.3.1 Artificial Boundary

An artificial boundary is defined three to four times the device radius away from the device. At this boundary, it is assumed that the electric fields fall off to zero. The position of the artificial boundary is important because the entire interior region up to the boundary,

must be discretized, and this increases the size of the problem without adding any useful information to the desired solution. Figure 3.1 shows an ice-covered insulator model with an artificial boundary.

Figure 3.2 shows the solution mesh for the computation of the potential distribution along the insulator.

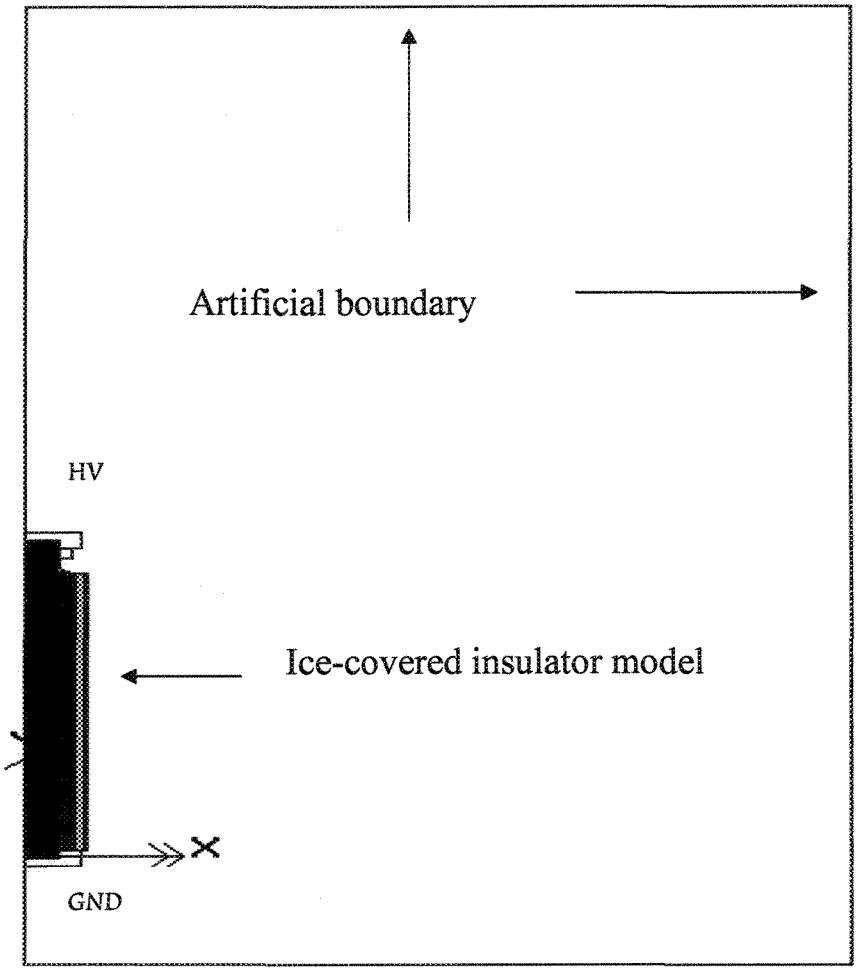

Figure 3.1: An ice-covered insulator with an artificial boundary.

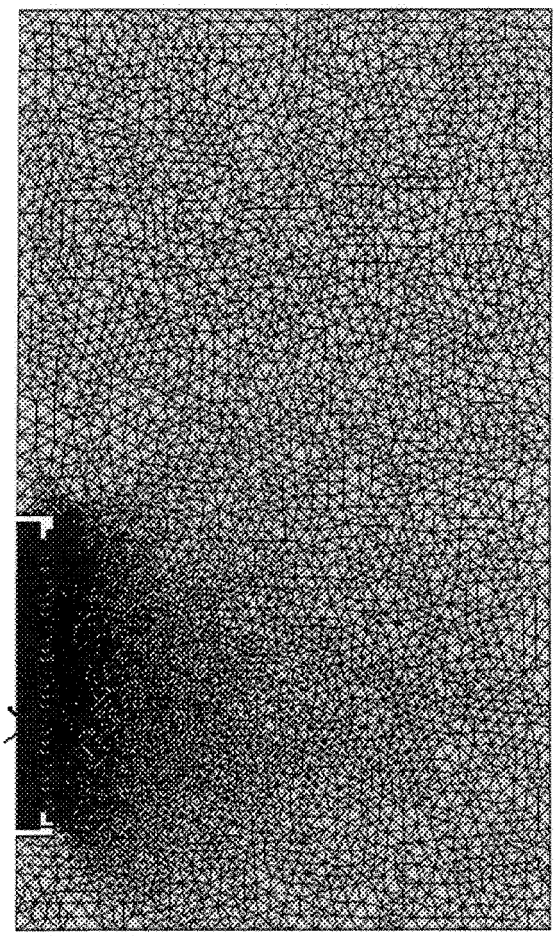

Figure 3.2: Solution mesh for the computation of potential distribution using an artificial boundary.

Figure 3.3 shows the voltage contours around an ice-covered insulator with a water film in presence of an icicle and an air gap computed by creating an artificial boundary around the insulator and Figure 3.4 shows the voltage contours close to the HV electrode.

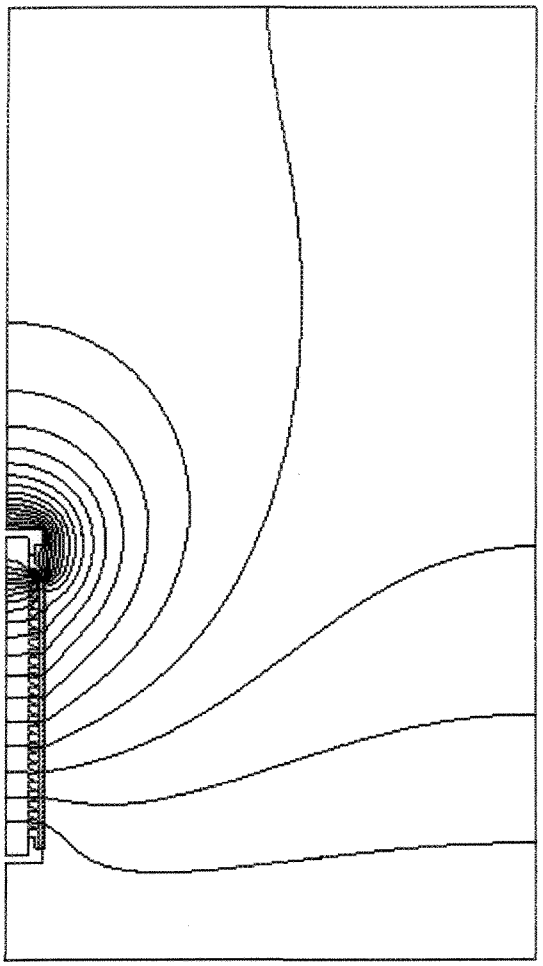

Figure 3.3: Voltage contours around an ice-covered insulator with a water film in presence of an icicle and an air gap computed by creating an artificial boundary around the insulator.

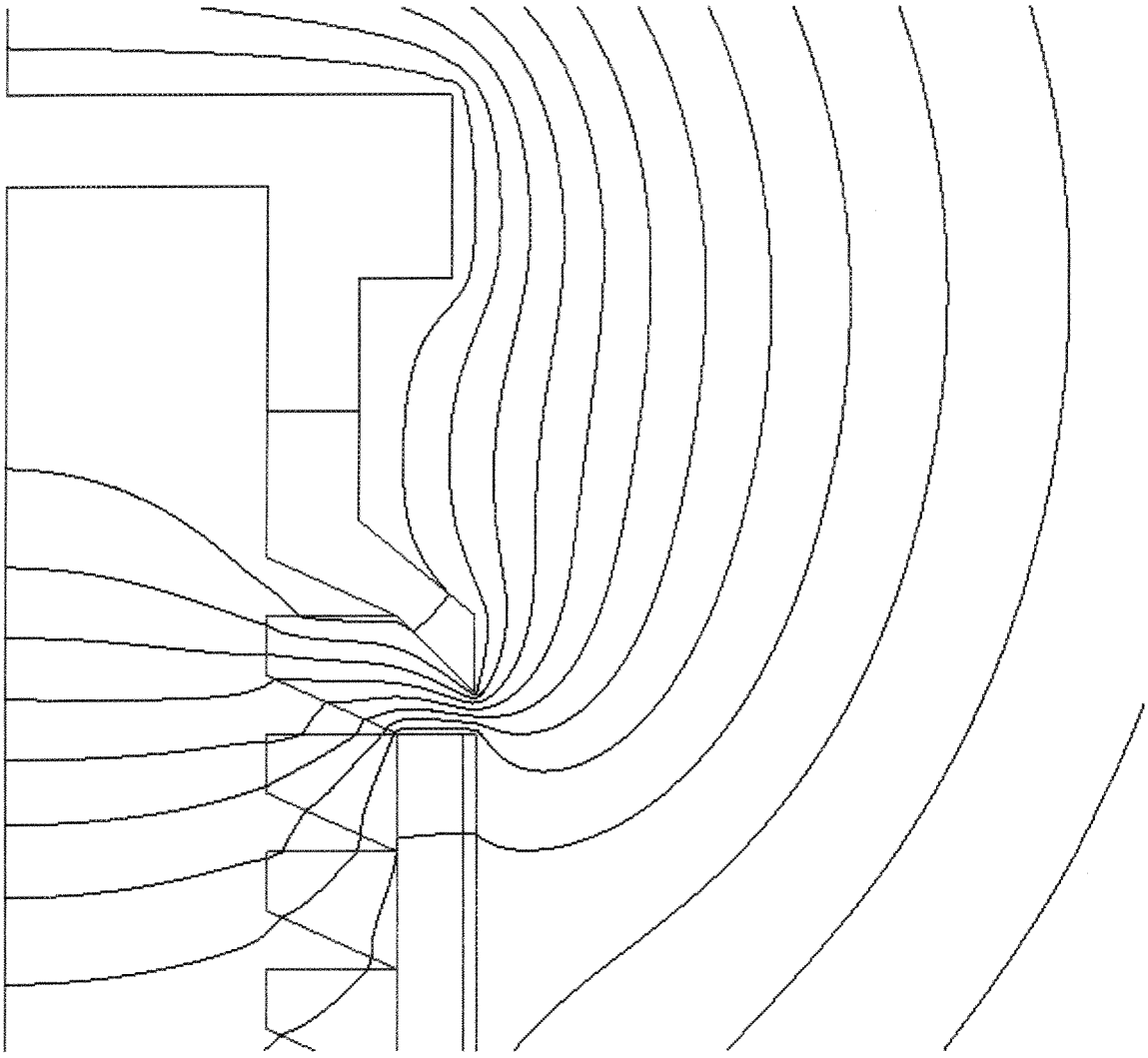

Figure 3.4: Voltage contours close to the HV electrode around an ice-covered insulator with a water film in presence of an icicle and an air gap computed by creating an artificial boundary around the insulator.

3.3.2 The Open Boundary Simulated by the Kelvin Transformation

In the Kelvin transformation, the region between the domain of interest and infinity is modeled simply by adding a circular boundary to the "interior" problem, a second mesh having a circular boundary with the same boundary node distribution as the inner region, and boundary constraints to force the equivalent boundary potentials on both regions to be identical. Infinity lies at the center of the second mesh. In effect, the second mesh represents the conformal transformation of all the space exterior to the first mesh into a circle [47, 48]. Using this idea, no deep knowledge of analysis is needed; very little extra computer time is necessary; and frequently fewer elements are required than for most other approximation methods to compute the potential and electric field distributions along the insulators under icing conditions.

The Kelvin transformation only transforms space and, strictly speaking, is not applicable to three-dimensional or rotationally symmetric geometries. It does not of itself in anyway transform the material properties. It is for this reason that an extra step in the derivation is necessary when dealing with non-two-dimensional translational systems. As a starting point, it is useful to consider the problem in network terms. Imagine a three-dimensional model based on a spherical geometry, with a defined centre. The main region of interest lies immediately around the centre and extends to a radius "a". Beyond that radius there exists only non-electric, non-conducting material. The network model is built up as a series of spherical shells. The outer region network could be rebuilt as a network within a sphere of radius "a". The successive radii within the new network are to be the transformed equivalent radii of the original outer network [47].

To complete the model, the extra step is to modify the impedances of the network so that the impedance seen looking into the new model from any pair of points, is identical to the impedance seen looking out from those same two points, in the original model. This change in impedance is achieved by applying a transformation to the material properties. This was first done by Ciric and Wong [49, 50]. Their approach was based on algebraic transformations, and they were able to effect great economy of effort in achieving solutions for a range of basic geometries. Later Freeman and Lowther [47] developed the technique to use an all enveloping sphere which can be applied to the solution of a general range of field problems using finite elements.

The transformation of the material properties is given by Ciric and Wong [49] as:

$$\varepsilon' = \varepsilon\left(\frac{r}{r'}\right), \tag{3.5}$$

$$r' = \frac{a^2}{r}, \tag{3.6}$$

where,

ε' is the permittivity at the transformed inner radius r',

ε is the permittivity at a radius, r.

Table 3.2 shows the relative permittivities of a series of spherical shells for the ice-covered insulator.

Table 3.2: Relative Permittivities of a series of spherical shells for the ice-covered insulator

Shell Number	Relative Permittivity
Exterior 1	1.28125
Exterior 2	2.17014
Exterior 3	4.51388
Exterior 4	15.6250
Exterior 5	500012.5

Figure 3.5 shows the insulator model for the computation of the potential distribution by simulating an open boundary by a form of Kelvin transformation.

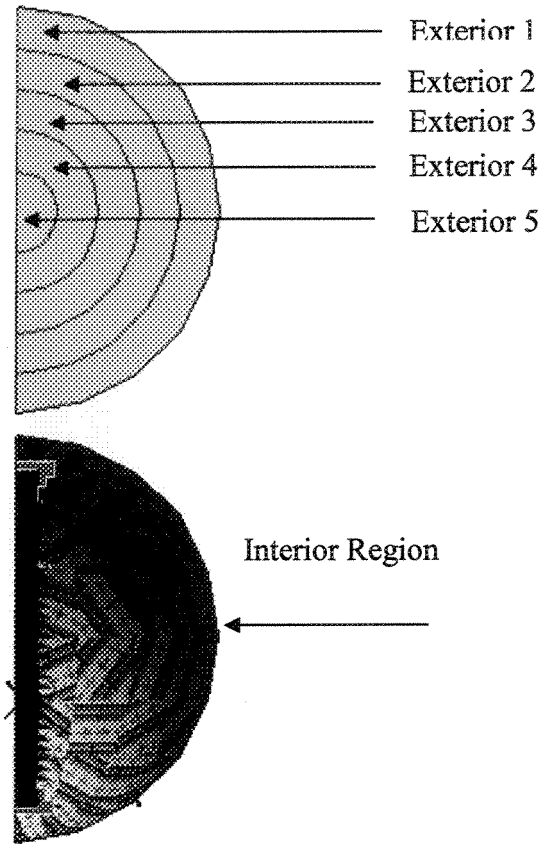

Figure 3.5: Insulator model for the computation of potential distribution using the Kelvin transformation.

Figure 3.6 shows the solution mesh for the computation of potential distribution by simulating an open boundary by the Kelvin transformation.

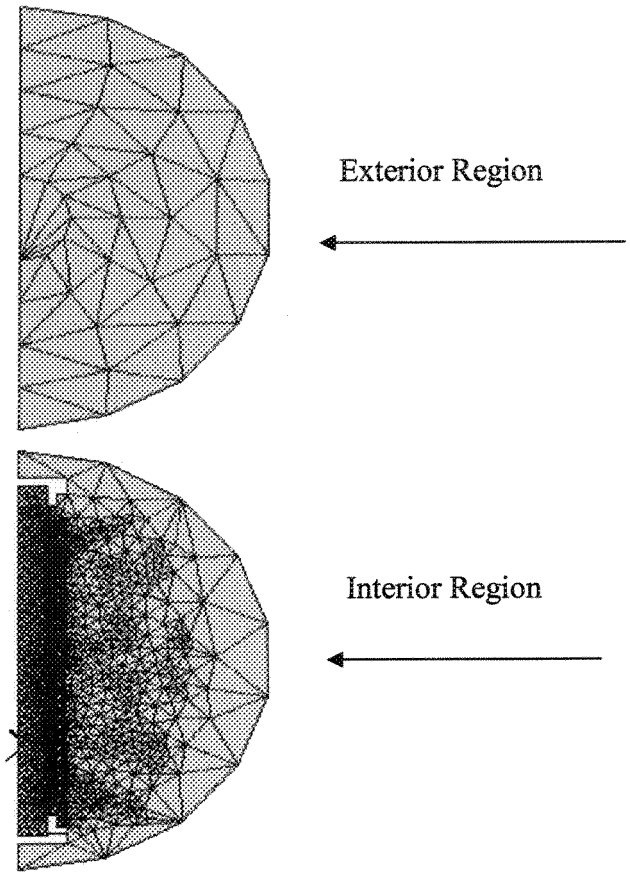

Figure 3.6: Solution mesh for the computation of electric field distribution using the Kelvin transformation.

Figure 3.7 and Figure 3.8 show voltage contours around an ice-covered insulator with a water film in the presence of an icicle and an air gap computed with an open boundary around the insulator simulated by the Kelvin transformation.

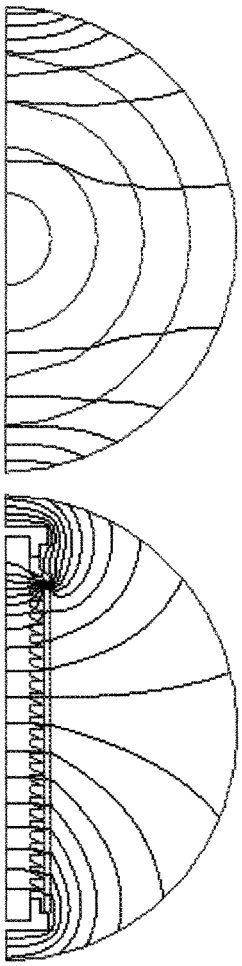

Figure 3.7: Voltage contours around an ice-covered insulator with a water film in presence of an icicle and an air gap computed with open boundary simulated by the Kelvin transformation.

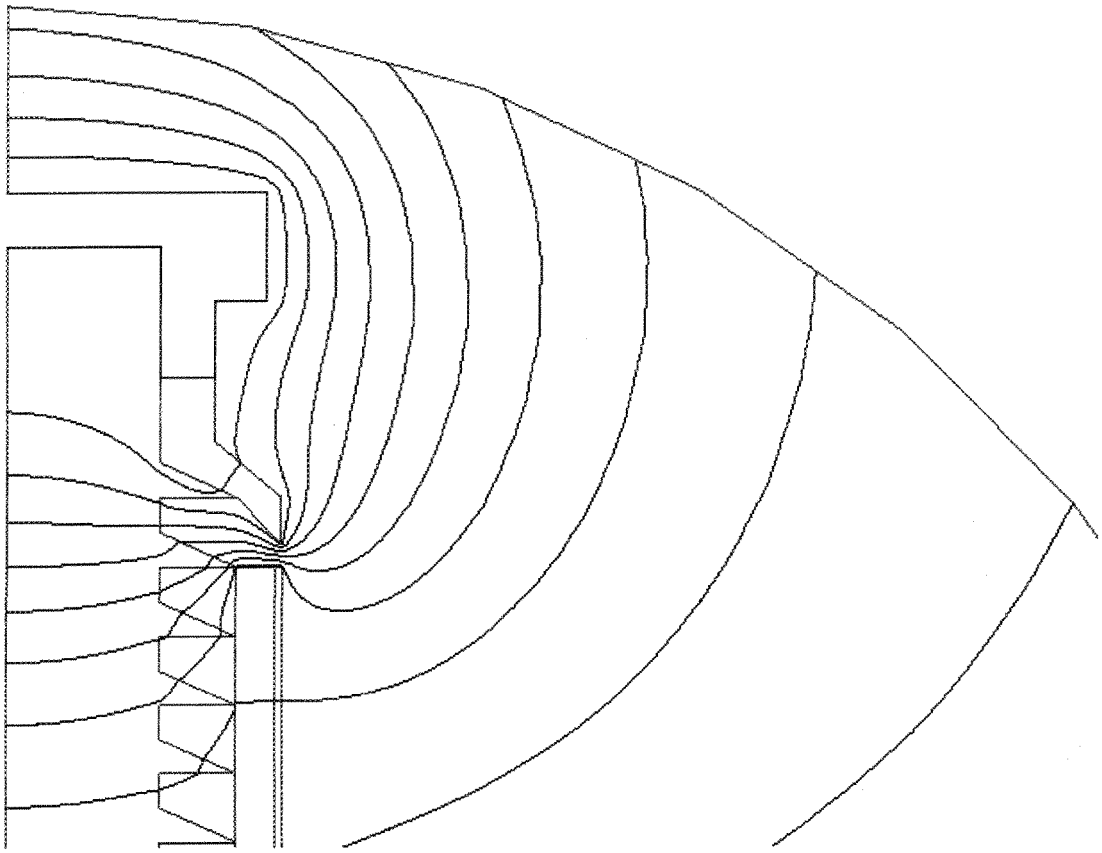

Figure 3.8: Voltage contours close to the HV electrode around an ice-covered insulator with a water film in presence of an icicle and an air gap computed with open boundary simulated by the Kelvin transformation.

3.4 Results and Discussion

Using an artificial boundary, the time taken for the computation of the potential distribution for a normal glazed ice-covered insulator using a Pentium 4 and 1.8GHz computer was 22 min 52 seconds.

For the Kelvin transformation, an air-box of radius 1.1 times the device radius is constructed to contain the model. Another circle with same radius represents the exterior region between the air-box and infinity. The time taken using a Pentium 4 and 1.8GHz computer for the computation of potential distribution using the Kelvin transformation was 8 minutes 38 seconds.

Figure 3.9 shows the comparison of the potential distributions computed using both the approximations and it is seen that the results are in agreement but the computation time is much less using the Kelvin transformation than that for an artificial boundary. The computation time is more important when the effects of a very thin semi-conducting glaze coating on the insulator for the potential and electric field distributions are studied. In some of these cases, the computation time is more than 100 hours using a Kelvin transformation.

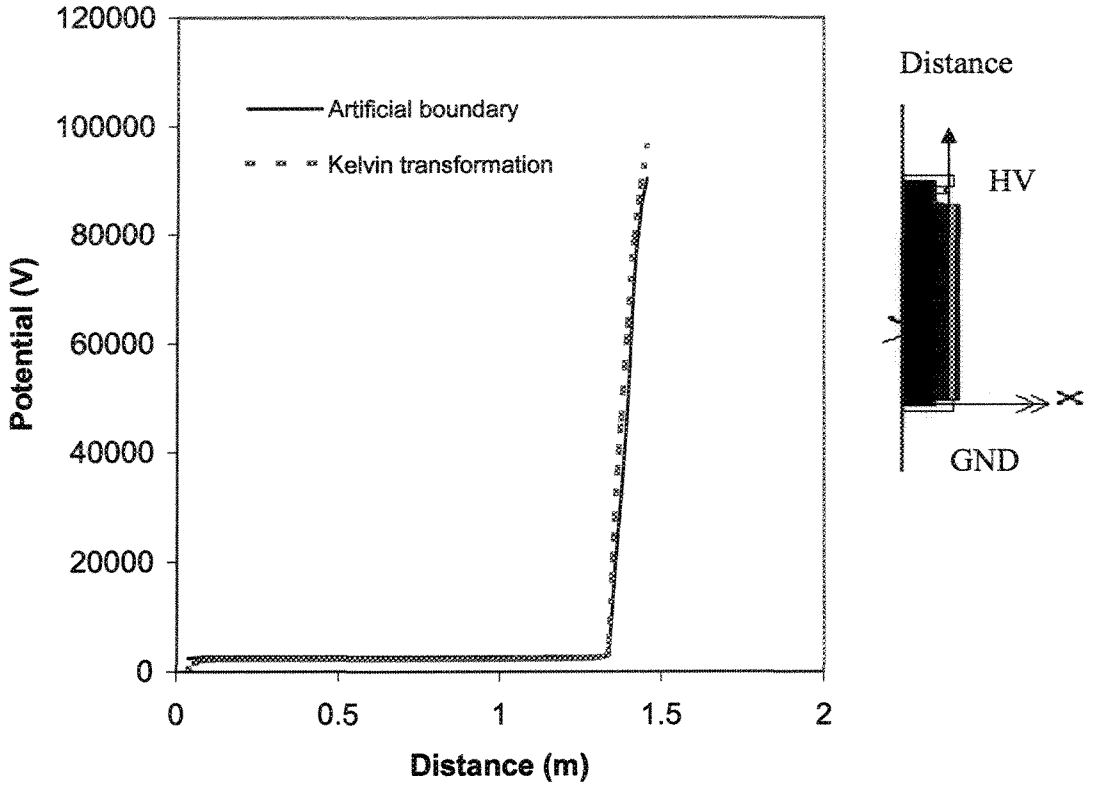

Figure 3.9: Comparison of the potential distributions along an ice-covered insulator in presence of an air gap and a water film on the surface, computed using an artificial boundary and an open boundary simulated by the Kelvin transformation.

The next chapter presents the proposed method for the computation of the electric field strengths at the four critical points in the radially outward direction from the axis of ice-free and ice-covered semi-conducting glazed insulators using the Finite Element Method under the lightning impulse and switching impulse voltages, and flashover performances of the insulators based on the electric field distributions.

CHAPTER 4

FLASHOVER PERFORMANCE OF AN INSULATOR BASED ON THE ELECTRIC FIELD DISTRIBUTION FOR TRANSIENT VOLTAGES

4.1 Overview

The ice accretion on the surface of an insulator is asymmetric, but insulators, in general, are axi-symmetric. Therefore, the field distribution around the insulator is really three-dimensional. The development of an ice-covered insulator flashover model, which can take into account the real experimental conditions, is little bit difficult, due to the complexity of the involved phenomena. Such complexity is the result of the non-uniformity of the ice deposits, the surrounding air temperature, the freezing water conductivity, the type of ice formed, the icing process, partial arcs, and the presence of space charge during the dry ice accretion. In order to develop such a model, many assumptions have been made, including the absence of space charge and partial arcs. In the semi-conducting glazed insulator, space charge does not have a major effect on the flashover voltage because of a flow of the continuous leakage current in the glaze, hence in this work the effects of space charge are neglected.

4.2 Ice Geometries

Computations are carried out for the two ice geometries described below:

4.2.1 The First Ice Geometry

In this case, there are two air-gaps formed along the insulator. The first air-gap appears near the HV electrode and the second near the grounded electrode. Figure 4.1 and Figure 4.2 show the ice geometry close to the HV electrode and the grounded electrode, respectively. The thicknesses of ice layer and the water film were 25.0 mm and 3.0 mm, respectively.

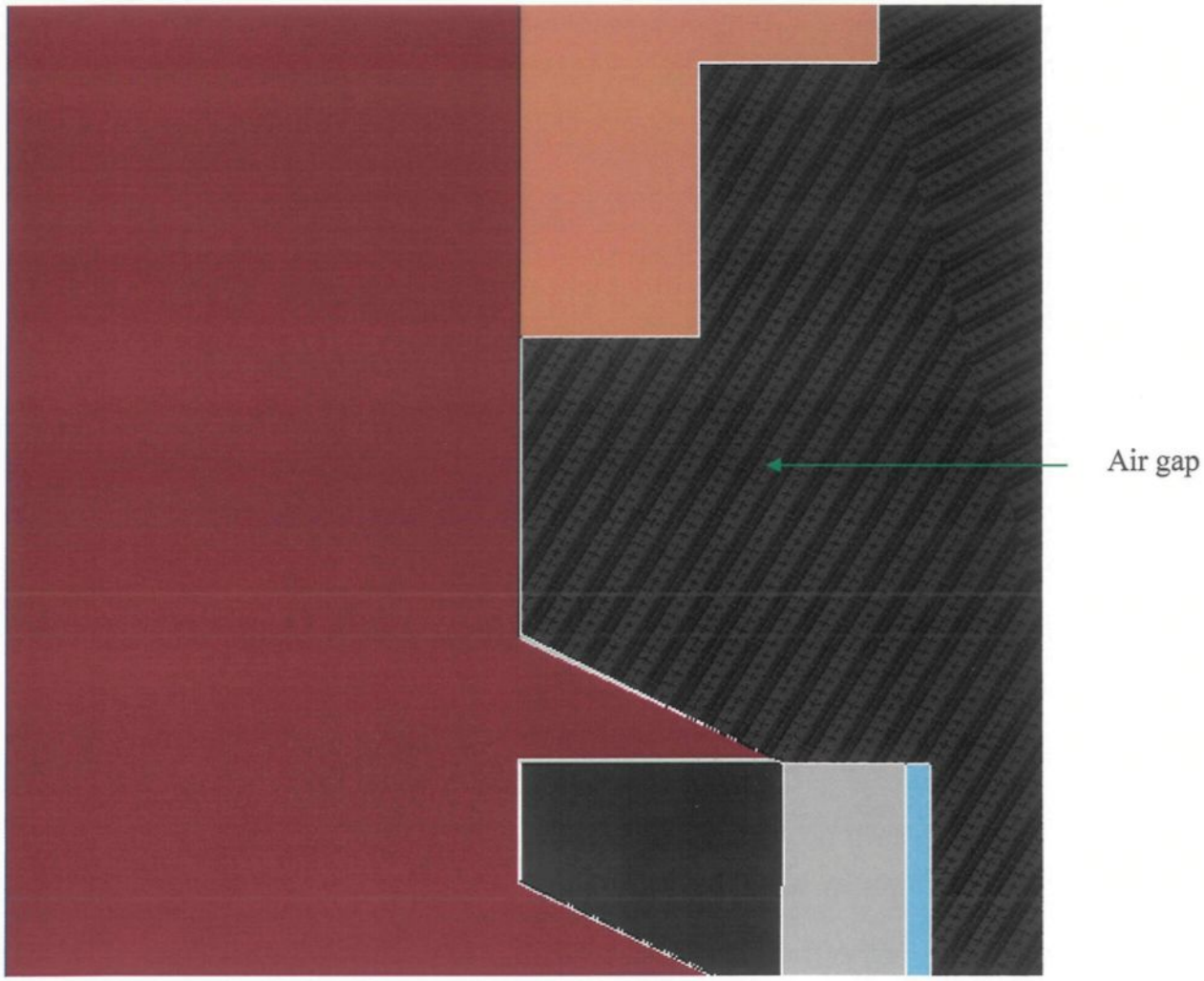

Figure 4.1: First ice geometry near the HV electrode.

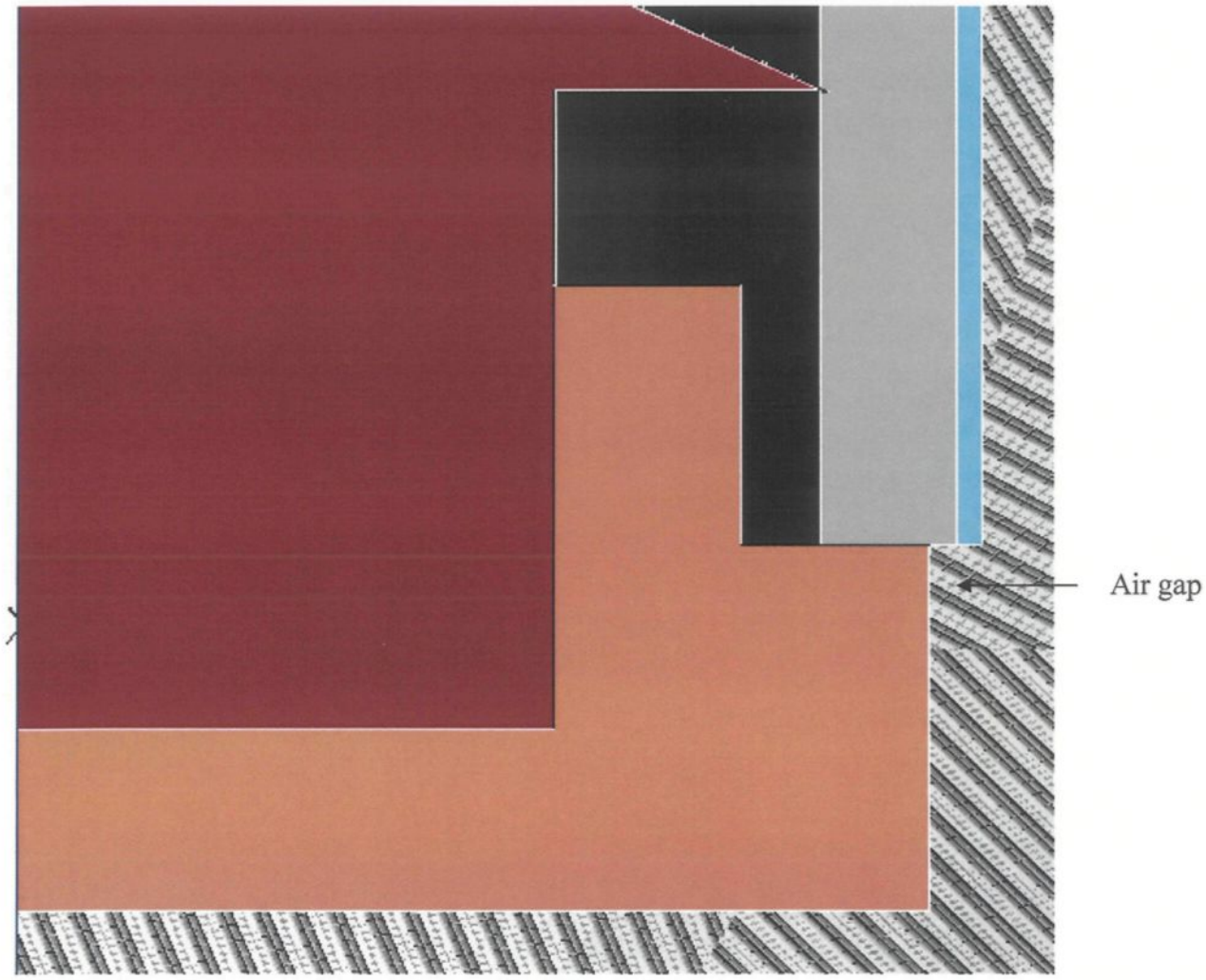

Figure 4.2: First ice geometry near the grounded electrode.

4.2.2 The Second Ice Geometry

In this ice geometry, there is only one air-gap formed near the HV electrode. This was the basis for a second set of simulations. The thicknesses of ice layer and the water film were 15.0 mm and 2.0 mm, respectively.

Figure 4.3 and Figure 4.4 show the ice geometry close to the HV electrode and the grounded electrode, respectively.

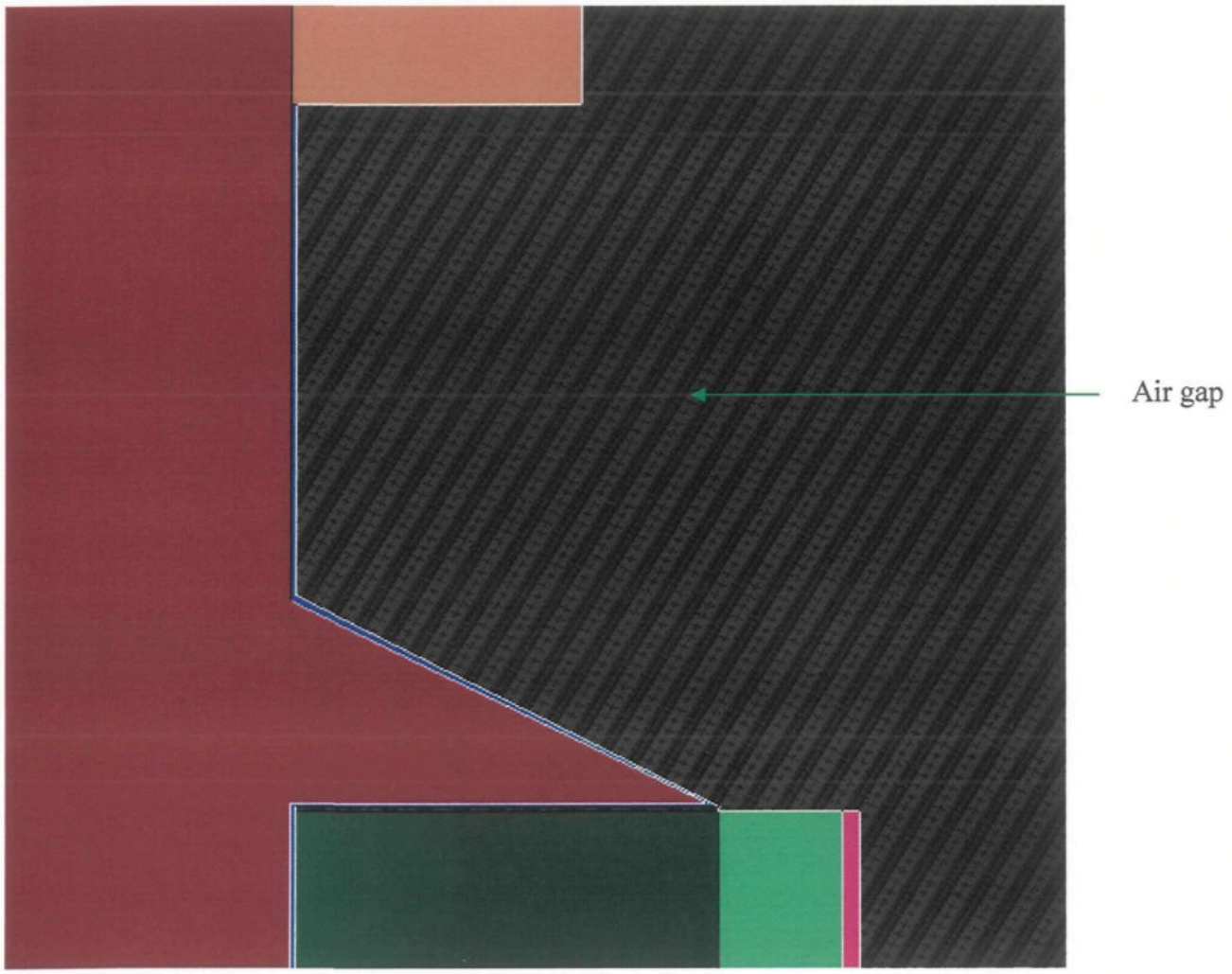

Figure 4.3: Second ice geometry near the HV electrode.

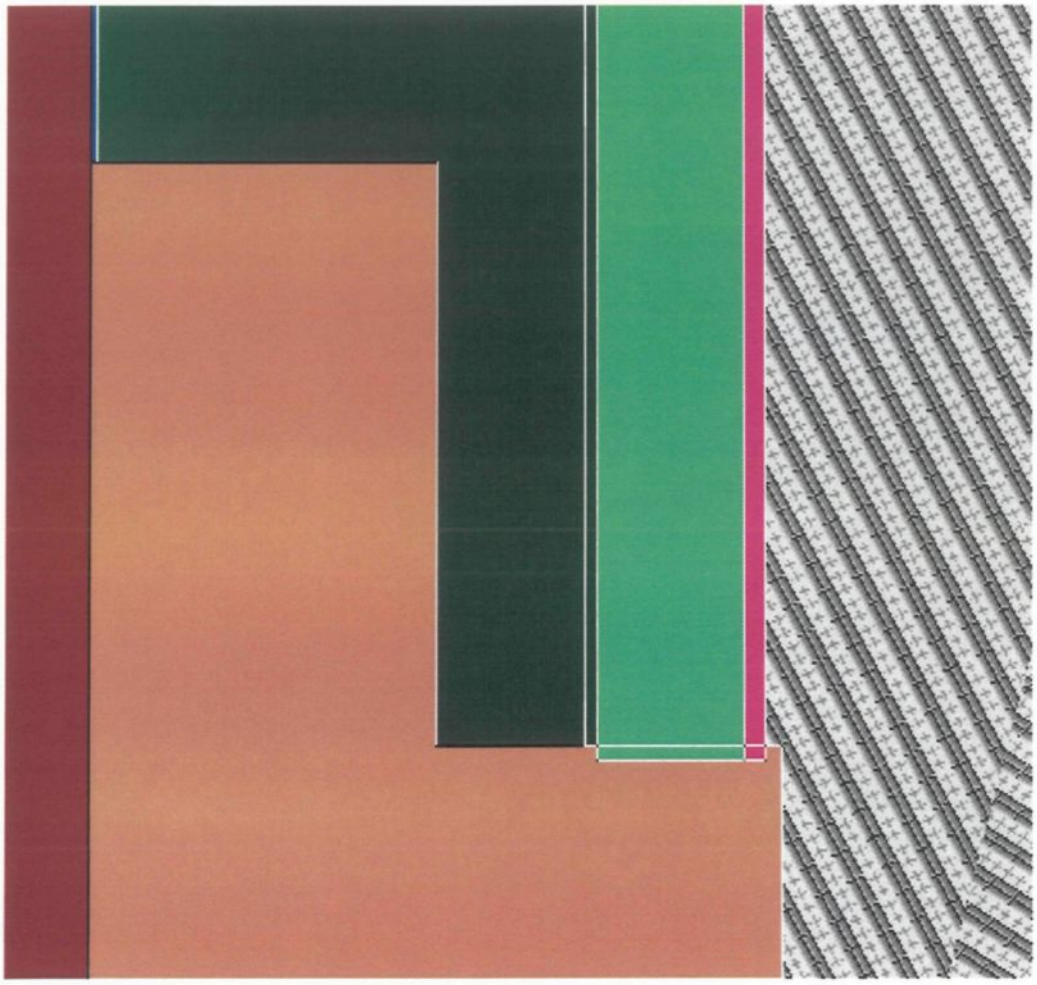

Figure 4.4: Second ice geometry near the grounded electrode.

4.3 Simulation Parameters

Table 4.1 and Table 4.2 show the simulation parameters for the first and second ice geometries, respectively.

Table 4.1: Simulation parameters for the first ice geometry

	Porcelain	Semi-conducting Glaze	Ice-layer	Water film
Relative Permittivity (ε_r)	6.0	16	75.0 for 60 Hz (variable)	81.0 (variable)
Conductivity (S/m)	0	0-2.20 (variable)	0	0.030
Thickness (mm)	-	0.5-5.0 (variable)	25.0	3.0

Table 4.2: Simulation parameters for the second ice geometry

	Porcelain	Semi-conducting Glaze	Ice-layer	Water film
Relative Permittivity (ε_r)	6.0	16	75.0 for 60 Hz (variable)	81.0 (variable)
Conductivity (S/m)	0	2.20×10^{-7} - 0.022 (variable)	0	0.015
Thickness (mm)	-	0.5	15.0	2.0

4.4 Computation of the Transient Electric Field Strengths

Electric field strengths as a function of time under the transient conditions were computed at the four critical points near the HV electrode in the radially outward direction from the axis of the insulator. These points were considered because the electric field strength was very high near the HV electrode. Figure 4.5 shows a critical point. The coordinates of the four critical points are (0.15, 1.35), (0.16, 1.35), (0.17, 1.35), and (0.20, 1.35) meters, respectively.

There are two types of the transient voltages studied in this work,

1. The lightning impulse voltage,
2. The switching impulse voltage.

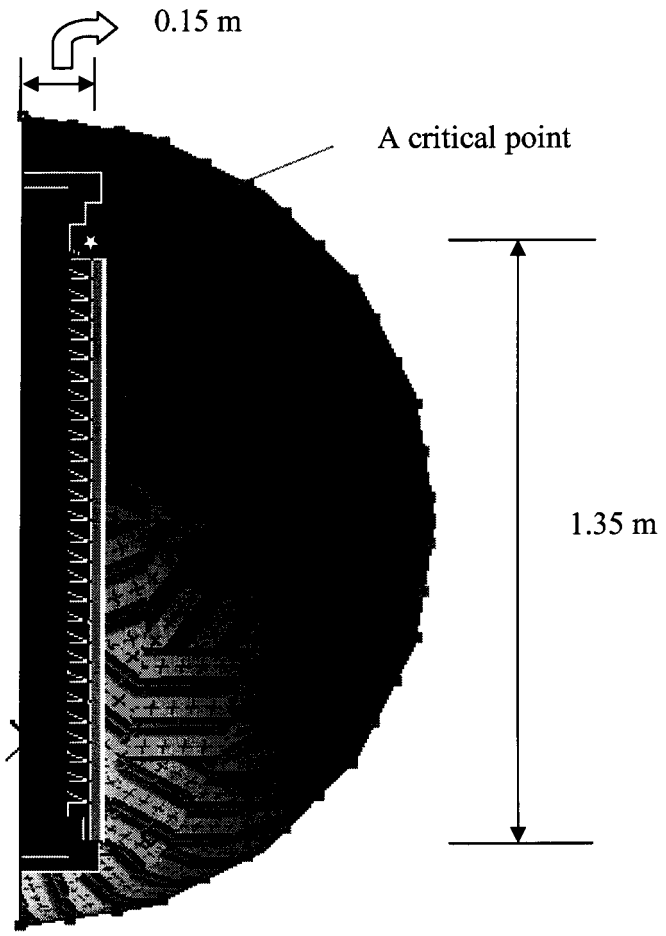

Figure 4.5: A critical point for the computation of the electric field strengths under the transient voltages.

Figure 4.6 shows the standard lightning impulse waveform (1.2/50 μs) applied on the HV electrode for the computation of the transient electric field strengths.

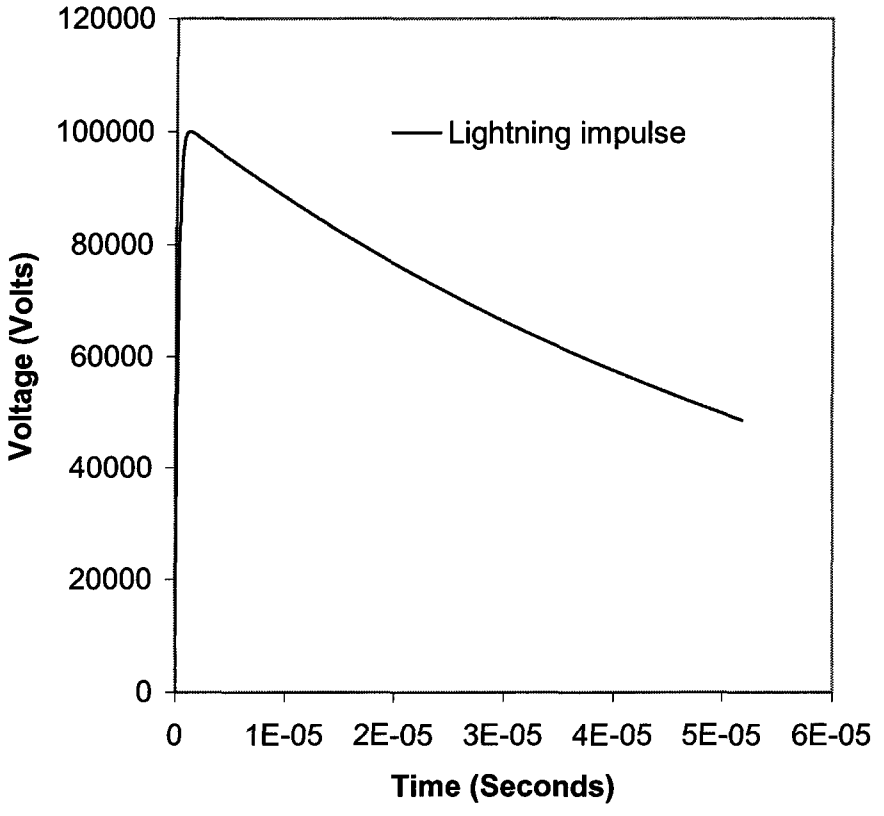

Figure 4.6: The lightning impulse waveform applied on the HV electrode.

The standard switching impulse waveform (250/2500 μs) is shown in Figure 4.7.

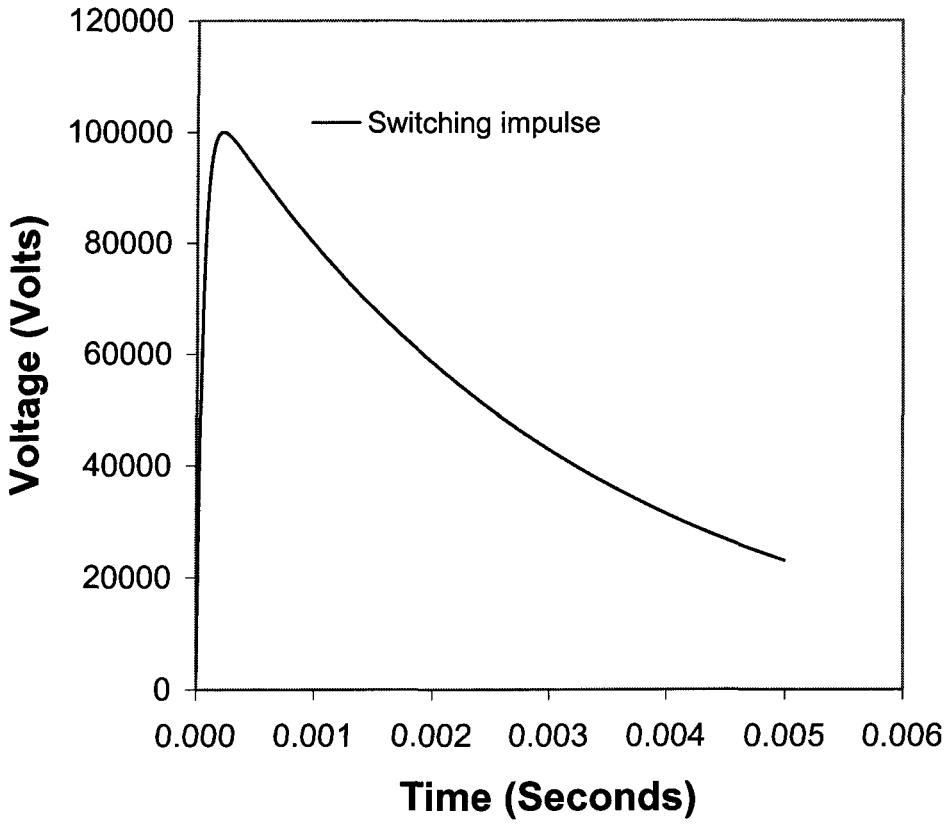

Figure 4.7: The switching impulse waveform applied on the HV electrode.

4.4.1 Using the First Ice Geometry

A semi-conducting glaze of thickness 0.5 mm and of conductivity 0.022 S/m is considered for the first ice-geometry.

Figure 4.8 and Figure 4.9 show the electric field strengths at the first critical point (0.15, 1.35) for a clean i.e. ice-free and a wet ice-covered insulator under a lightning and a switching impulse voltage, respectively.

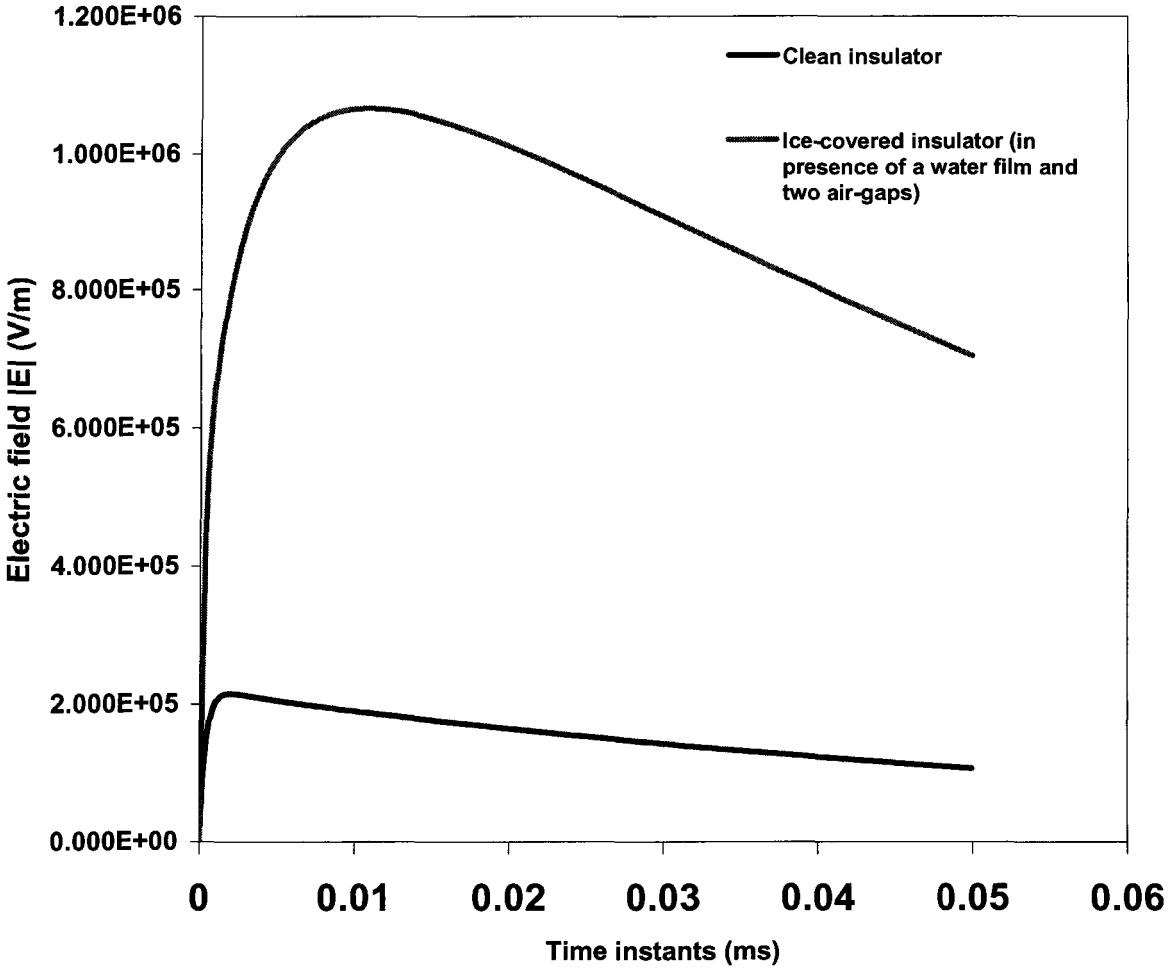

Figure 4.8: Electric field strengths at the first critical point for a clean and a wet ice-covered insulator for a lightning impulse voltage.

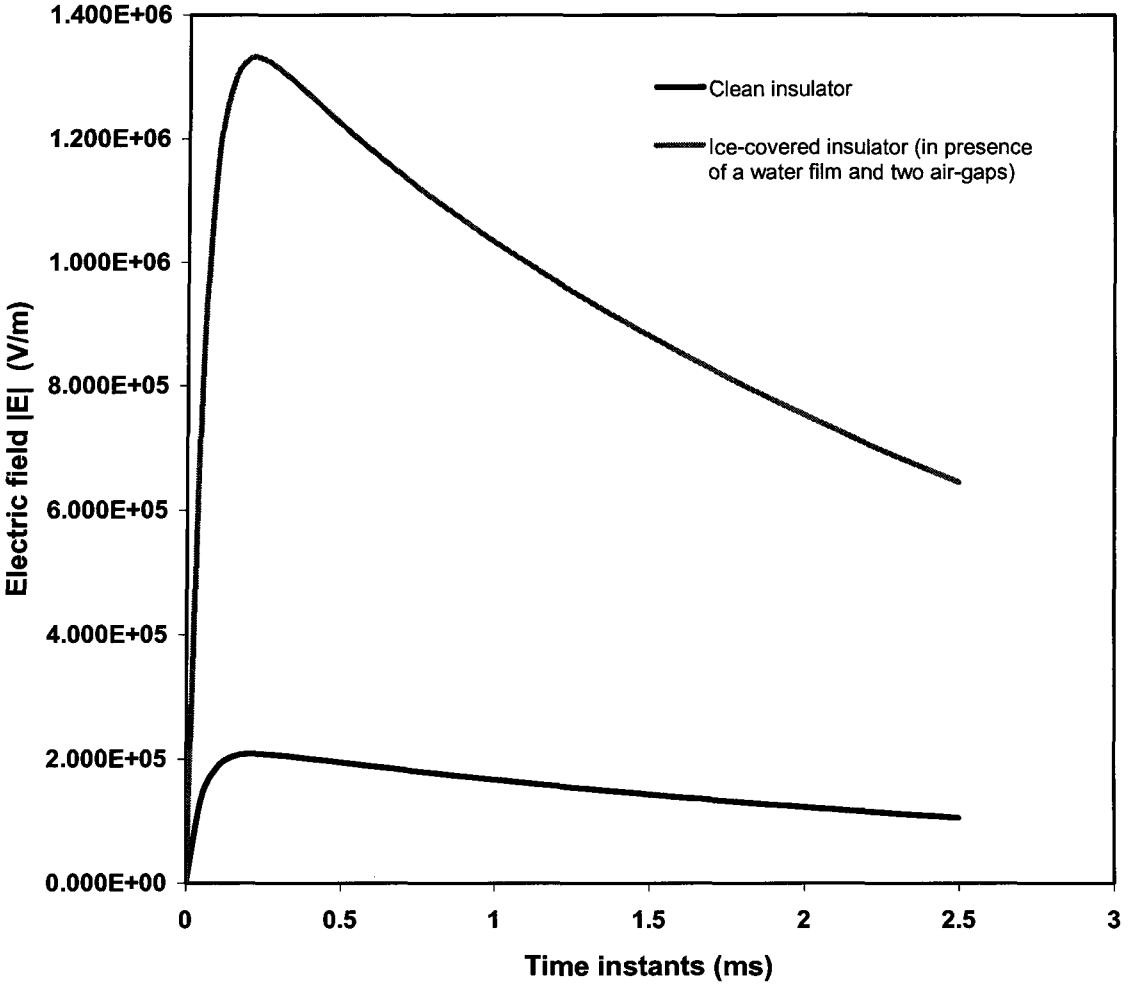

Figure 4.9: Electric field strengths at the first critical point for a clean and a wet ice-covered insulator for a switching impulse voltage.

Figure 4.10 shows the comparison of the electric field strengths at the first critical point (0.15, 1.35) of a clean semi-conducting glazed insulator. It is observed that the electric field strength is higher for a lightning impulse voltage than that for a switching impulse voltage.

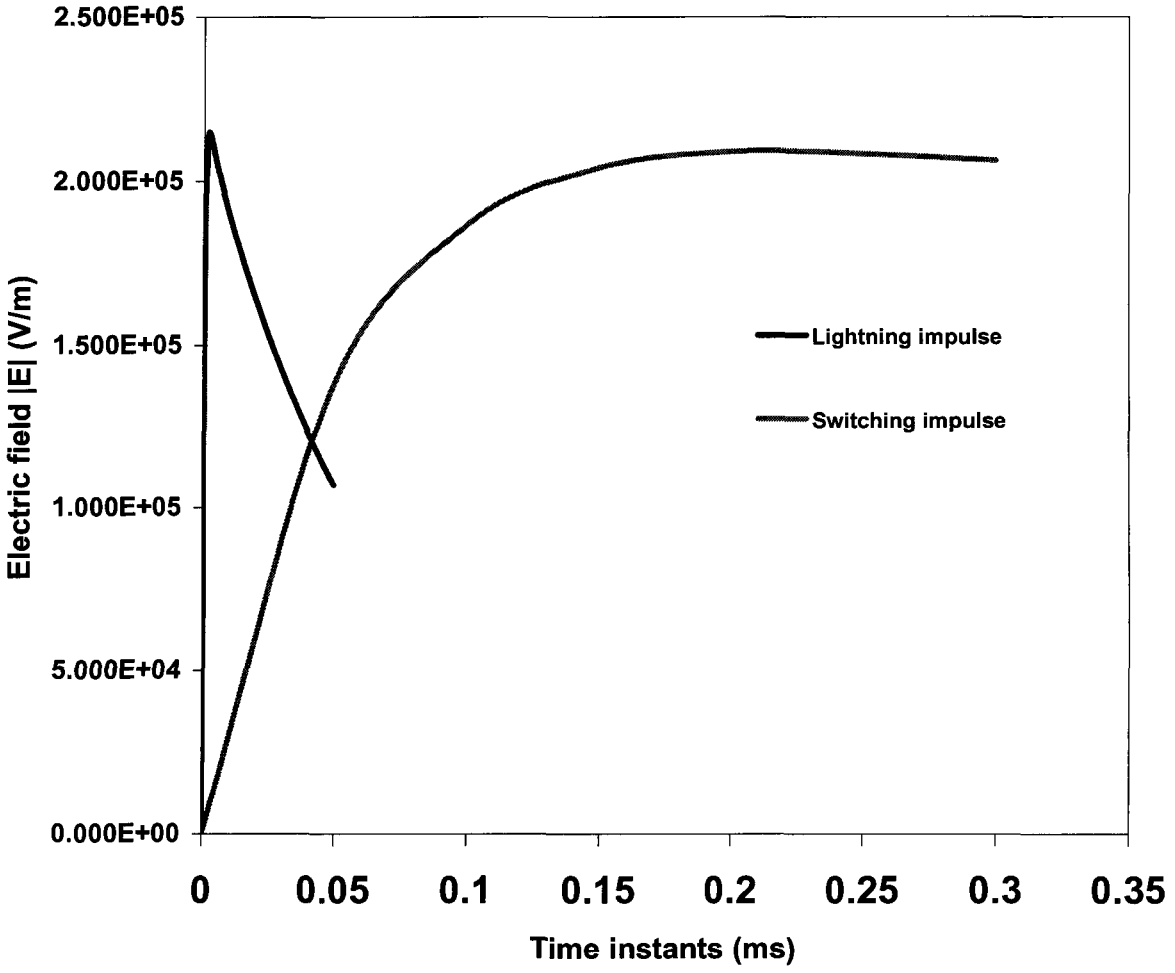

Figure 4.10: Electric field strengths at the first critical point near the HV electrode of a clean semi-conducting glazed insulator for the lightning and switching impulse voltages.

Figure 4.11 shows the comparison of the maximum electric field strengths at the three critical points in the radially outward direction near the HV electrode of a clean semi-conducting glazed insulator for the lightning and switching impulse voltages. It is observed that the maximum electric field strength is higher for a lightning impulse voltage than that for a switching impulse voltage.

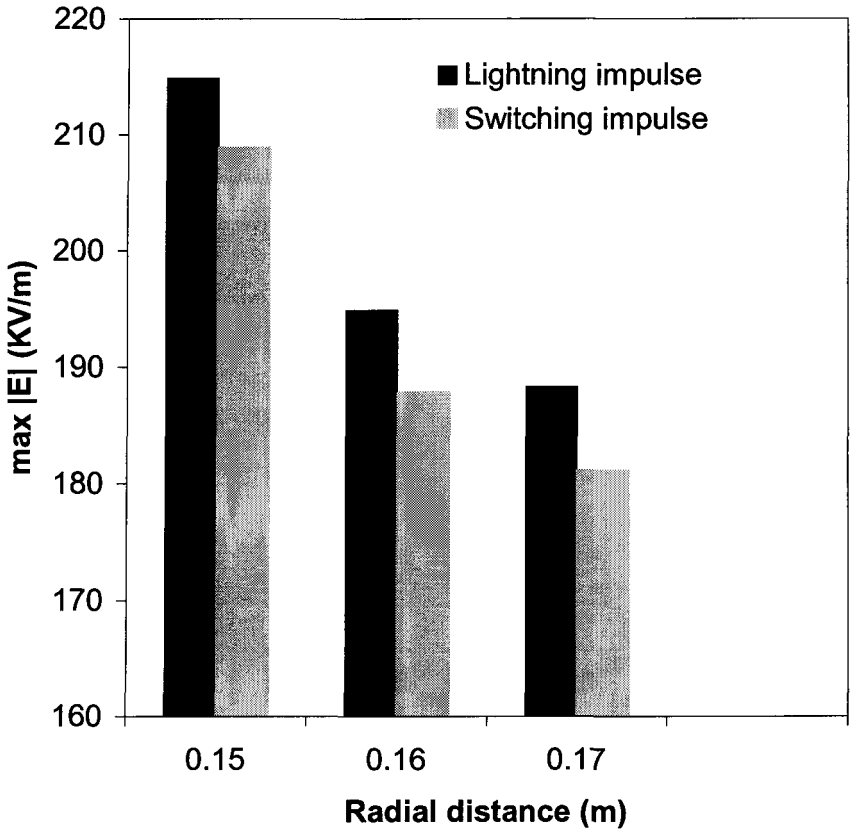

Figure 4.11: Maximum electric field strengths for the lightning and switching impulse voltages near the HV electrode of a clean semi-conducting glazed insulator.

Figure 4.12 shows the comparison of the electric field strengths at the first critical point (0.15, 1.35) of a wet ice-covered semi-conducting glazed insulator. It is observed that the electric field strength is higher for a switching impulse voltage than that for a lightning impulse voltage.

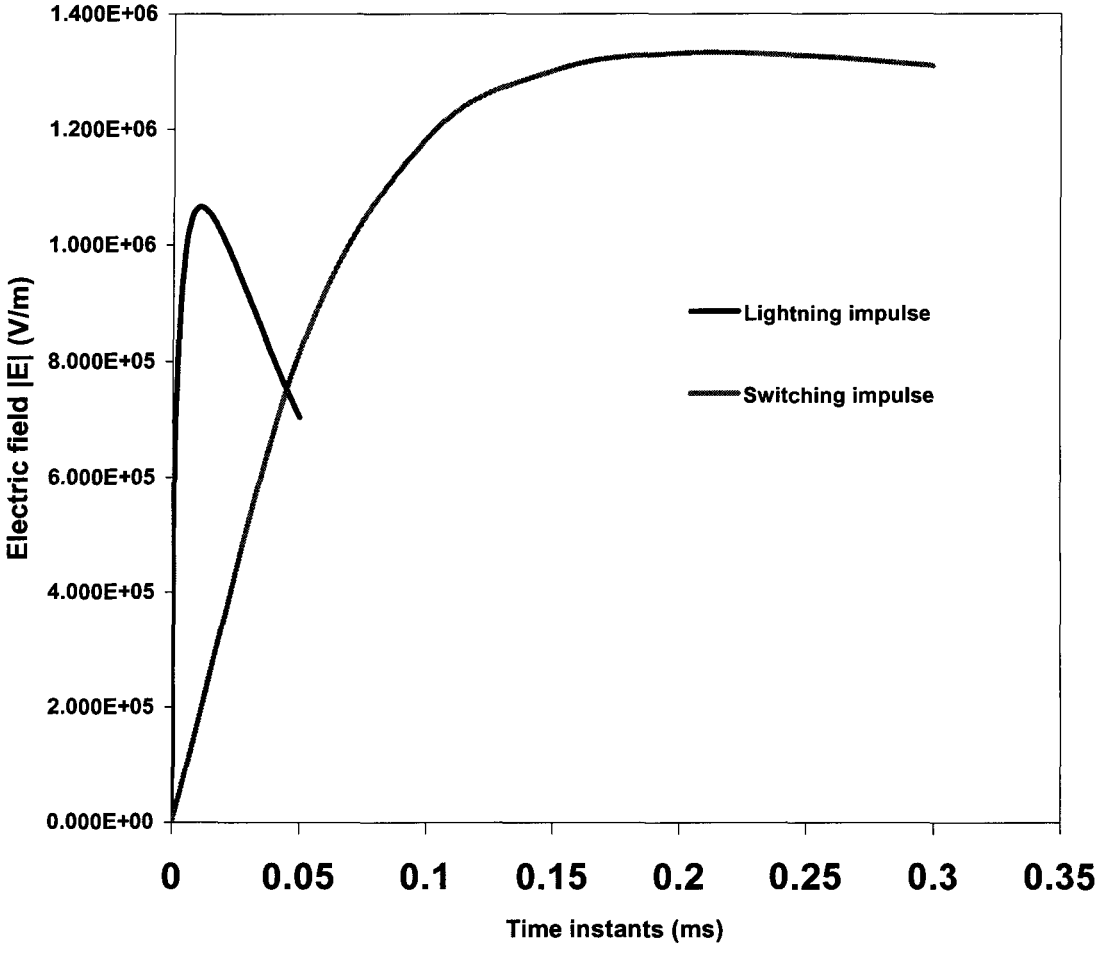

Figure 4.12: Electric field strengths for the lightning and switching impulse voltages at the first critical point near the HV electrode of a wet ice-covered semi-conducting glazed insulator in the presence of a water film and two air-gaps.

Figure 4.13 shows the comparison of the maximum electric field strengths at the three critical points in the radially outward direction near the HV electrode of a wet ice-covered semi-conducting glazed insulator. It is observed that the maximum electric field strength is higher for a switching impulse than that for a lightning impulse voltage.

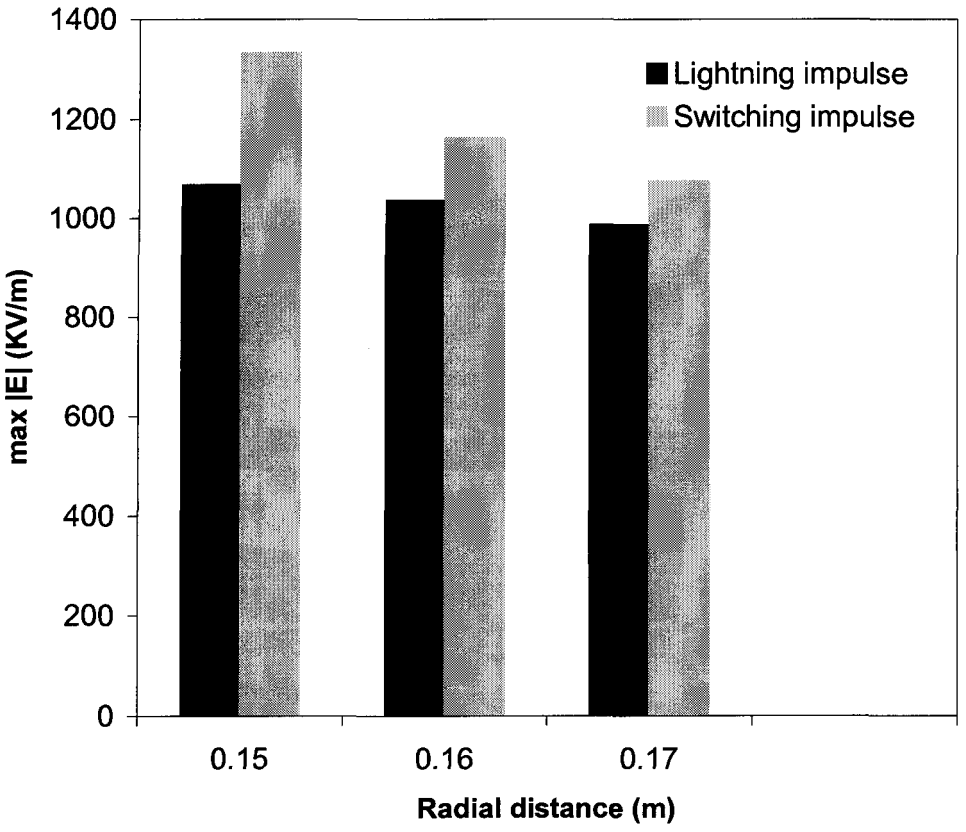

Figure 4.13: The maximum electric field strengths for the lightning and switching impulse voltages near the HV electrode of a wet ice-covered semi-conducting glazed insulator in the presence of a water film and two air-gaps.

4.4.2 Using the Second Ice Geometry

Computations have been done for the two types of the semi-conducting glaze (thickness 0.5 mm) with different conductivities.

4.4.2.1 The First Semi-conducting Glaze

The conductivity of the first semi-conducting glaze is 2.20×10^{-7} S/m.

Figure 4.14 and Figure 4.15 show the electric field strengths at the first critical point (0.15, 1.35) for a clean and a wet ice-covered insulator under the lightning and switching impulse voltages, respectively.

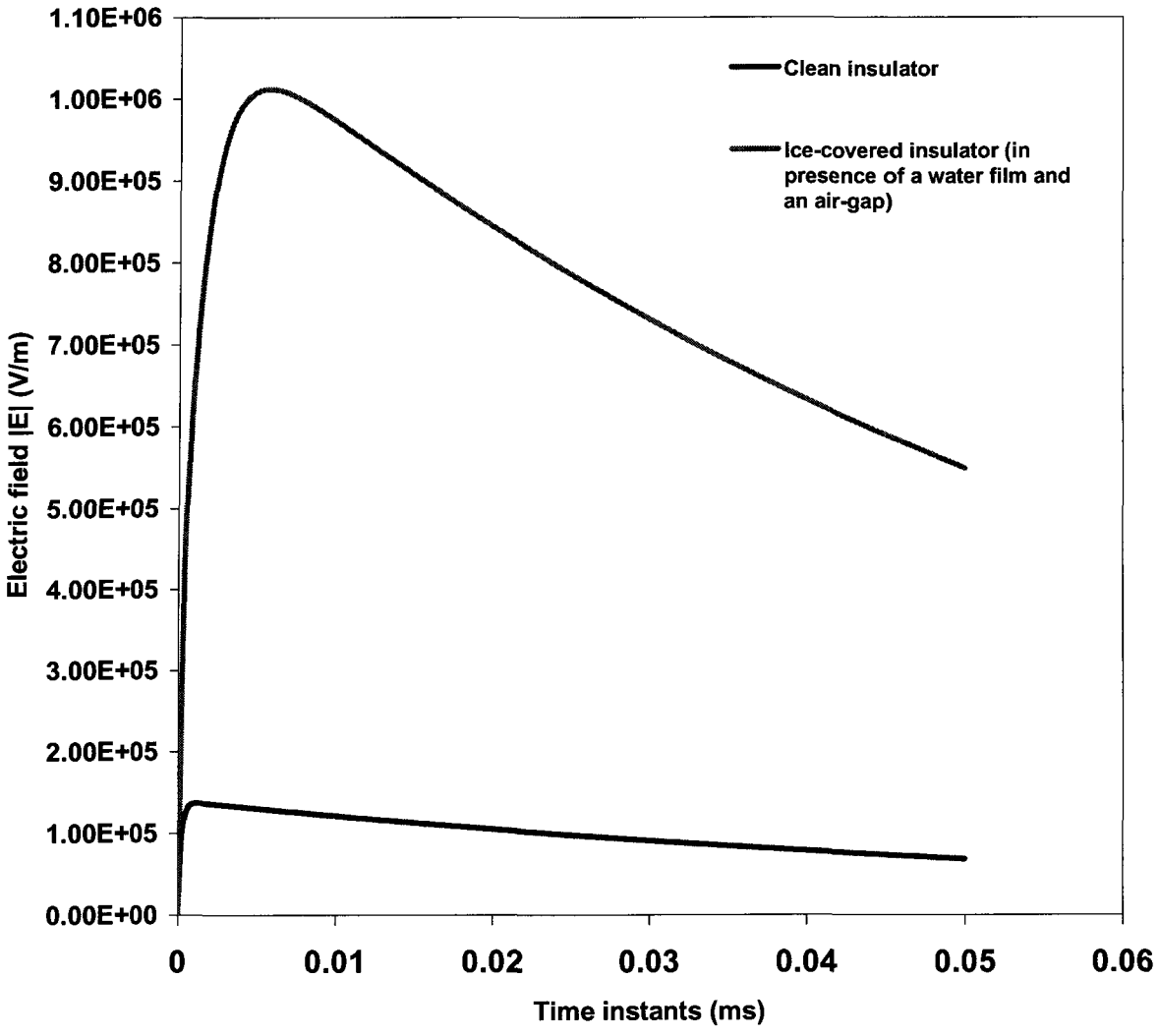

Figure 4.14: Electric field strengths at the first critical point for a clean and a wet ice-covered insulator for a lightning impulse voltage using the second ice geometry.

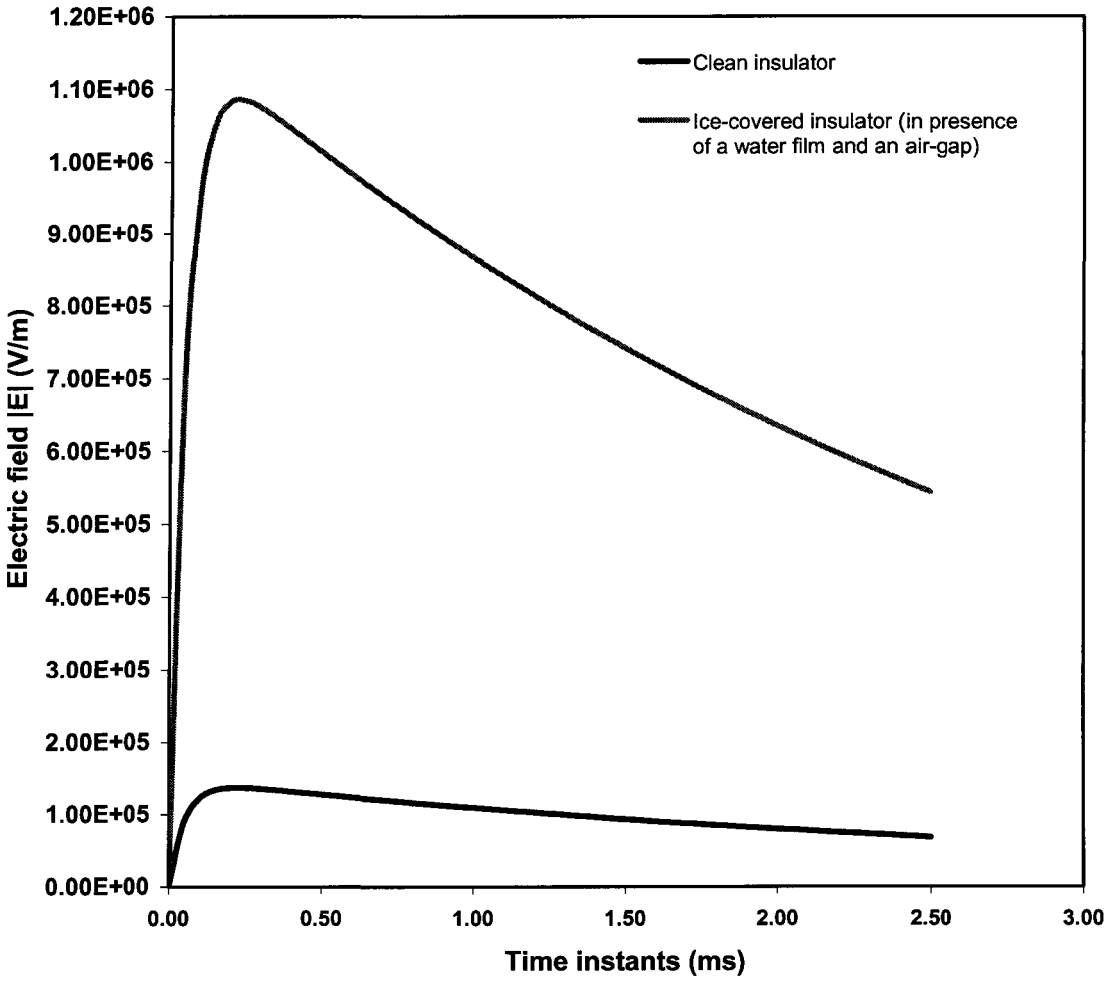

Figure 4.15: Electric field strengths at the first critical point for a clean and a wet ice-covered insulator for a switching impulse voltage using the second ice geometry.

Figure 4.16 shows the comparison of the electric field strengths for the lightning and the switching impulse voltages at the first critical point (0.15, 1.35) near the HV electrode of a clean semi-conducting glazed (conductivity 2.20×10^{-7} S/m) insulator.

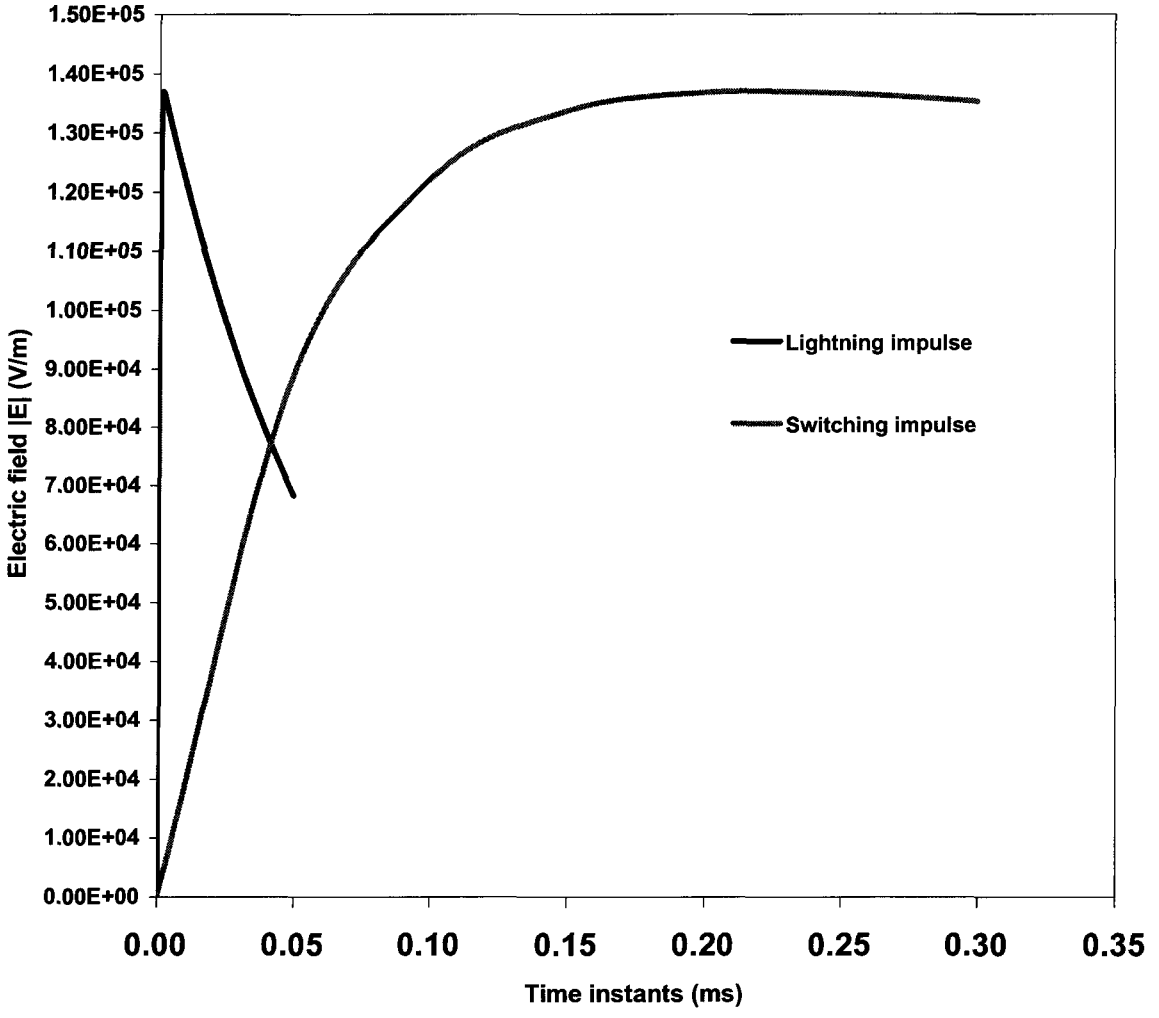

Figure 4.16: Electric field strengths at the first critical point near the HV electrode of a clean semi-conducting glazed insulator for the lightning and switching impulse voltages.

Figure 4.17 shows the comparison of the maximum electric field strengths at the two critical points near the HV electrode in the radially outward direction from the axis of a clean semi-conducting glazed (conductivity 2.20×10^{-7} S/m) insulator. It is observed that the electric field strength is higher for a lightning impulse than that for a switching impulse voltage.

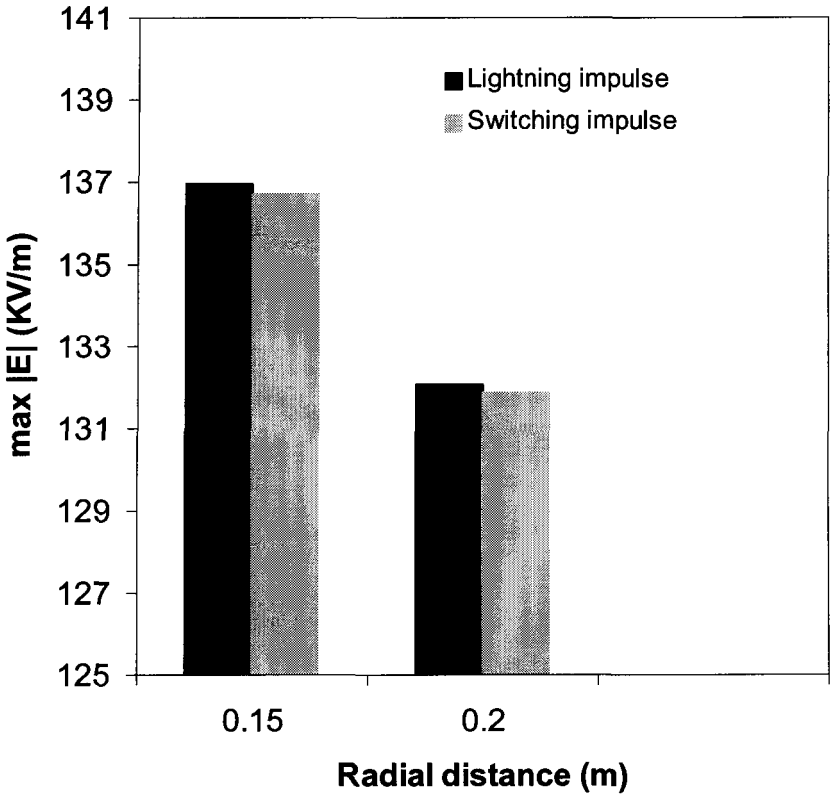

Figure 4.17: The maximum electric field strengths for the lightning and switching impulse voltages near the HV electrode of a clean semi-conducting glazed insulator.

Figure 4.18 shows the comparison of the electric field strengths at the first critical point (0.15, 1.35) of a wet ice-covered semi-conducting glazed insulator.

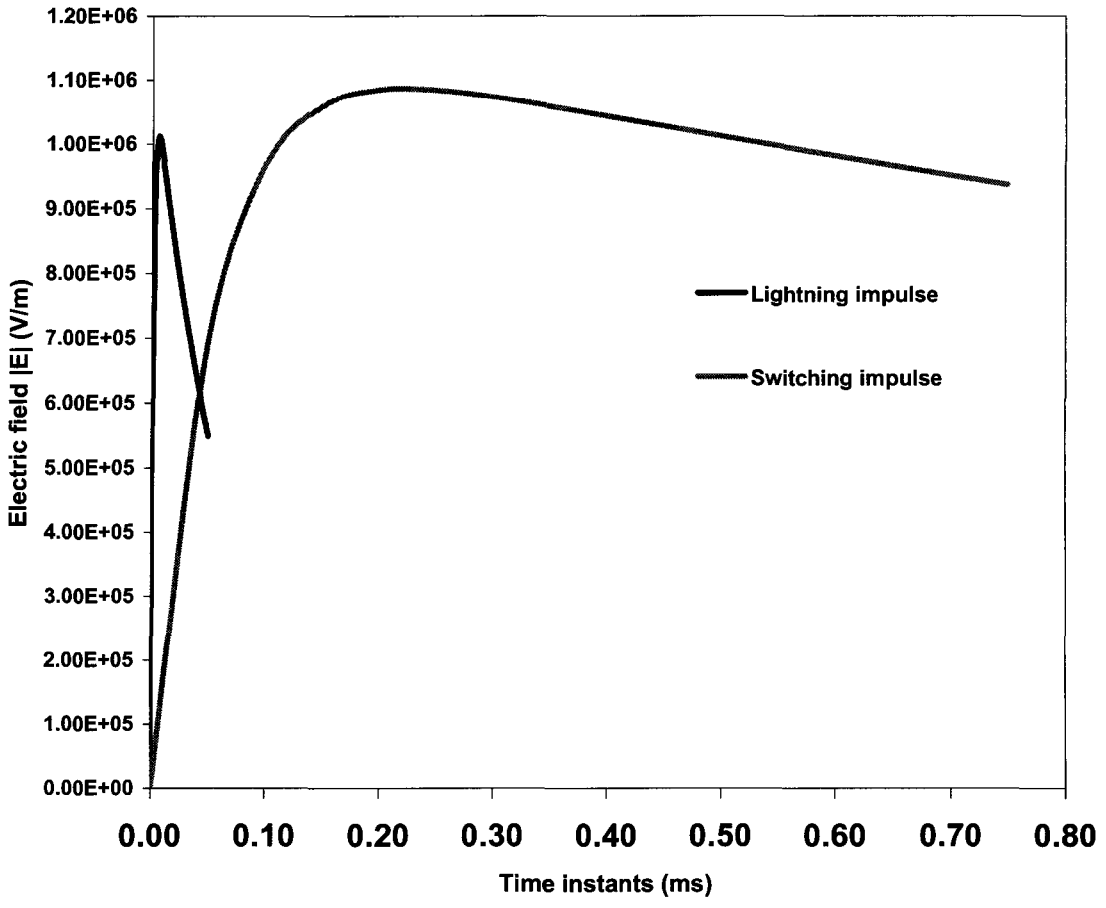

Figure 4.18: Electric field strengths for the lightning and switching impulse voltages at the first critical point near the HV electrode of a wet ice-covered semi-conducting glazed insulator in the presence of a water film and an air-gap.

Figure 4.19 shows the comparison of the maximum electric field strengths at the two critical points of a wet ice-covered semi-conducting glazed insulator. It is observed that the maximum electric field strength for a switching impulse is higher than that for a lightning impulse voltage.

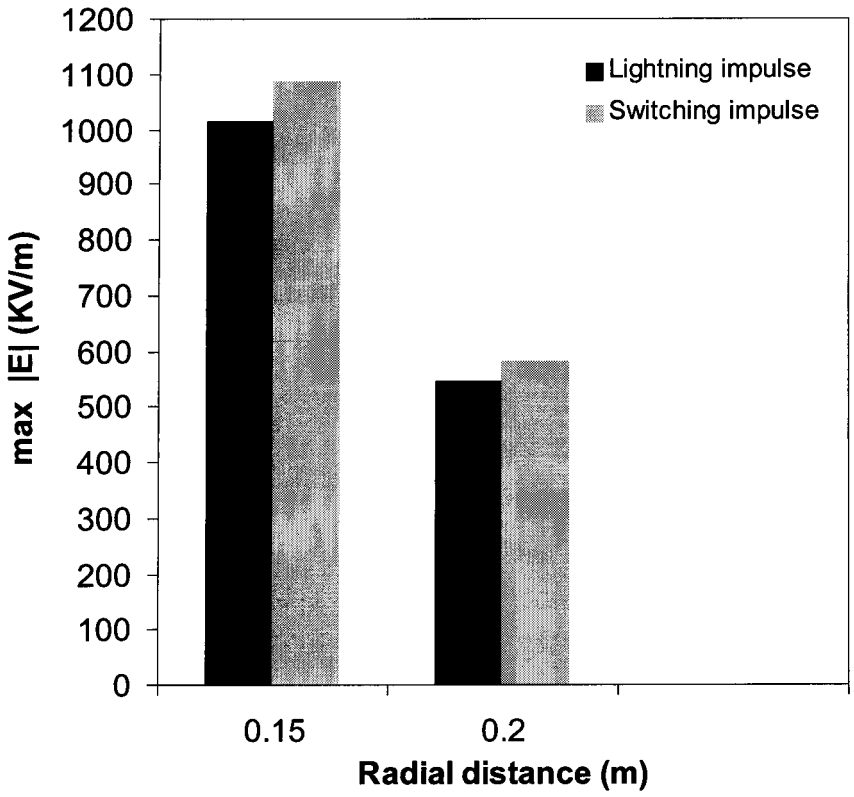

Figure 4.19: The maximum electric field strengths for the lightning and switching impulse voltages near the HV electrode of a wet ice-covered semi-conducting glazed insulator in the presence of a water film and an air-gap.

4.4.2.2 The Second Semi-conducting Glaze

The conductivity of the second semi-conducting glaze is 0.022 Siemens/m.

Figure 4.20 and Figure 4.21 show the transient electric field strengths at the first critical point (0.15, 1.35) excited by the lightning and switching impulse voltages, respectively, for a clean and a wet ice-covered insulator.

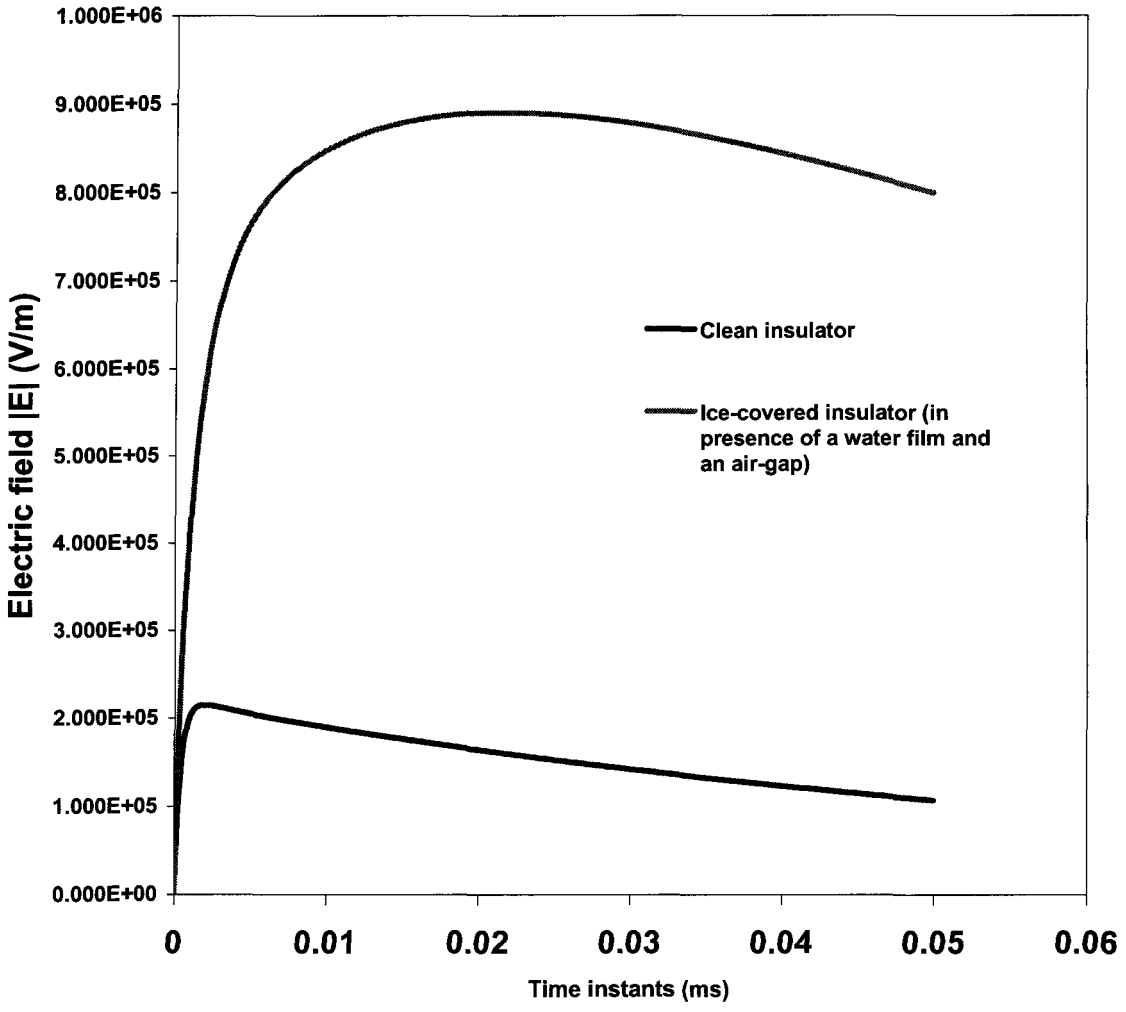

Figure 4.20: Electric field strengths at the first critical point for a clean and a wet ice-covered insulator for a lightning impulse voltage using the second ice geometry.

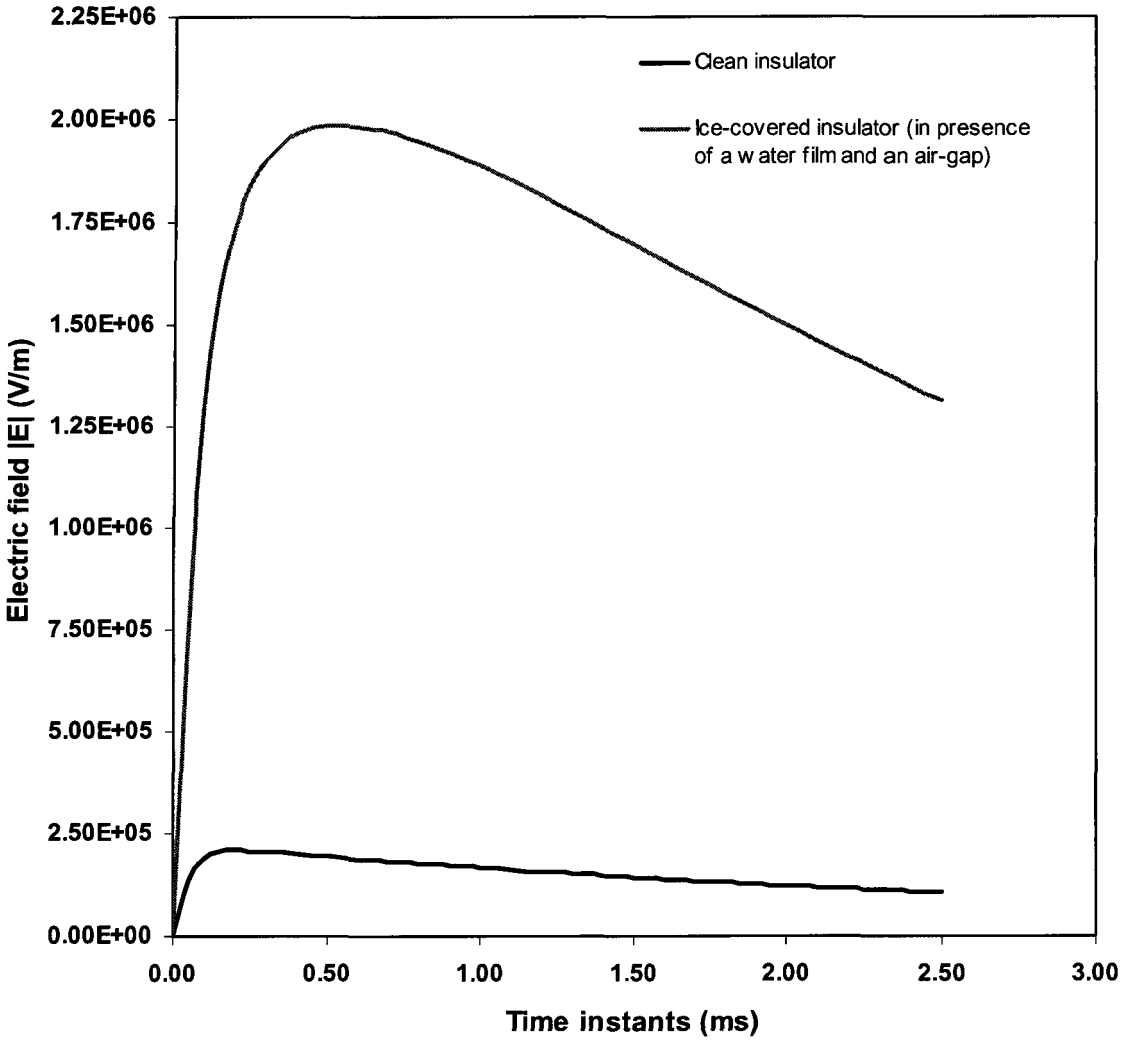

Figure 4.21: Electric field strengths at the first critical point for a clean and a wet ice-covered insulator for a switching impulse voltage using the second ice geometry.

Figure 4.22 (this is the same as Figure 4.11 with additional data but just repeated for convenience) shows the comparison of the maximum electric field strengths at the four critical points of a clean semi-conducting glazed (conductivity 0.022 S/m) insulator.

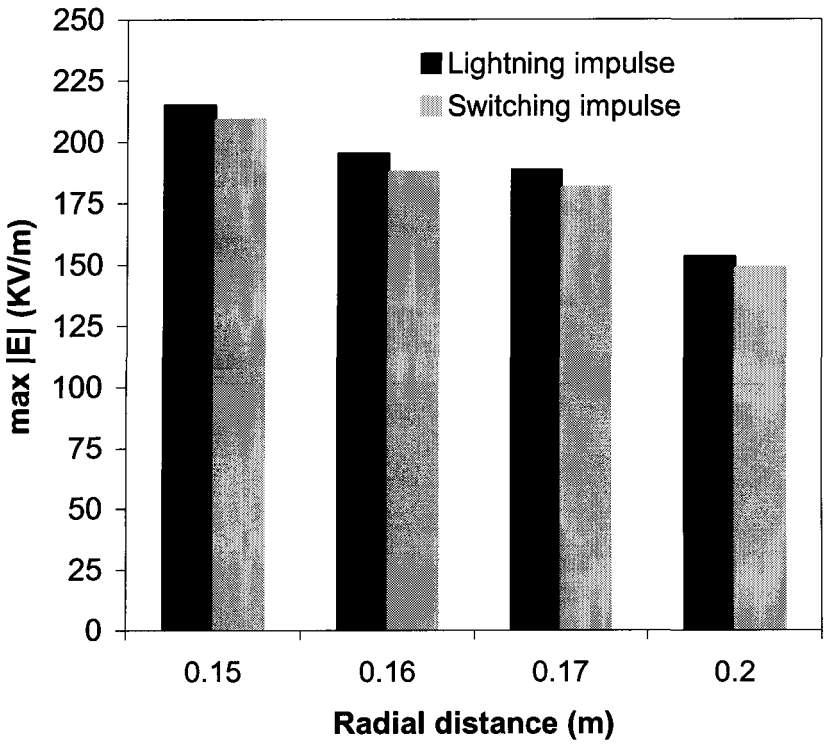

Figure 4.22: The maximum electric field strengths for the lightning and switching impulse voltages near the HV electrode of a clean semi-conducting glazed insulator.

Figure 4.23 shows the comparison of the electric field strengths at the first critical point (0.15, 1.35) of a wet ice-covered semi-conducting glazed insulator.

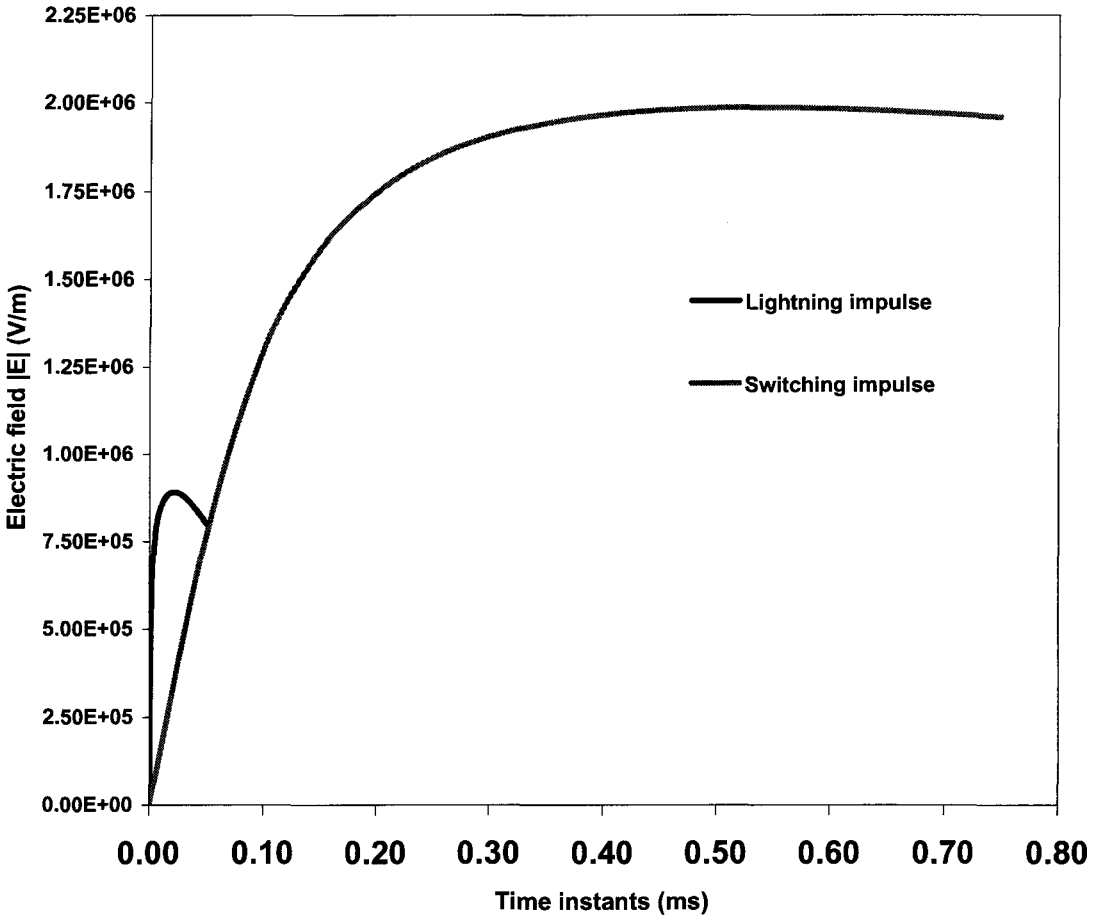

Figure 4.23: Electric field strengths for the lightning and switching impulse voltages at the first critical point near the HV electrode of an ice-covered semi-conducting glazed insulator in the presence of a water film and an air-gap.

Figure 4.24 shows the comparison of the maximum electric field strengths at the four critical points near the HV electrode of a wet ice-covered semi-conducting glazed insulator. It is observed that the maximum electric field strength is higher for a switching impulse than it is for a lightning impulse voltage.

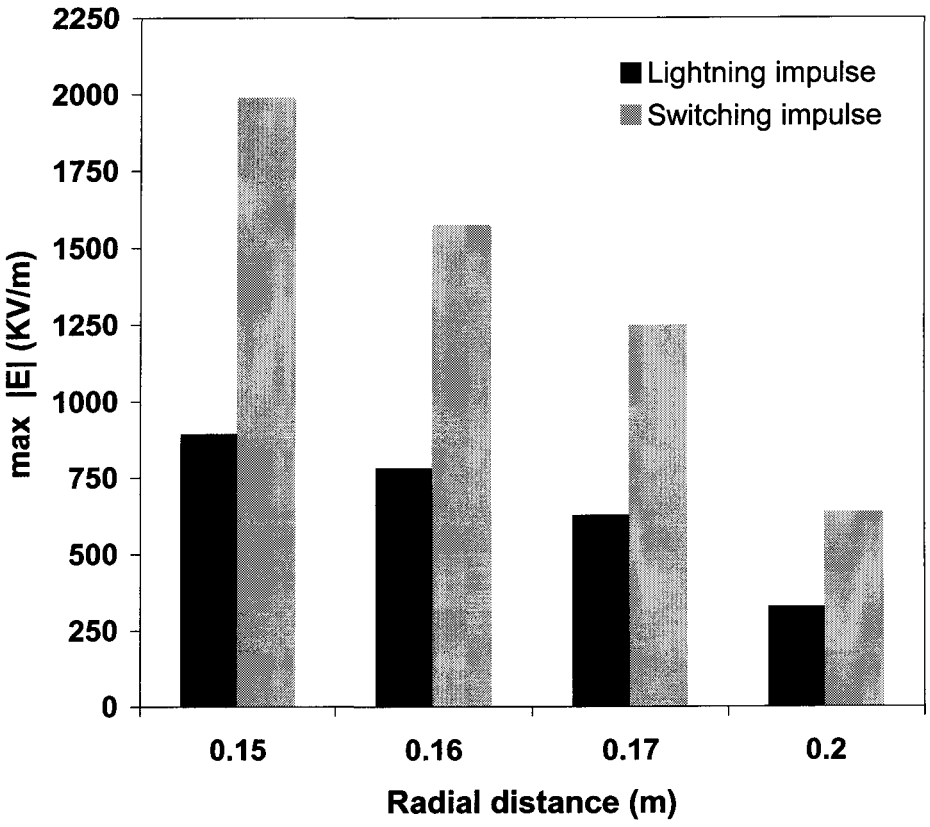

Figure 4.24: The maximum electric field strengths for the lightning and switching impulse voltages near the HV electrode of an ice-covered semi-conducting glazed (conductivity 0.022 S/m) insulator in the presence of a water film and an air-gap.

4.5 Effects of a Change in the Ice Permittivity for the Impulse Voltages

Figure 4.25 shows the comparison of the electric field strengths for a lightning impulse voltage at the first critical point (0.15, 1.35) of a wet ice-covered semi-conducting glazed (thickness 0.5 mm, conductivity 0.022 S/m) insulator using the second ice geometry taking the ice permittivity to be 75 and 5.

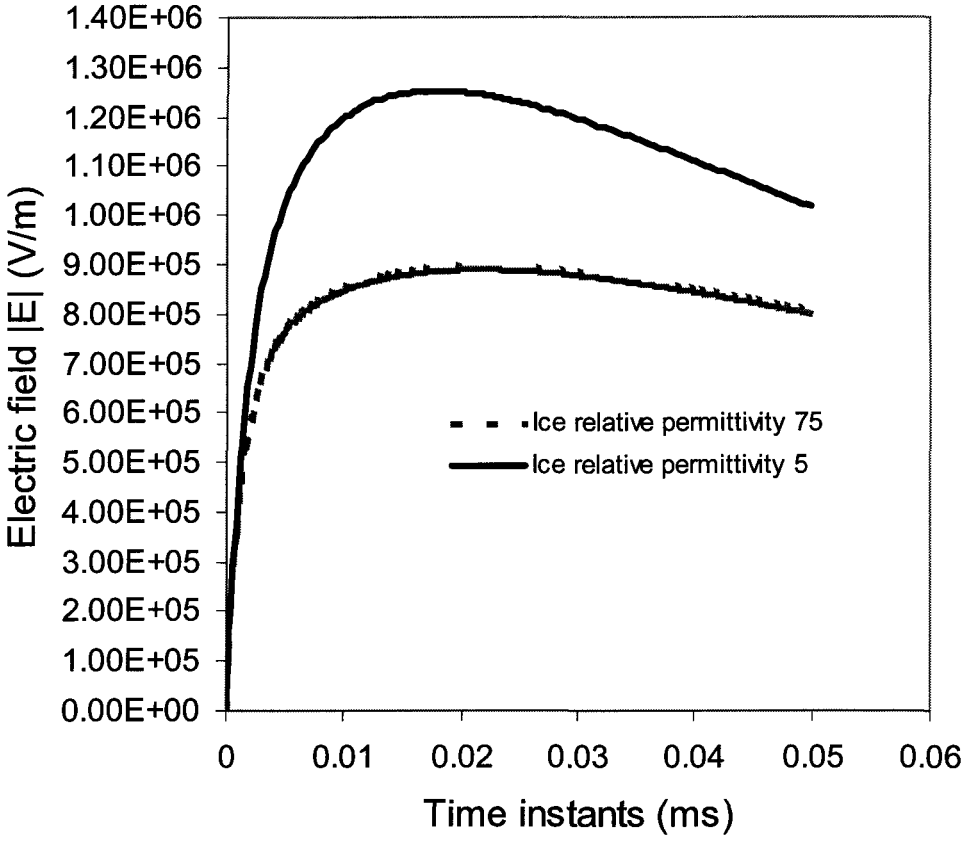

Figure 4.25: Comparison of the electric field strengths for a lightning impulse voltage at the first critical point of an ice-covered semi-conducting glazed insulator in the presence of a water film and an air-gap taking the ice permittivity to be 75 and 5.

Figure 4.26 shows the comparison of the electric field strengths excited by a switching impulse voltage at the first critical point of a wet ice-covered semi-conducting glazed (thickness 0.5 mm, conductivity 0.022 S/m) insulator using the second ice geometry taking the ice permittivity to be 75 and 40.

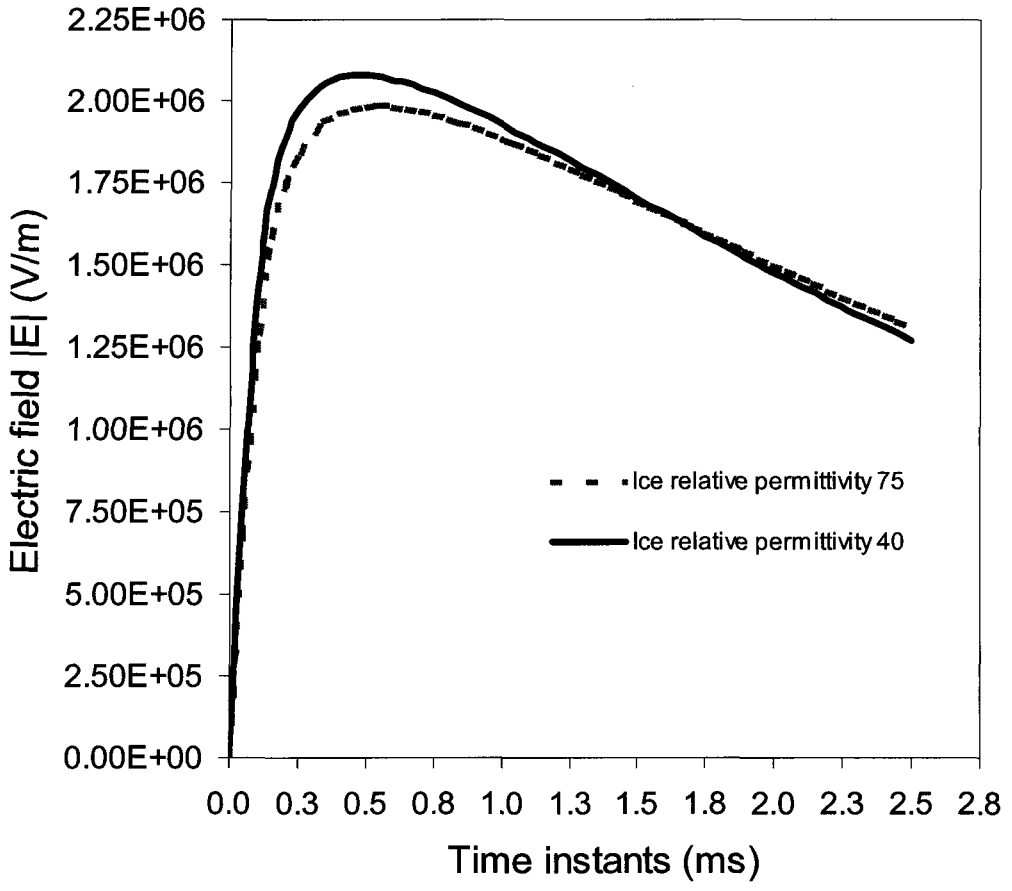

Figure 4.26: Comparison of the electric field strengths for a switching impulse voltage at the first critical point of an ice-covered semi-conducting glazed insulator in the presence of a water film and an air-gap taking the ice permittivity to be 75 and 40.

4.6 Results and Discussion

For the wet ice-covered insulator, it is observed from the Figure 4.12, Figure 4.13, Figure 4.18, Figure 4.19, Figure 4.23, and the Figure 4.24 that the electric field strength is higher for a switching impulse voltage than that for a lightning impulse voltage. Based on the simulation results, it is concluded that a switching impulse is the limiting factor in the design of a semi-conducting glazed insulator under icing conditions. It is also seen from the Figure 4.20 and the Figure 4.21 that the time instants at the maximum electric field strengths for the lightning impulse and the switching impulse voltages are 21.6 μs (peak voltage 1.2 μs) and 550.0 μs (peak voltage 250.0 μs), respectively. It is concluded that the electric field strength becomes maximum after the peak voltage for the wet ice-covered semi-conducting glazed insulator under a lightning impulse and a switching impulse voltage. This is because of a change in the equivalent impedance of the system due to high value of conduction current in the water film under icing conditions.

For the clean insulator, it can be seen from the Figure 4.10, Figure 4.11, Figure 4.16, Figure 4.17 and the Figure 4.22 that the electric field strength is higher for a lightning impulse voltage than that for a switching impulse voltage. Based on the simulation results, it is concluded that a lightning impulse is the limiting factor in the design of a clean semi-conducting glazed insulator. It is also observed from the Figure 4.20 and the Figure 4.21 that the time instants at the maximum electric field strengths for the lightning impulse and the switching impulse voltages are 2.0 μs (peak voltage 1.2 μs) and 200.0 μs (peak voltage 250.0 μs), respectively. It is concluded that the electric field strength becomes maximum after the peak voltage under a lightning impulse voltage, and before the peak voltage under

a switching impulse voltage, for the clean semi-conducting glazed insulator. This is due to the fact that a continuous leakage current flows in the semi-conducting glaze of the insulator that has a major effect on the equivalent impedance of the system under ice-free conditions.

It is also observed from the Figure 4.22 and Figure 4.24 that the wet ice, accumulated on the insulator, has a little effect on the electric field distribution around the insulator for a lightning impulse voltage, but it has a major effect on the electric field distribution for a switching impulse voltage. This is because of the rise time of a lightning impulse is much lower than that of a switching impulse voltage.

The next chapter deals in detail the flashover tests done in a climate chamber for the ice-free as well as ice-covered semi-conducting glazed insulators under the lightning and switching impulse voltages to validate the proposed model.

CHAPTER 5

EXPERIMENTAL VALIDATION

5.1 Overview

To verify the simulation results, flashover tests were done in a climate room of dimensions 6.2×5.7×3.8 meter on a semi-conducting glazed insulator covered with a glaze ice of thickness 1.5 cm in the presence of a water film and an air gap. The conductivity of the water used to form the glaze ice was taken as 80 μS/cm. The dripping water conductivity was measured after the flashover test and it was found to be 300 μS/cm. The increase resulted from the salt (NaCl) that was deposited on the surface during the ice accumulation process while the service voltage was applied. The length of the tested insulator was taken as 80 cm. Flashover tests were performed for the positive and negative lightning impulse and switching impulse voltages.

5.2 Experimental Set-up

Figure 5.1 shows the experimental setup used during the ice deposit process.

Figure 5.2 shows the experimental setup used during the flashover performance test. Impulse voltages were generated using a Marx generator and shaped to a standard lightning impulse voltage (1.2/50 μS) and a switching impulse voltage (250/2500 μS) using external resistors. The test sample was kept in the climate room. The voltage was applied through a bushing.

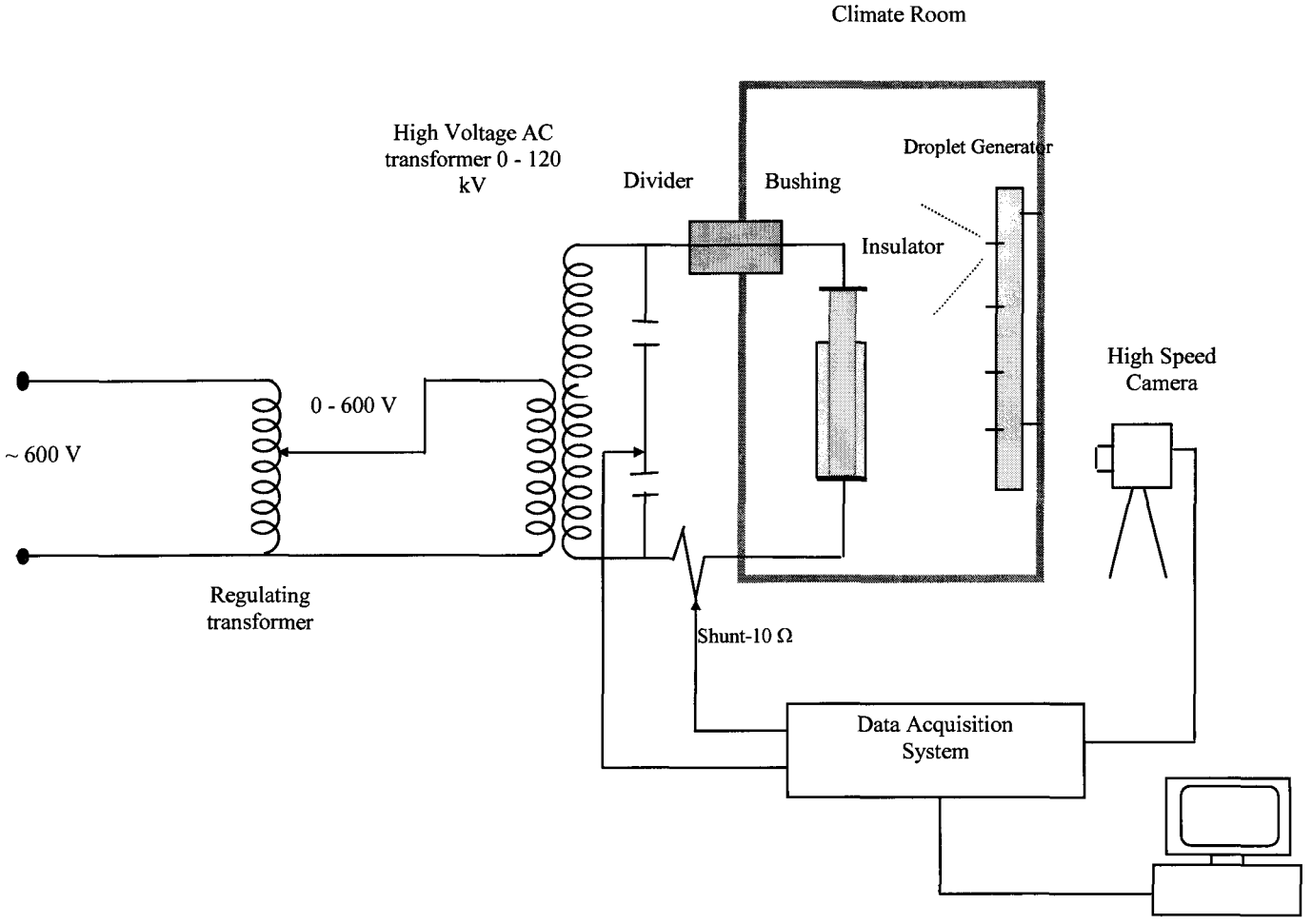

Figure 5.1: The ice deposit process.

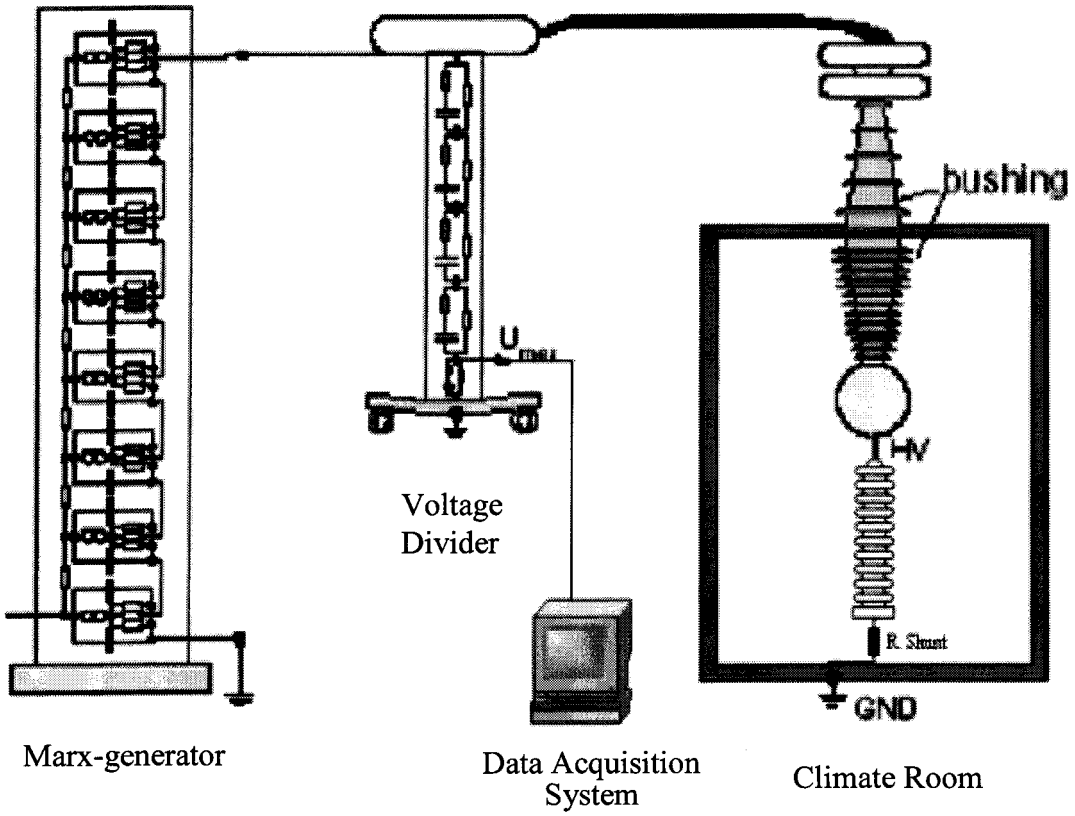

Figure 5.2: The flashover performance test.

5.3 Ice Deposit Method

Natural conditions were simulated as closely as possible by depositing artificial ice on the energized insulators in the climate room. The testing conditions were also adjusted to enable the growth of wet ice on the same insulators. This type of ice is associated with the highest probability of flashover [27]. In the climate room, parameters such as air temperature and wind velocity, as well as both the vertical and horizontal components of precipitation intensities, were controlled and kept constant following the instructions provided in [24].

The service voltage was applied to the test insulator during the whole icing period. This is necessary for a more realistic simulation of the natural icing of insulator equipment in the field [24]. In fact, the electric field affects ice accretion during its formation [23], particularly the progression of icicles and, consequently, the formation of the air gaps i.e. ice-free areas. The location, number, and length of these air gaps are major factors in the electric field distortion [52, 53], and consequently, the flashover voltage level.

Table 5.1 shows the test conditions used for the experiments.

Table 5.1: The experimental test conditions

Chamber dimensions	6.2×5.7×3.8 m
Accumulation voltage	64 kV, 60 Hz, AC
Test voltages	Lightning and Switching Impulse, up-and-down method ($V_{50\%}$)
Accumulation temperature	-12°C
Ice thickness	15 mm
Type of ice	Glaze
Conductivity	80 µS/cm at 20°C

5.4 Ice Test Preparation Prior to Flashover

A preparation period is needed between the end of the ice accretions at subzero air temperature and the moment when the test voltage is applied for the flashover voltage evaluation. The procedure may be adjusted according to two approaches, that is, performing the test under the "icing regime" or under the "melting regime" [24].

In this work, testing was done under the "icing regime." The test insulator was exposed to conditions as close as possible to those in the field (e.g. freezing rain conditions).

Testing under the "icing regime" corresponds to the case where the flashover performance test is carried out shortly after the ice accretion is completed and a water film is still present on the ice surface [23]. In such a case, the preparation period is short, typically about 2 to 3 minutes. This gives enough time for taking pictures, adjusting the test setup and installing/removing the collector receiving dripping water from the test insulator. Immediately after this period, the flashover test voltage is applied.

5.5 Ice Test Flashover Performance Evaluation

High leakage currents from an appropriate power supply, including both partial and flashover arcs, generally change the length and shape of air gaps i.e. ice-free areas formed along the ice-covered insulator, modify the ice surface conductivity, and will sometimes totally shed the ice deposit. These changes will affect the flashover voltages of the test insulators [24]. Therefore, the flashover test under one condition was achieved for any ice accretion sequence.

5.6 Experimental Results

The flashover voltages and time instants of breakdowns under various conditions are shown in Table 5.2, Table 5.3, Table 5.4 and Table 5.5.

Table 5.2: The flashover voltage under the lightning impulse voltage for the clean i.e. ice-free semi-conducting glazed insulator

Test No.	Peak voltage (kV)	Time instant at breakdown (μs)	State
1	350.0		Withstand
2	360.0		Withstand
3	370.0		Withstand
4	380.0		Withstand
5	390.0		Withstand
6	400.0		Withstand
7	410.0		Withstand
8	420.0		Withstand
9	430.0		Withstand
10	440.0		Withstand
11	450.0		Withstand
12	460.0	12.21	Breakdown
13	450.0	32.74	Breakdown
14	440.0		Withstand
15	450.0	14.59	Breakdown
16	440.0		Withstand
17	450.0	23.08	Breakdown
18	440.0		Withstand
19	450.0	17.63	Breakdown
20	440.0		Withstand
21	450.0	19.99	Breakdown
22	440.0		Withstand
23	450.0	20.44	Breakdown
24	440.0		Withstand
25	450.0	22.08	Breakdown
26	450.0		Withstand
27	450.0	16.56	Breakdown
28	450.0	13.95	Breakdown
29	450.0	19.20	Breakdown
30	450.0		Withstand
31	450.0	34.35	Breakdown
32	450.0		Withstand
33	450.0		Withstand
34	450.0	15.12	Breakdown

Table 5.3: The flashover voltage under the switching impulse voltage for the clean semi-conducting glazed insulator

Test no.	Peak voltage (kV)	Time instant at breakdown (μs)	State
1	480.0		Withstand
2	490.0		Withstand
3	500.0		Withstand
4	510.0		Withstand
5	520.0		Withstand
6	530.0		Withstand
7	540.0		Withstand
8	550.0	285.1	Breakdown
9	540.0	149.8	Breakdown
10	530.0		Withstand
11	540.0		Withstand
12	550.0	172.8	Breakdown
13	540.0	210.4	Breakdown
14	530.0	101.0	Breakdown
15	520.0	117.4	Breakdown
16	510.0		Withstand
17	520.0		Withstand
18	530.0	155.3	Breakdown
19	520.0	150.8	Breakdown
20	510.0		Withstand
21	520.0	136.4	Breakdown
22	510.0		Withstand
23	520.0		Withstand
24	530.0	189.3	Breakdown
25	520.0	147.1	Breakdown
26	510.0	191.4	Breakdown
27	500.0		Withstand
28	510.0		Withstand
29	520.0		Withstand

Table 5.4: The flashover voltage under the lightning impulse voltage for the ice-covered semi-conducting glazed insulator

Test no.	Peak voltage (kV)	Time instant at breakdown (μs)	State
1	300.0		Withstand
2	300.0		Withstand
3	310.0		Withstand
4	320.0		Withstand
5	330.0		Withstand
6	340.0		Withstand
7	350.0		Withstand
8	360.0		Withstand
9	370.0		Withstand
10	380.0		Withstand
11	390.0		Withstand
12	400.0		Withstand
13	410.0		Withstand
14	420.0		Withstand
15	430.0	27.7	Breakdown
16	420.0		Withstand
17	430.0		Withstand
18	440.0		Withstand
19	450.0	19.5	Breakdown
20	440.0		Withstand
21	450.0		Withstand
22	460.0	17.9	Breakdown

Table 5.5: The flashover voltage under the switching impulse voltage for the ice-covered semi-conducting glazed insulator

Test no.	Peak voltage (kV)	Time instant at breakdown (μs)	State
1	350.0		Withstand
2	360.0	767.1	Breakdown
3	350.0		Withstand
4	360.0		Withstand
5	370.0	261.2	Breakdown
6	360.0	1035.0	Breakdown
7	350.0		Withstand
8	360.0	521.8	Breakdown
9	350.0		Withstand
10	360.0		Withstand
11	370.0	414.9	Breakdown
12	360.0		Withstand
13	370.0		Withstand
14	380.0	375.1	Breakdown
15	370.0	292.5	Breakdown
16	360.0	402.1	Breakdown
17	350.0		Withstand
18	360.0	420.1	Breakdown
19	350.0	382.1	Breakdown
20	340.0	358.9	Breakdown
21	330.0		Withstand
22	340.0		Withstand

5.7 Determination of the 50% Flashover Voltage

The 50% flashover voltage for the semi-conducting glazed insulator is calculated according to the following equation [54],

$$V_{50} = \frac{\left(\sum (n_i V_i)\right)}{N}, \qquad (5.1)$$

Where,

V_i is an applied voltage level,

n_i is the number of individual tests carried out at the same applied voltage level V_i,

N is the total number of "valid" tests.

The 50% flashover voltage for the studied semi-conducting glazed insulator is calculated in the following conditions:

1. The clean insulator,
2. The ice-covered insulator.

5.7.1 The Clean Insulator

5.7.1.1 The Lightning Impulse Voltage

The data in Table 5.2 are used to compute the 50% flashover voltage.

$$V_{50\%} = (460 \times 1 + 450 \times 16 + 440 \times 6)/23 = 447.8 \text{ kV}.$$

5.7.1.2 The Switching Impulse Voltage

The data from

Table 5.3,

$$V_{50\%} = (550 \times 2 + 540 \times 3 + 530 \times 4 + 520 \times 7 + 510 \times 5 + 500 \times 1)/22 = 524.1 \text{ kV}.$$

5.7.2 The Ice-covered Insulator

5.7.2.1 The Lightning Impulse Voltage

The data from Table 5.4,

$$V_{50\%} = (430 \times 2 + 420 \times 1 + 440 \times 2 + 450 \times 2 + 460 \times 1)/8 = 440.0 \text{ kV}.$$

5.7.2.2 The Switching Impulse Voltage

The data from Table 5.5,

$$V_{50\%} = (330 \times 1 + 340 \times 2 + 360 \times 8 + 350 \times 5 + 370 \times 4 + 380 \times 1)/21 = 357.1 \text{ kV}.$$

5.8 Results and Discussion

Figure 5.3 shows the 50% impulse flashover voltages under the icing and clean conditions for the test conditions mentioned in the previous sections. It is observed that the switching impulse is the limiting factor in the design of the semi-conducting glazed insulator under icing conditions. This is contrary to clean conditions where the lightning impulse is the limiting factor.

It can be seen, from the Table 5.2, Table 5.3, Table 5.4, and the Table 5.5, that the flashover occurs after the peak voltage for the clean as well as the wet ice-covered semi-conducting glazed insulator under the lightning impulse voltage, and before the peak voltage for the clean semi-conducting glazed insulator and after the peak voltage for the wet ice-covered semi-conducting glazed insulator under the switching impulse voltage.

It is also seen from the Figure 5.3 that the wet ice, accumulated on the insulator, has a very little effect on the flashover voltage of the semi-conducting glazed insulator under the lightning impulse voltage, but it significantly reduces the flashover voltage under the switching impulse voltage. All the trends in data are in agreement with the simulation results.

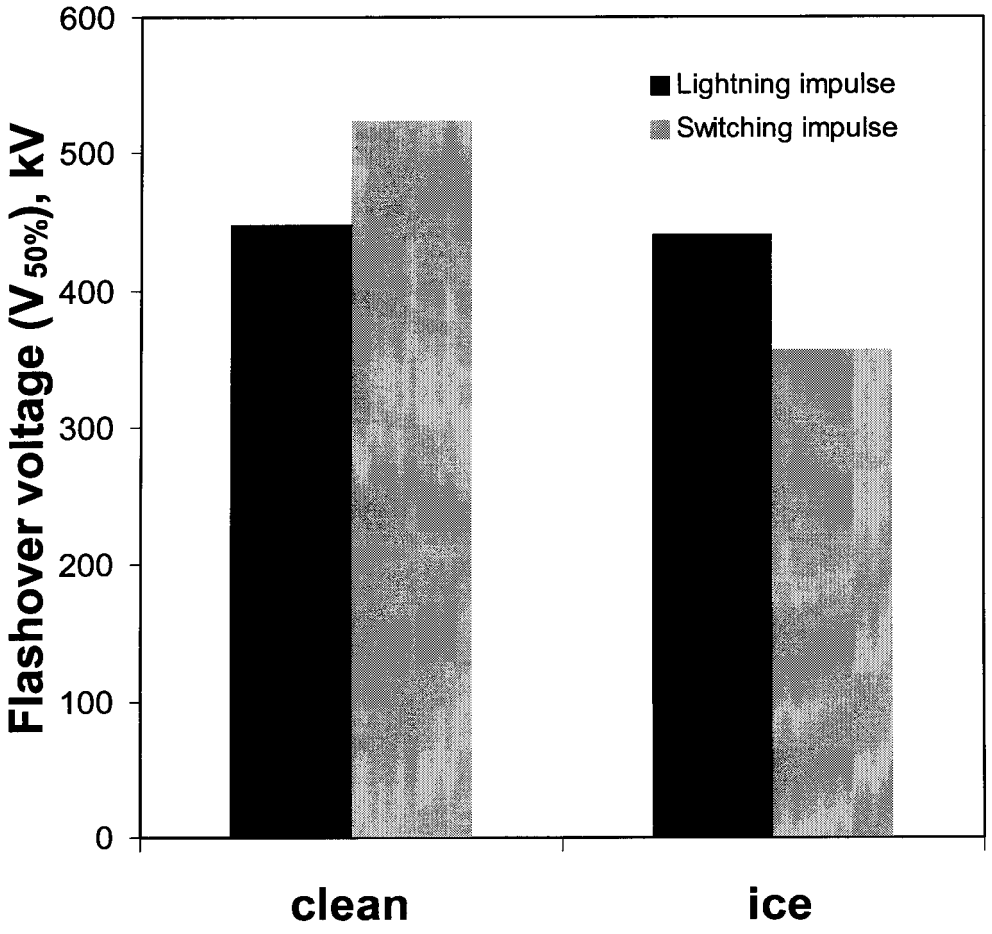

Figure 5.3: The impulse flashover performance of a semi-conducting glazed standard post insulator (experimental results).

The next chapter discusses the proposed method for the computation of potential distributions along the tip of sheds of ice-free and ice-covered insulators under the sinusoidal voltages equivalent to lightning and switching impulses using the Finite Element Method, and flashover performances of the insulators based on the potential distributions.

CHAPTER 6

FLASHOVER PERFORMANCE OF AN INSULATOR BASED ON THE ELECTRIC FIELD DISTRIBUTION WHEN SINUSOIDAL VOLTAGES ARE APPLIED

6.1 Overview

In this chapter, computations have been done for the sinusoidal voltages equivalent to the lightning and switching impulse voltages as those are faster computationally and avoid long transient solutions but results are almost as useful. Flashover performance can be studied by computing the electric field strengths around the insulator. When the electric field strength, at any point, exceeds the corona onset field, discharges occur at that point and may lead to flashover. Computation of the electric field strength, can involve a large error, because of the numerical differentiation of the potential at any point. Hence potential distributions along the insulators have been computed in this chapter. By visible inspection of the potential distributions, flashover performance has been studied.

6.2 Computation of Potential Distributions for Power Frequency and Impulse Voltages

The potential distributions have been computed along the Station Post insulator surface starting from the HV electrode down to the grounded electrode for uniform ice

accretions from the point of view of the surface flashover. Maxwell's equations are solved with the usual boundary conditions (Dirichlet, Neuman or mixed) on the dielectric interfaces. Computations have been carried out for power frequency as well as for switching impulse (SI) and lightning impulse (LI) voltages in the whole domain for clean (ice-free) normal glazed and the semi-conducting glazed insulators, as well as for insulators covered with dry and wet ice (uniformly distributed) in the presence of air-gaps.

6.2.1 The Wet Ice-covered Insulator

6.2.1.1 The Power Frequency Voltage

Figure 6.1 shows the potential distributions along the insulator for a power frequency (60 Hz) voltage with a peak of 100 kV using the first ice geometry. It is observed from the figure that the conductivity of the semi-conducting glaze does not have a major effect on the potential distribution for this excitation. This is due to the fact that the displacement current is negligible in the ice layer for a low frequency voltage and there is a saturation in the conduction current in the semi-conducting glaze and water film when the conductivity exceeds a certain value. The potential distribution is almost same for both conductivities, i.e. 0.022 and 2.2 Siemens/metre and there is no further improvement if the conductivity of the semi-conducting glaze of thickness 0.5 mm exceeds 0.022 Siemens/m. Further improvement can only be obtained by increasing the thickness of the semi-conducting glaze to 5.0 mm with a conductivity of 0.022 Siemens/m.

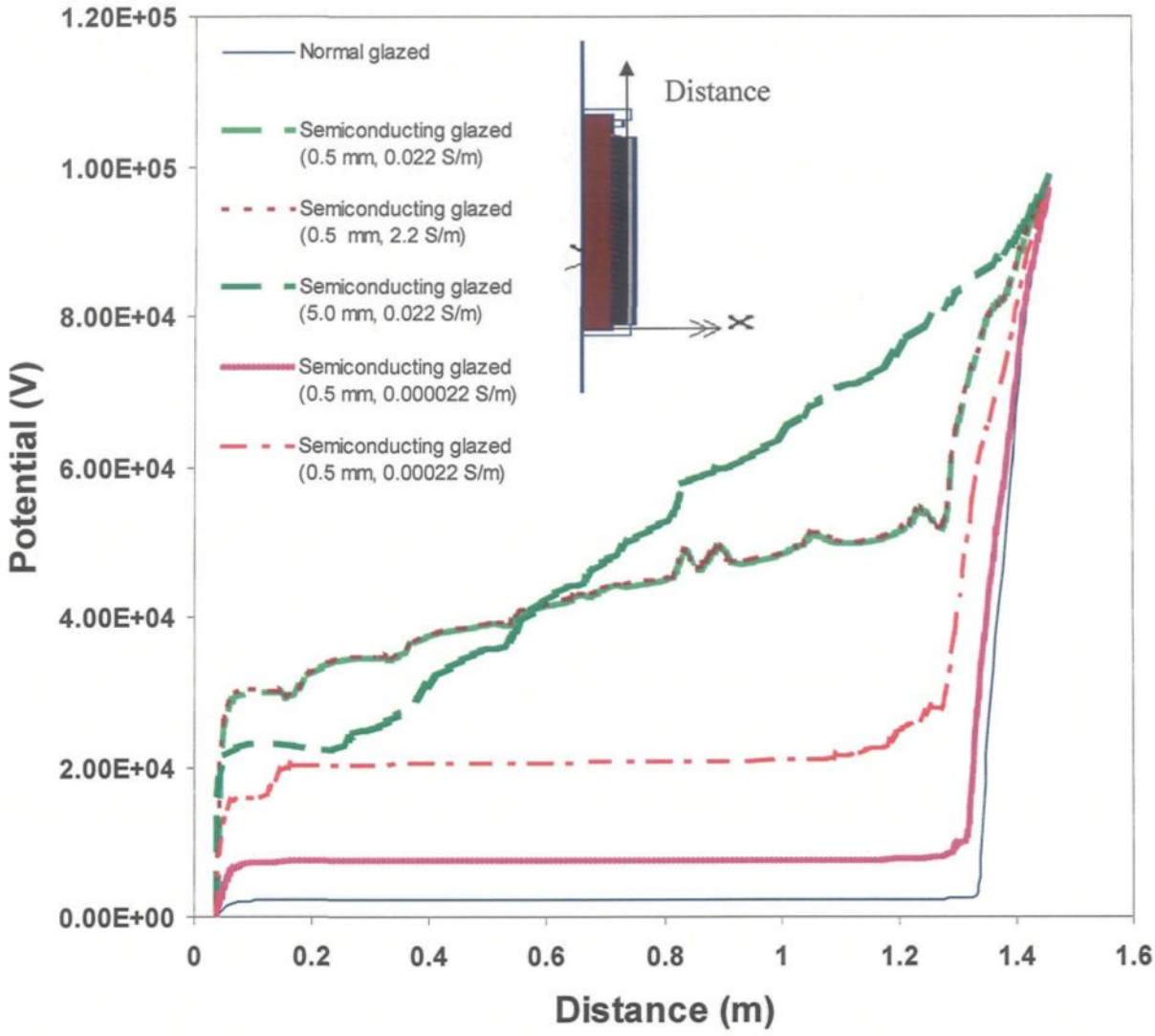

Figure 6.1: Potential distributions along the ice-covered insulators for the power frequency (60 Hz) voltage.

6.2.1.2 The Impulse Voltages

Next the sinusoidal voltages equivalent (same rise time) to impulse voltages are considered [51].

For the switching impulse,

$$t_r = 250\mu s,$$

$$F_{eq} = 1/\pi t_r = 1.3KHz. \quad (6.1)$$

For the lightning impulse,

$$t_r = 1\mu s,$$

$$F_{eq} = 1/\pi t_r = 320KHz. \quad (6.2)$$

Where,

t_r is the rise time of the impulse,

F_{eq} is the equivalent frequency of the impulse.

Figure 6.2 shows voltage contours around the normal glazed standard insulator covered with glaze ice, in the presence of air-gaps, for a 320 KHz sinusoidal voltage equivalent to a lightning impulse voltage using the first ice geometry. It is observed that most of the voltage drops occur across the air gap and thus the possibility of electric discharges near the HV electrode resulting in flashover is a maximum in this situation. This is in agreement with previous results using the Boundary Element Method [45].

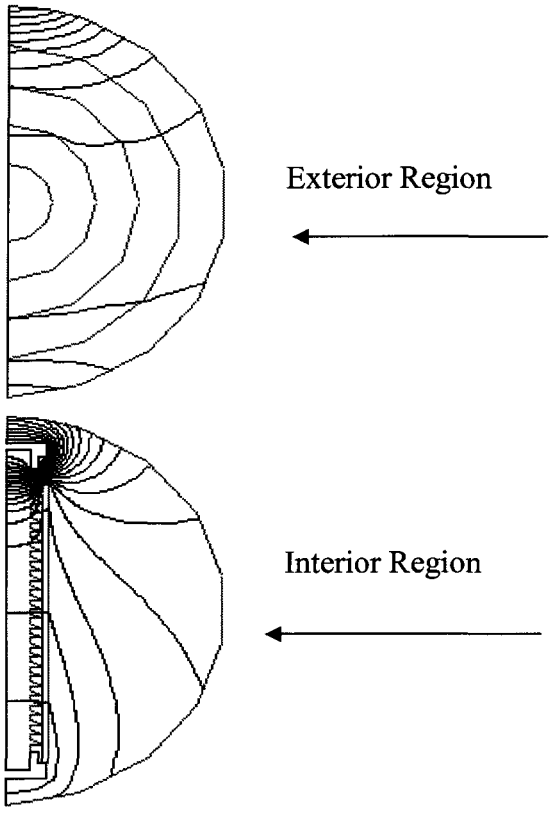

Figure 6.2: Voltage contours around the normal glazed standard insulator covered with a wet glaze ice in presence of air gaps for an equivalent lightning impulse voltage.

The normal glazed insulator is coated with a glaze with zero conductivity and two types of the semi-conducting glazed insulator have been considered for this excitation. In the first type, the thickness of the semi-conducting glaze is 0.5 mm. In the second, the thickness of the semi-conducting glaze is 5.0 mm. The conductivity of the semi-conducting glaze varies from 0.022 Siemens/m to 2.2 Siemens/m. Figure 6.3 shows the comparison of the potential distributions at the tip of the sheds for an equivalent lightning impulse voltage using the first ice geometry. It is seen that a semi-conducting glaze coating of thickness 0.5 mm and a conductivity of 2.2 Siemens/m makes the potential distribution linear. A linear potential distribution can also be obtained by increasing the thickness of the semi-conducting glaze to 5.0 mm with a conductivity of 0.022 Siemens/m only.

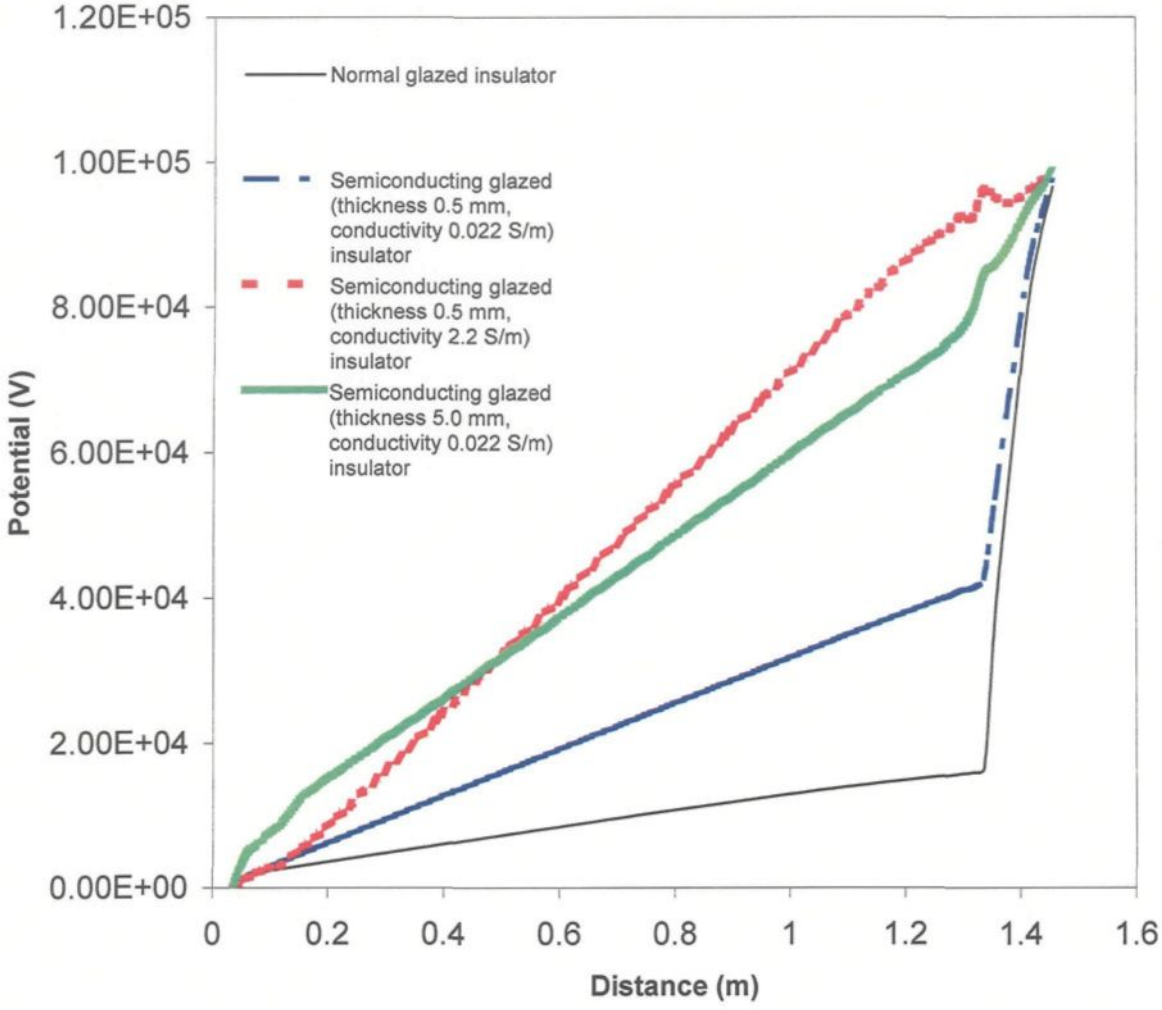

Figure 6.3: Comparison of the potential distributions along the normal glazed and the semi-conducting glazed insulators using the first ice geometry for a 320 KHz sinusoidal voltage equivalent to a lightning impulse voltage.

The results for a 1.3 KHz sinusoidal voltage (equivalent to a switching impulse voltage), for the above configuration are shown in Figure 6.4. It is seen that a thin semi-conducting glaze coating makes the potential distribution less linear for an equivalent switching impulse compared to an equivalent lightning impulse voltage because of a high value of the displacement current in the ice layer for a high frequency voltage. It is also seen that the conductivity of the semi-conducting glaze of thickness 0.5 mm has no further effects if its value exceeds 2.2 Siemens/m. Further improvement can only be obtained by increasing the thickness of the semi-conducting glaze to 5.0 mm with a conductivity 0.022 Siemens/m and it has no further effects if its value exceeds 0.022 Siemens/m.

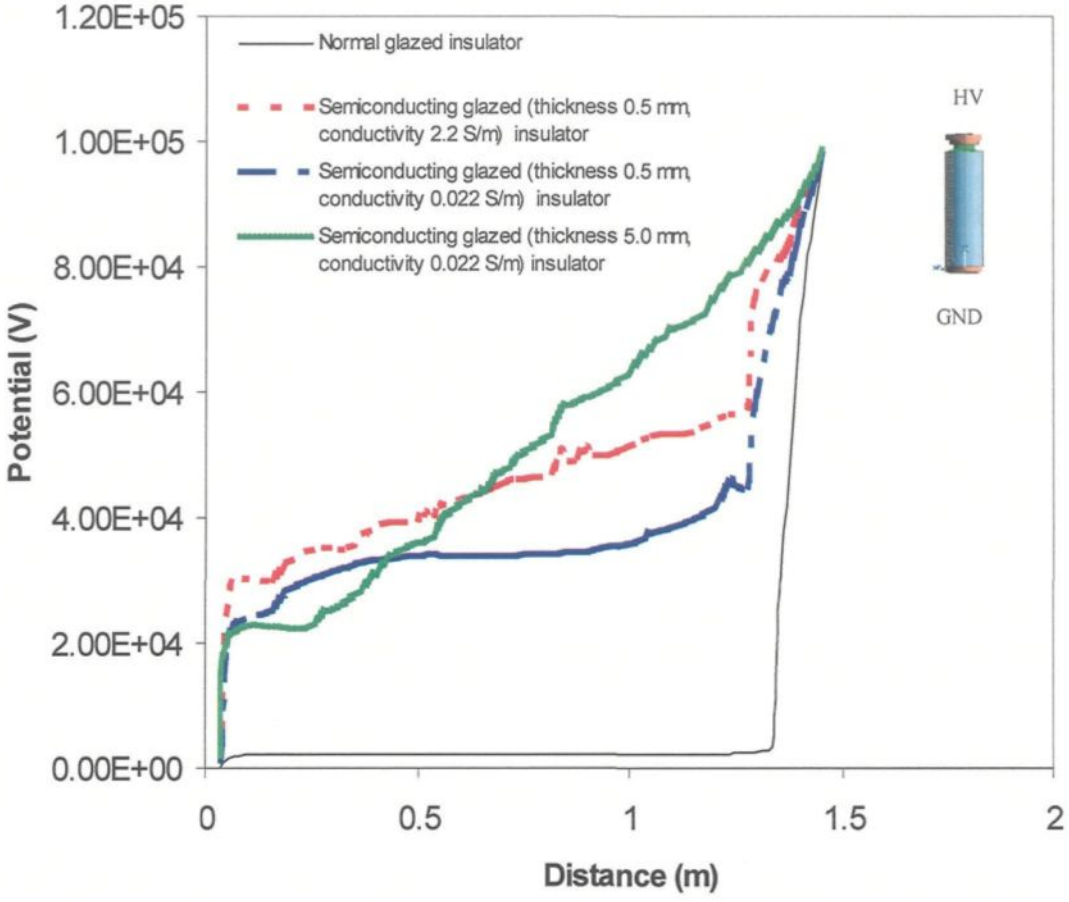

Figure 6.4: Comparison of the potential distributions along the normal glazed and the semi-conducting glazed insulators using the first ice geometry for a 1.3 KHz sinusoidal voltage equivalent to a switching impulse voltage.

The potential distributions along a semi-conducting glazed insulator under an equivalent switching impulse voltage using the first ice geometry, for ice relative permittivities of 40 and 75 (cf. equation 2.3), with the semi-conducting glaze thickness set to 0.5 mm and the conductivity at 2.20 S/m are shown in Figure 6.5. It can be seen from the figure that the permittivity of the ice does not have a major effect on the potential distribution for a switching impulse voltage.

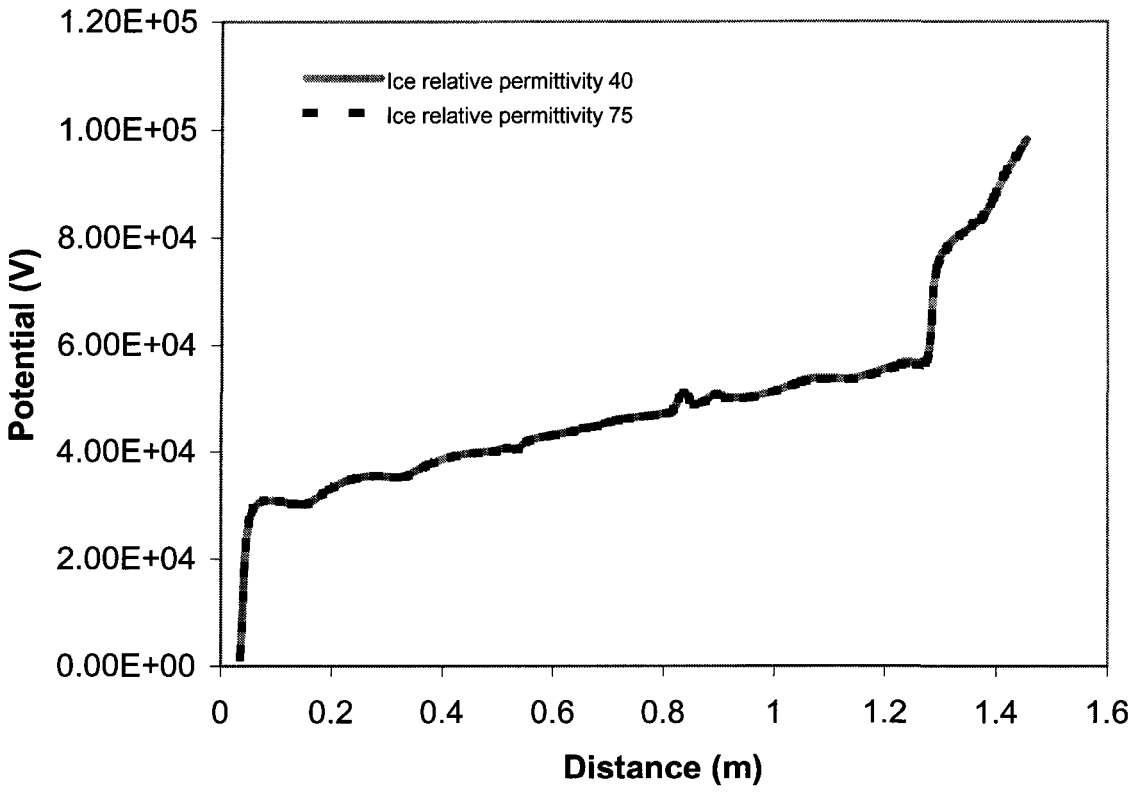

Figure 6.5: Effects of the ice permittivity for a 1.3 KHz sinusoidal voltage equivalent to a switching impulse voltage with the semi-conducting glaze of thickness 0.5 mm and conductivity 2.20 S/m.

Figure 6.6 shows the potential distributions along the insulator for a power frequency voltage, and the sinusoidal voltages equivalent to a lightning impulse and a switching impulse, for the second ice geometry with a semi-conducting glaze conductivity of 2.20×10^{-5} S/m. It is observed that the potential distribution is more linear for a lightning impulse than that for a switching impulse voltage because of a high value of the displacement current in the ice layer for a high frequency voltage.

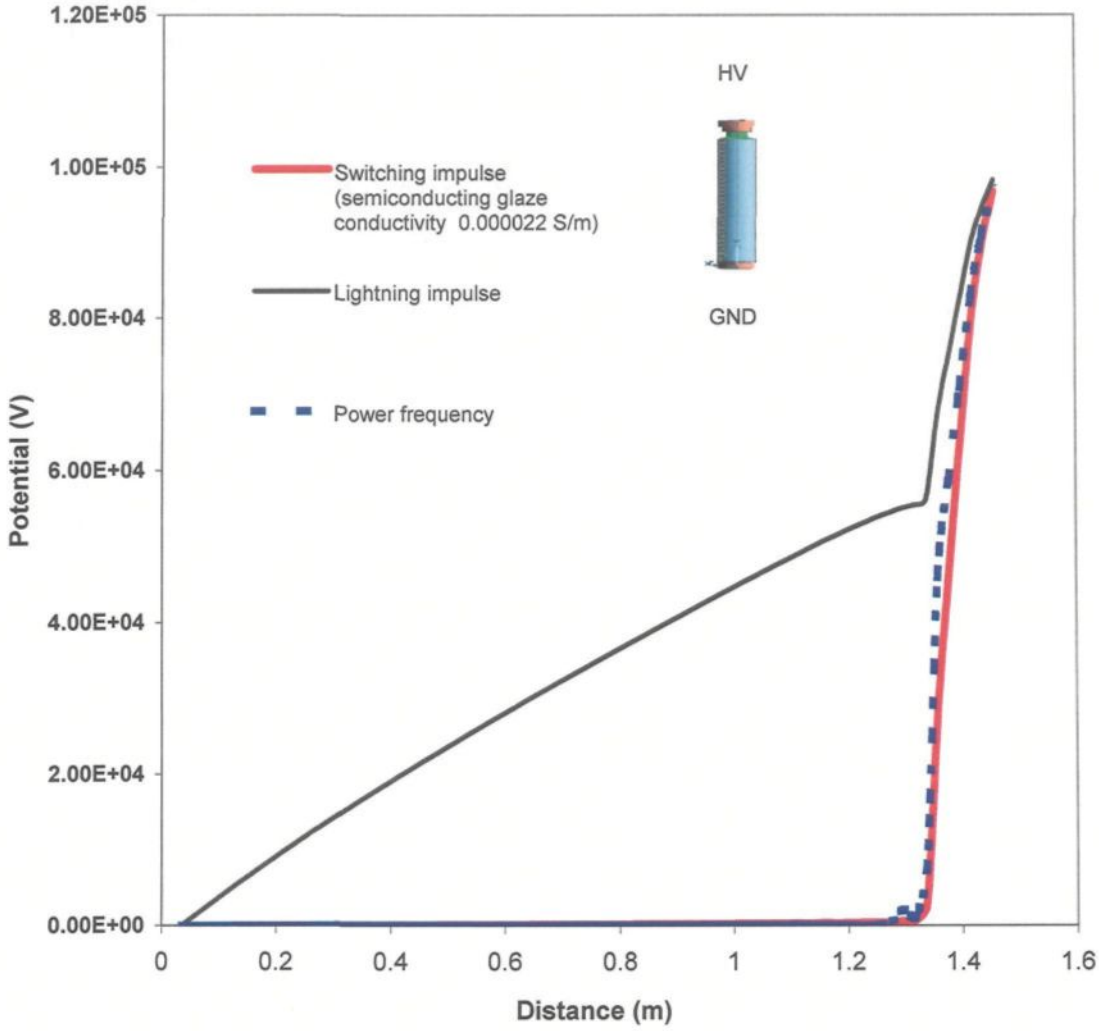

Figure 6.6: Comparison of the potential distributions for a switching impulse, a lightning impulse and a power frequency voltage for the second ice geometry with a semi-conducting glaze conductivity of 2.20×10^{-5} S/m.

The results for the second ice geometry with a semi-conducting glaze conductivity of 0.022 and 2.2 S/m are shown in Figure 6.7 and Figure 6.8 respectively.

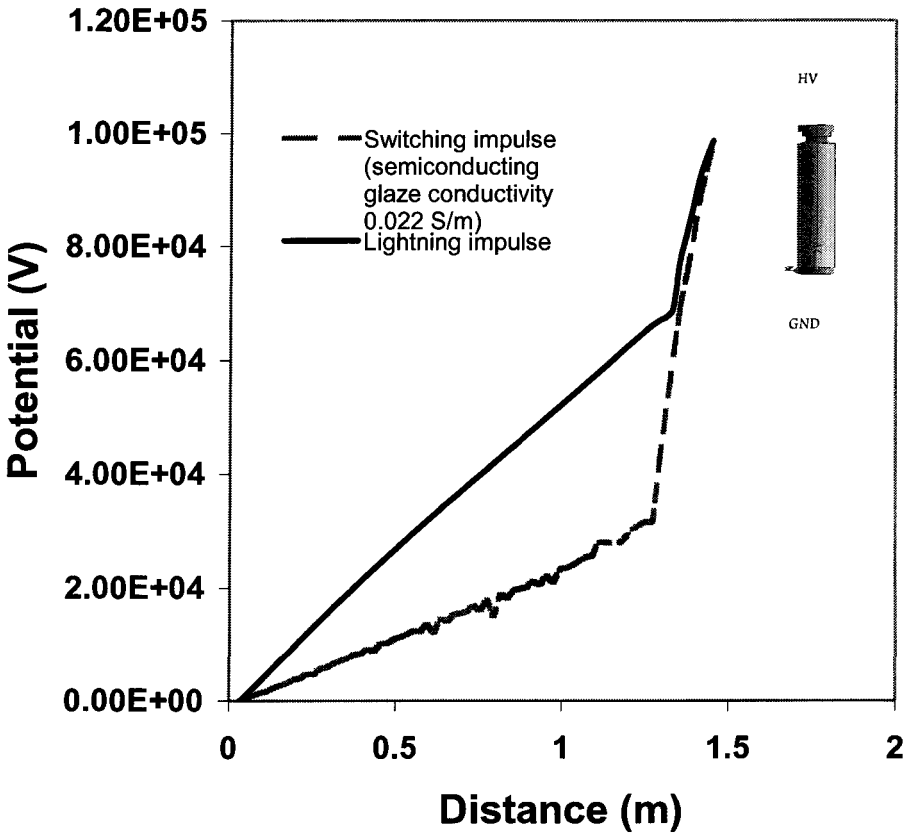

Figure 6.7: Comparison of the potential distributions for a switching impulse and a lightning impulse voltage for the second ice geometry with a semi-conducting glaze conductivity of 0.022 S/m.

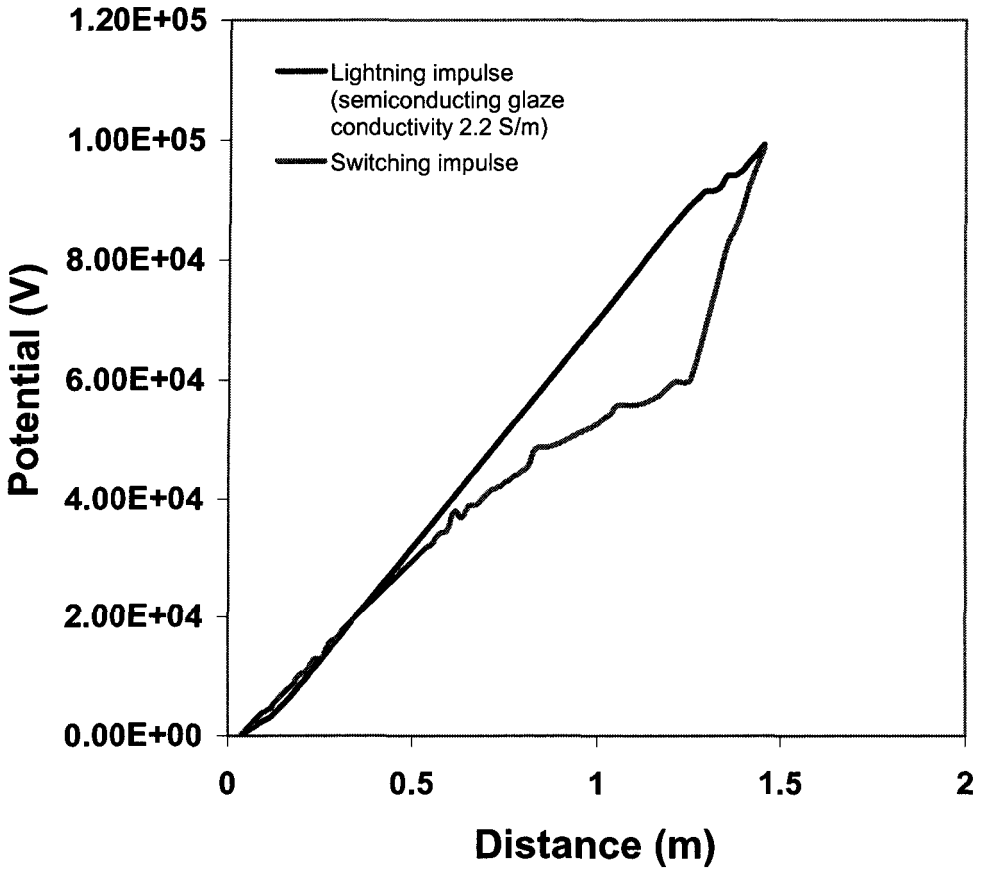

Figure 6.8: Comparison of the potential distributions for a switching impulse and a lightning impulse voltage for the second ice geometry with a semi-conducting glaze conductivity of 2.2 S/m.

The potential distributions for an equivalent lightning impulse voltage, for the second ice geometry with the ice relative permittivities (cf. equation 2.3) set to 5 and 75, with a semi-conducting glaze conductivity of 0.022 S/m are shown in Figure 6.9. It is seen that the permittivity of the ice has a very little effect on the results.

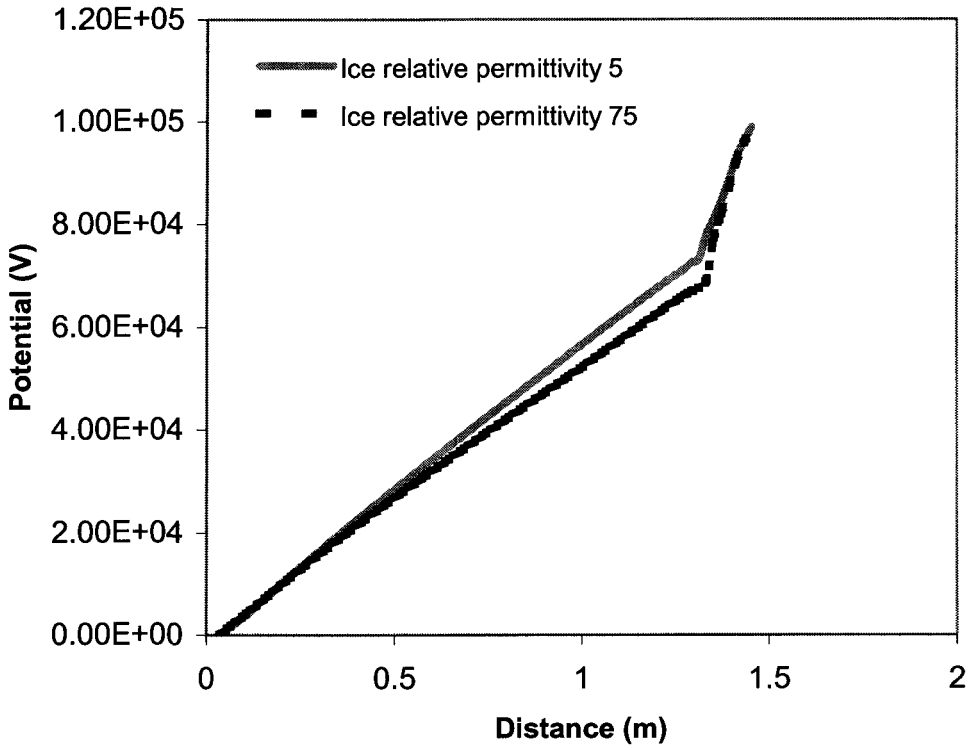

Figure 6.9: Effects of the ice permittivity for a lightning impulse voltage with a semi-conducting glaze conductivity of 0.022 S/m.

6.2.2 The Dry Ice-covered Insulator

In this case, there is no water film on the surface of an ice-covered insulator. All the simulations have been done for the second ice geometry shown in Figure 4.3 and Figure 4.4, without a water film.

The comparisons of the results for power frequency and impulse voltages for the second ice geometry without a water film for a semi-conducting glaze conductivity of 2.20×10^{-5} and 0.022 S/m are shown in Figure 6.10 and Figure 6.11 respectively. It is seen that the potential distribution is more linear for a switching impulse than it is for a lightning impulse voltage.

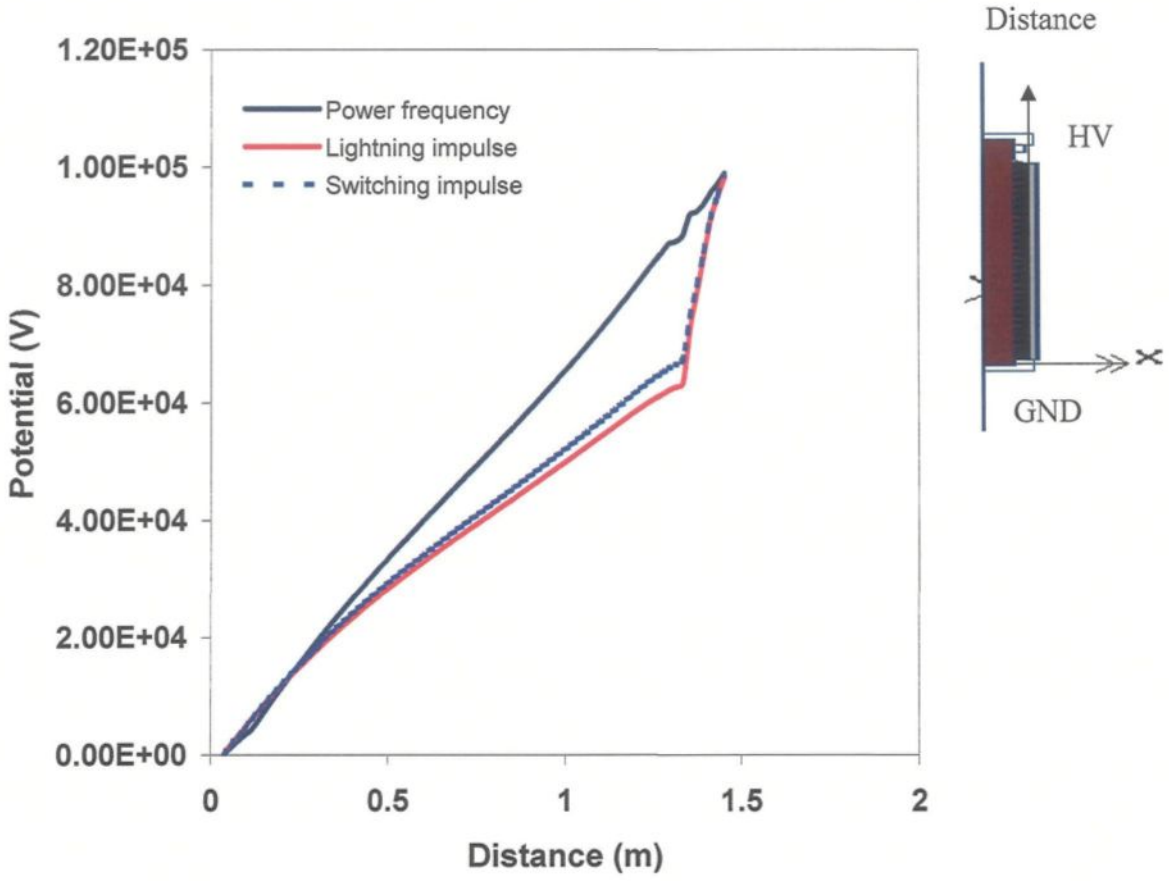

Figure 6.10: Comparison of the potential distributions for the power frequency and the impulse voltages for the second ice geometry without a water film for a semi-conducting glaze conductivity of 2.20×10^{-5} S/m.

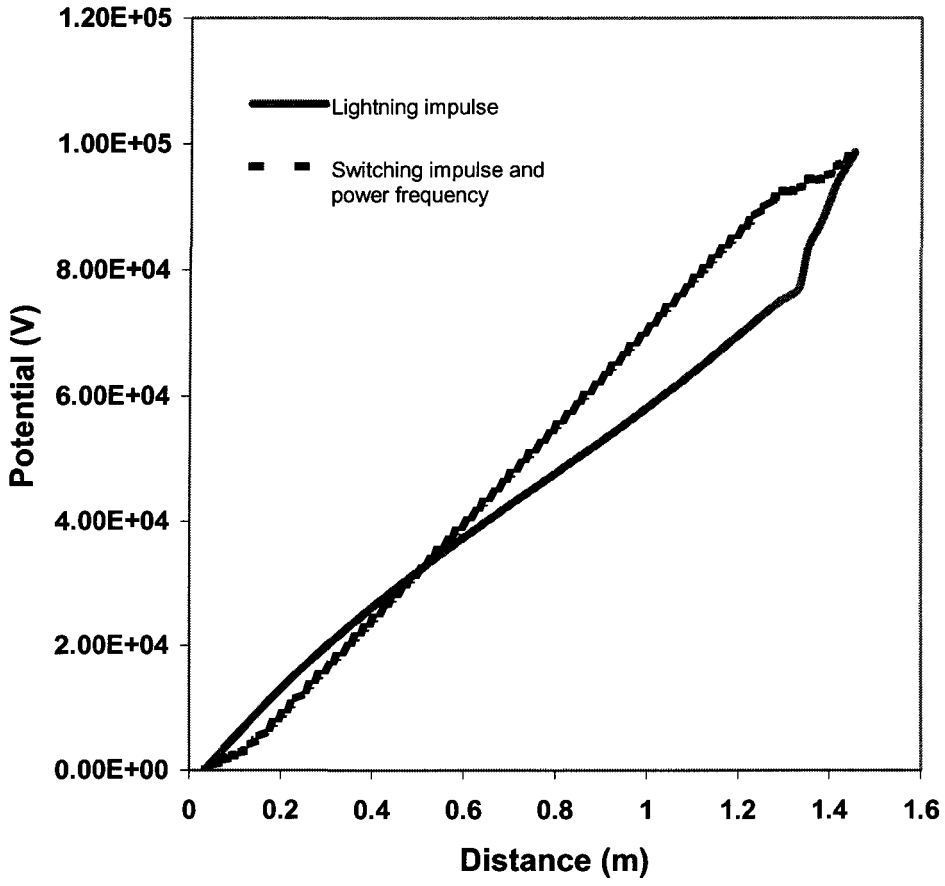

Figure 6.11: Comparison of the potential distributions for the power frequency and the impulse voltages for the second ice geometry without a water film for a semi-conducting glaze conductivity of 0.022 S/m.

6.2.3 The Clean Insulator

The potential distributions along the clean insulator at the tip of the sheds, coated with a semi-conducting glaze of thickness 0.5 mm and of conductivities 2.20×10^{-5}, 2.20×10^{-4}, 2.20×10^{-3}, and 2.20×10^{-2} S/m are shown in Figure 6.12, Figure 6.13, Figure 6.14, and Figure 6.15, respectively. It is observed that the potential distribution is more linear for a switching impulse voltage than it is for a lightning impulse voltage.

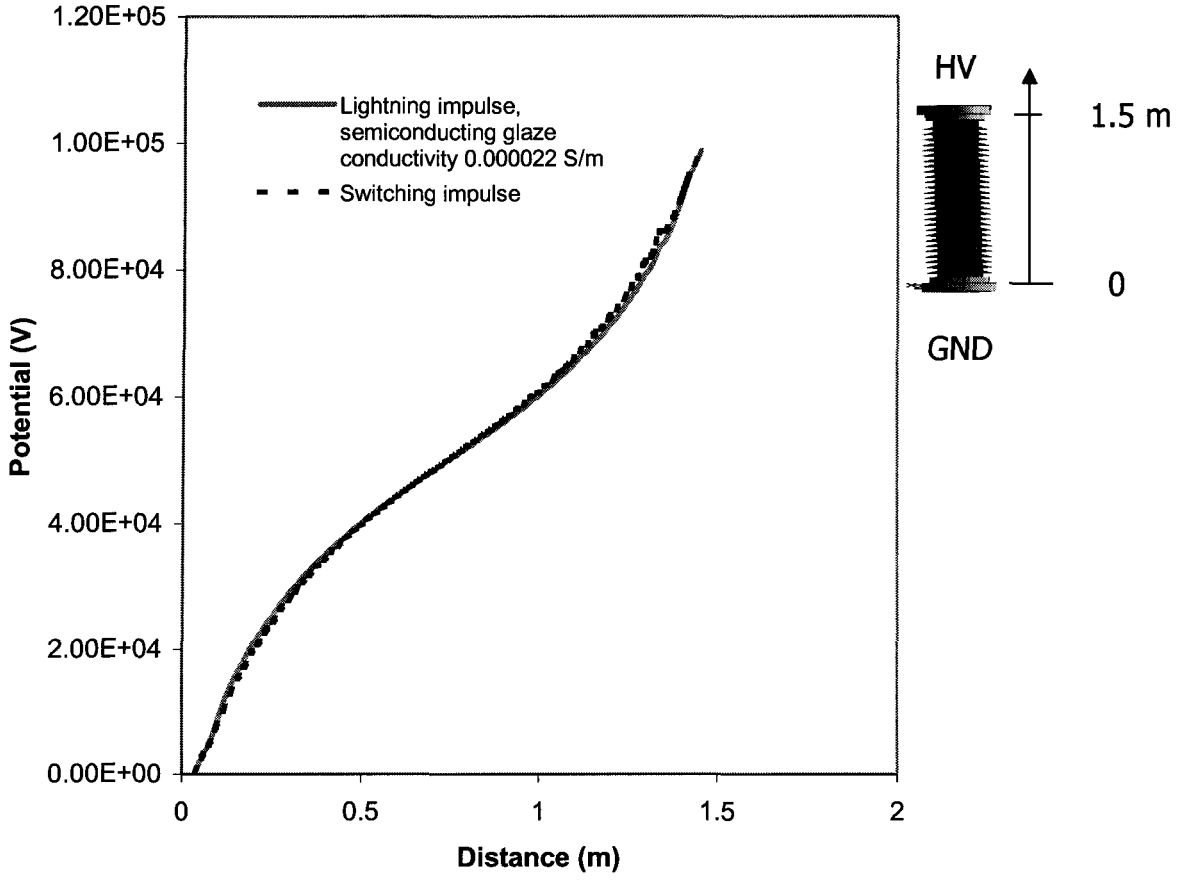

Figure 6.12: Potential distributions along a clean insulator coated with a semi-conducting glaze of conductivity 2.20×10^{-5} S/m for the lightning and switching impulse voltages.

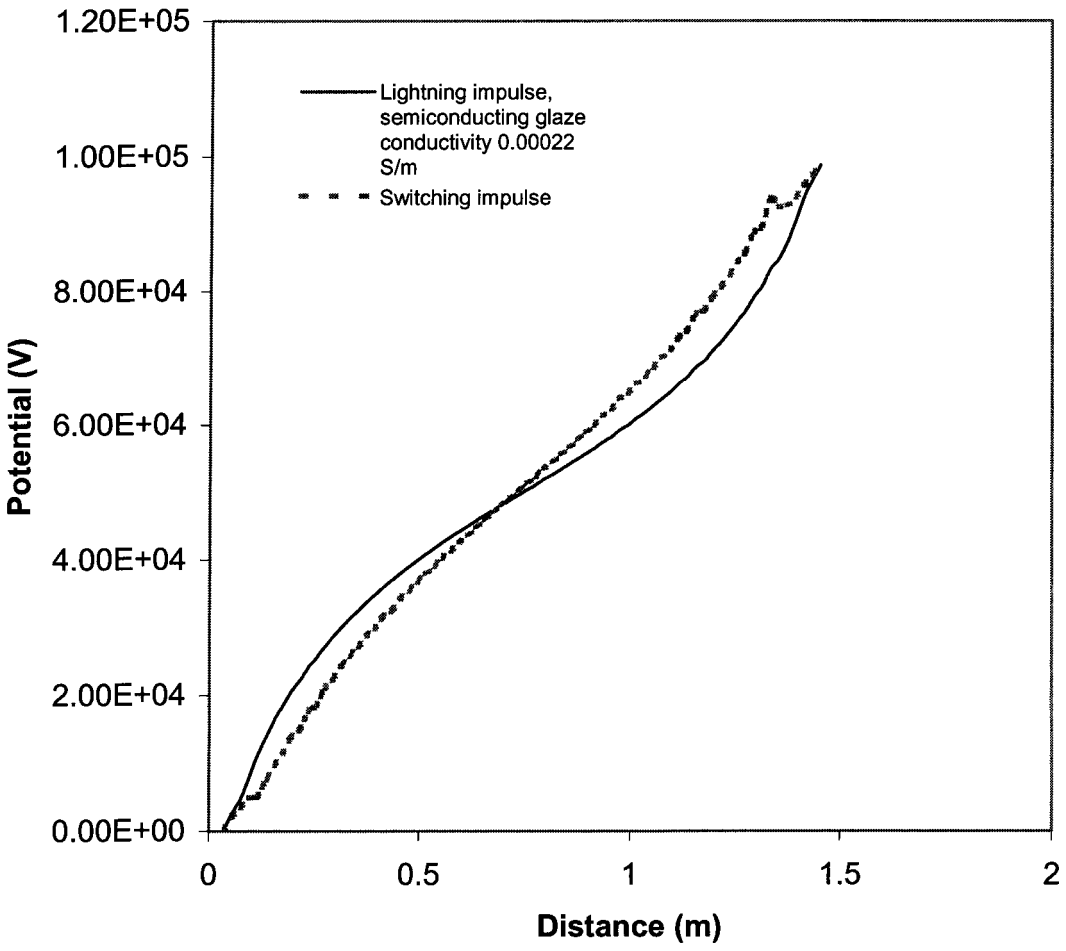

Figure 6.13: Potential distributions along a clean insulator coated with a semi-conducting glaze of conductivity 2.20×10^{-4} S/m for the lightning and the switching impulse voltages.

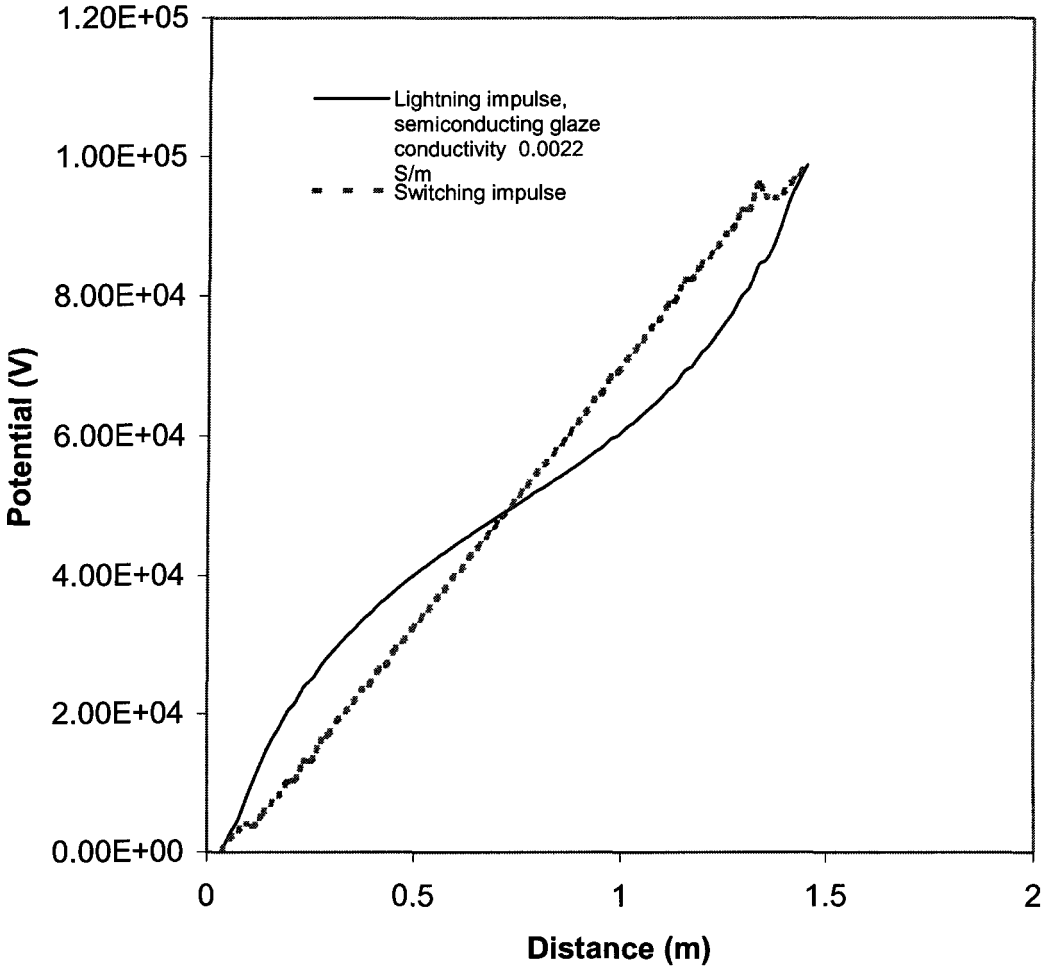

Figure 6.14: Potential distributions along a clean insulator coated with a semi-conducting glaze of conductivity 0.0022 S/m for the lightning and switching impulse voltages.

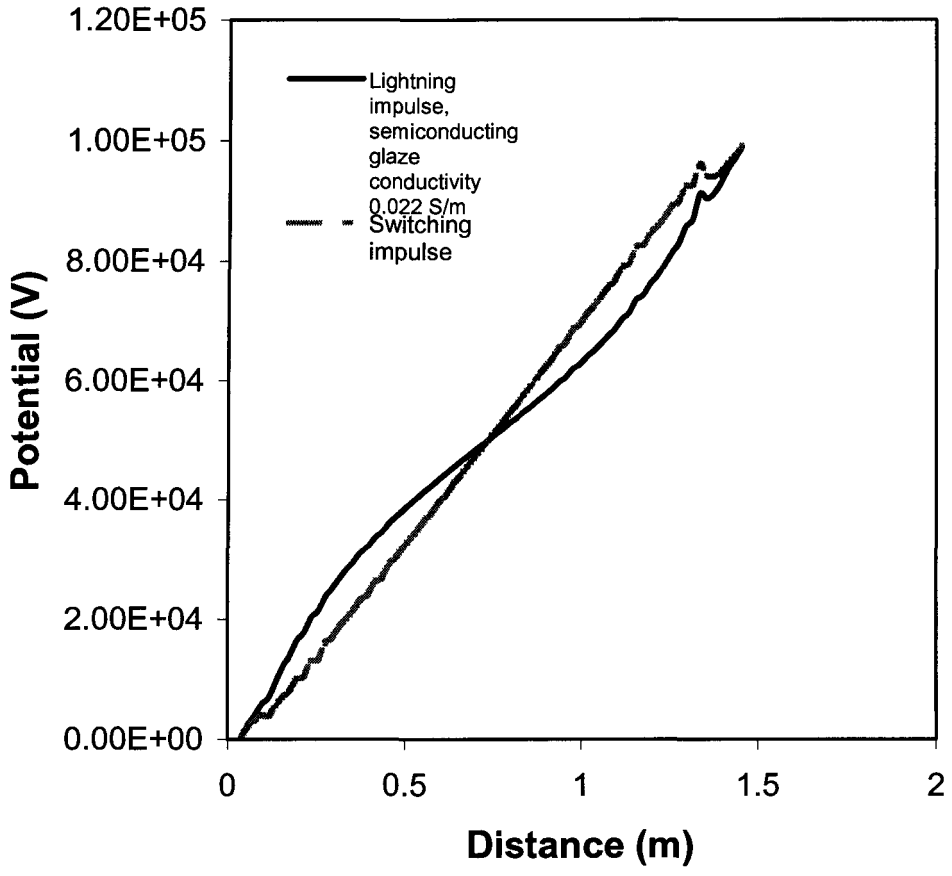

Figure 6.15: Potential distributions along a clean insulator coated with a semi-conducting glaze of conductivity 0.022 S/m for the lightning and switching impulse voltages.

6.3 Results and Discussion

For the wet ice-covered insulator, it can be seen from Figure 6.3, Figure 6.4 Figure 6.6, Figure 6.7, and Figure 6.8 that the potential distribution is more linear for an equivalent lightning impulse than that for an equivalent switching impulse voltage. This is because of higher value of displacement current in the ice layer for an equivalent lightning impulse than that for an equivalent switching impulse voltage. It is concluded that the switching impulse is the limiting factor in the design of the wet ice-covered semi-conducting glazed insulator.

For the dry ice-covered insulator, it is observed from the Figure 6.10 and Figure 6.11 that the potential distribution is more linear for a switching impulse than it is for a lightning impulse voltage. It is concluded that the lightning impulse is the limiting factor in the design of the dry ice-covered semi-conducting glazed insulator.

For the clean insulator, it can be seen from the Figure 6.12, Figure 6.13, Figure 6.14, and Figure 6.15 that the potential distribution is more linear for a switching impulse than that for a lightning impulse voltage. It is concluded that the lightning impulse is the limiting factor in the design of the clean semi-conducting glazed insulator.

It is seen from the Figure 6.3, Figure 6.6, Figure 6.7, Figure 6.8, Figure 6.12, Figure 6.13, Figure 6.14, and the Figure 6.15 that the potential distributions for a lightning impulse voltage both along the wet ice-covered semi-conducting glazed insulator and along the

clean semi-conducting glazed insulator, are almost linear. It is concluded that wet ice accumulated on the insulator has very little effect on the potential distribution along the insulator for a lightning impulse voltage. It can also be observed from the Figure 6.4, Figure 6.6, Figure 6.7, Figure 6.8, Figure 6.12, Figure 6.13, Figure 6.14, and the Figure 6.15 that while the potential distribution for a switching impulse voltage is not linear along the insulator when it is covered with wet ice, it is linear when the insulator is clean. It is concluded that the wet ice accumulated on the insulator has a major effect on the potential distribution for a switching impulse voltage. This is because of the conduction current is negligible in the ice layer and the displacement current is much higher for an equivalent lightning impulse than that for an equivalent switching impulse voltage.

The next chapter gives the important conclusions arising out of this study and topics for future research in the area of electric field computations under transient voltages around the insulators.

CHAPTER 7

CONCLUSION

The effects of the semi-conducting glaze coating on the potential and electric field distributions along a standard HV post insulator for power frequency, lightning impulse and switching impulse voltages under icing conditions, have been studied using the finite element method. A thin semi-conducting glaze requires a large number of elements for FEM analysis in the open boundary problems. To reduce the number of elements and hence the computation time, the open region around the insulator is simulated by a form of Kelvin transformation.

The conclusions from the core of the thesis presented, are divided in three parts as follows:

1. Simulation of an open boundary around an insulator for the field computations,
2. Flashover performance of an insulator based on the electric field distribution for transient voltages,
3. Flashover performance of an insulator based on the electric field distribution for sinusoidal voltages.

7.1 Simulation of an Open Boundary around an Insulator for the Field Computations

There is a great savings in the computation time by using a form of Kelvin transformation for the semi-conducting glazed insulator where the computation time in some cases is more than 100 hours using a form of Kelvin transformation. Results from both the methods are compared, and they are found to be in agreement, cf. Figure 3.9.

7.2 Flashover Performance of an Insulator based on the Electric Field Distribution for Transient Voltages

1. For the wet ice-covered insulator, it is found that the electric field strength at the mentioned critical point is higher for a switching impulse voltage than that for a lightning impulse voltage. It is concluded that a switching impulse is the limiting factor in the design of a wet ice-covered semi-conducting glazed insulator.

2. For the clean insulator, it is found that the electric field strength at the mentioned critical point is higher for a lightning impulse voltage than that for a switching impulse voltage. It is concluded that a lightning impulse is the limiting factor in the design of a clean semi-conducting glazed insulator.

3. It is also found that the wet ice, accumulated on the insulator, has very little effect on the electric field distribution around the insulator for a lightning impulse

voltage, but the wet ice has a major effect on the electric field distribution for a switching impulse voltage.

4. From the simulation results, confirmed by the experimental results, it is found that the flashover occurs after the peak voltage for the clean as well as the ice-covered semi-conducting glazed insulator under the lightning impulse voltage.

5. From the simulation results, confirmed by the experimental results, it is found that the flashover occurs before the peak voltage for the clean semi-conducting glazed insulator, and the flashover occurs after the peak voltage for the ice-covered semi-conducting glazed insulator under the switching impulse voltage.

7.3 Flashover Performance of an Insulator based on the Electric Field Distribution for the Sinusoidal Voltages

1. All the simulation results (trends in data) of sinusoidal voltages are in agreement with the equivalent transient solutions (trends in data) and experimental results (trends in data) and hence it is concluded that the equivalent sinusoidal simulation for impulse voltage produces good results and is an effective technique.

2. When the semi-conducting glazed insulator is covered with dry ice (no water film), a lightning impulse is the limiting factor in the design of the semi-conducting glazed insulator like the clean insulator because the potential distribution is more linear along the studied semi-conducting glazed insulator for a switching impulse voltage. It is due to presence of a water film and an air-gap that the limiting factor changes from the lightning impulse to the switching impulse for the ice-covered insulator.

3. Under clean conditions, whether or not the lightning impulse voltage should be the limiting factor in the design of the semi-conducting glazed insulator depends upon the conductivity of the semi-conducting glaze coating, as observed by the simulation results. If the conductivity of the semi-conducting glaze coating becomes lower than 2.20×10^{-5} S/m, cf. Figure 6.12, flashover voltages of the semi-conducting glazed insulator are almost same for both the lightning and the

switching impulse voltages. This is in agreement with the laboratory experiments for the normal glazed insulator [44].

4. Under icing conditions, when the insulator is covered with a wet glaze ice in the presence of the air-gap, it is found that most of the voltage drops occur across the air-gap. In this case, the semi-conducting glaze coating makes the potential distributions more linear along the insulator and hence improves the flashover performance considerably, as confirmed by the laboratory experiments [55].

5. There is no further improvement in potential distribution along the studied insulator if the conductivity of the semi-conducting glaze of thickness 0.5 mm exceeds 2.2 Siemens/m for the impulse voltages, cf. Figure 6.4.

6. Further improvement in potential distribution is obtained by increasing the thickness of the semi-conducting glaze and there is no further improvement in potential distribution if the conductivity of the semi-conducting glaze of thickness 5.0 mm exceeds 0.022 Siemens/m for the impulse voltages, cf. Figure 6.4.

7. The conductivity of the semi-conducting glaze coating does not have a major effect on the potential distribution along the insulator and hence does not have a major effect on the electrical performance of the insulator for the power frequency voltage.

8. There is no further improvement in the potential distribution along the studied insulator if the conductivity of the semi-conducting glaze of thickness 0.5 mm exceeds 0.022 Siemens/m for the power frequency voltage, cf. Figure 6.1.

7.4 Scope for the Future Research

The following are the topics, which the author wishes to emphasize for any future research in the field computations around the ice-covered insulators:

- The impulse waveform could be transformed into a Fourier series, the field computation could be done for each frequency using the master slave approach in the parallel processing, where the master computer instructs each slave computer to perform the field computation for a particular frequency. When the slave computer finishes the field computation for a particular frequency, it informs the master computer and then master computer instructs it to perform the field computation for another frequency until the field computations for all the frequencies are done. For each frequency, the permittivity of the ice is to be taken as given by the equation (2.3). The electric field strength around the insulator under the impulse voltage is the algebraic sum of the electric field strengths under all the frequencies. Results could be compared with the results presented in this thesis for the impulse voltages.

- The effects of the space charge and partial arcs on the dry ice-covered normal glazed insulator have not been discussed in this thesis and this could form a topic of another research study.

References

1. M. Farzaneh and O. T. Melo, "Flashover performance of insulators in the presence of short icicles", Int. J. Offshore Polar Eng., Vol. 4, No. 2, pp. 112-118, 1994.

2. W. A. Chisholm et al., "The cold-fog test", IEEE Trans. Power Delivery, Vol. 11, pp. 1874-1880, Oct. 1996.

3. E. A. Cherney, "Flashover performance of artificially contaminated and iced long-rod transmission line insulators", IEEE Trans. Power App. Syst., Vol. PAS-99, pp. 46-52, Feb. 1980.

4. J. F. Drapeau and M. Farzaneh, "Ice accumulation characteristics on Hydro-Quebec HV insulators", Proc. 6th Int. Workshop Atmospheric Icing of Structures, Budapest, Hungary, 1993, pp. 225-230.

5. L. Gu et al., "AC flashover characteristics of EHV line insulators for high altitude contamination regions", Proc. Int. Conf. Properties Application Dielectric Materials, 1988.

6. L. Shu, C. Sun, J. Zhang, and L. Gu, "AC flashover performance on iced and polluted insulators for high altitude regions", Proc. 7th Int. Symp. High Voltage Eng., Vol. 4, Dresden, Germany, 1991, 43.13, pp. 303-306.

7. V. Sklenicka and J. Vokalek, "Insulators in icing conditions: Selection and measures for reliability increasing", Proc. 7th Int. Workshop Atmospheric Icing Structures, Chicoutimi, QC, Canada, 1996, pp. 72–76.

8. J. S. Forest, "The performance of high voltage insulators in polluted atmospheres", Conf. Paper IEEE Winter Meeting, New York, 1969.

9. K. Kannus and K. Lahti, "Electrical behavior of high voltage insulator strings under rime ice", Proc. 9th Int. Workshop Atmospheric Icing Structures, Chester, U.K., 2000, p. 8.

10. H. Matsuda, H. Komuro, and K. Takasu, "Withstand voltage characteristics of insulator strings covered with snow or ice", IEEE Trans. Power Delivery, Vol. 6, pp. 1243–1250, July 1991.

11. T. Fujimura, K. Naito, Y. Hasegawa, and K. Kawaguchi, "Performance of insulators covered with snow or ice", IEEE Trans. Power App. Syst., Vol. PAS-98, pp. 1621–1631, Sept./Oct. 1979.

12. R. Matsuoka, S. Ito, K. Sakanishi, and K. Naito, "Flashover on contaminated insulators with different diameters", IEEE Trans. Elect. Insulation, Vol. 26, No. 6, pp. 1140–1146, 1991.

13. M. Yasui, K. Naito, and Y. Hasegawa, "AC withstand voltage characteristics of insulator string covered with snow", IEEE Trans. Power Delivery, Vol. 3, pp. 828–838, April 1988.

14. S. M. Fikke, J. E. Hanssen, and L. Rolfseng, "Long range transported pollution and conductivity on atmospheric ice on insulators", IEEE Trans. Power Delivery, Vol. 8, pp. 1311–1321, July 1993.

15. S. M. Fikke, T. M. Ohnstad, T. Telstad, H. Förster, and L. Rolfseng, "Effect of long range airborne pollution on outdoor insulation", NORD-IS 94, 1994, 1.6.

16. A. Meier and W. M. Niggli, "The influence of snow and ice deposits on supertension transmission line insulator strings with special reference to high altitude operations", in Proc. IEEE Conf. Publ. 44, London, U.K., 1968, pp. 386–395.

17. D. Wu, K. A. Halsan, and S. M. Fikke, "Artificial ice tests for long insulator strings", Proc. 7th Int. Workshop Atmospheric Icing Structures, Chicoutimi, QC, Canada, 1996, pp. 67–71.

18. D. Wu and R. Hartings, "Correlation between the AC withstand voltage and insulator lengths under icing tests", Proc. 9th Int. Workshop Atmospheric Icing Structures, Chester, U.K., 2000, p. 6.

19. M. Kawai, "AC flashover test at project UHV on ice-coated insulators", IEEE Trans. Power App. Syst., Vol. PAS-89, pp. 1800–1804, Nov./Dec. 1970.

20. M. D. Charneski, G. L. Gaibrois, and B. F. Whitney, "Flashover tests on artificially iced insulators", IEEE Trans. Power App. Syst., Vol. PAS-101, pp. 2429–2433, Aug. 1982.

21. H. M. Schneider, "Artificial ice tests on transmission line insulators – A progress report", in the IEEE/Power Eng. Soc. Summer Meeting, San Fran-cisco, CA, USA, 1975, A75–491–1, pp. 347–353.

22. Z. Vuckovic and Z. Zdravkivic, "Effect of polluted snow and ice accretion on high voltage transmission line insulators", Proc. 5th Int. Workshop Atmospheric Icing Structures, Tokyo, Japan, 1990, B4–3.

23. M. Farzaneh, "Ice Accretion on H.V. Conductors and Insulators and Related Phenomena", Invited article, Philosophical Transactions, The Royal Society, Londres, No. 358, pp. 1-35, 2000.

24. M. Farzaneh et al, "Insulator Icing Test Methods and Procedures", IEEE Trans. Power Delivery, Vol. 18, pp. 1503-1515, October 2003.

25. M. Farzaneh and J. Kiernicki, "Flashover problems caused by ice build-up on insulators", IEEE Electr. Insul. Mag., Vol. 11, pp.5-17, March/April 1995.

26. M. Farzaneh and J. F. Drapeau, "AC flashover performance of insulators covered with artificial ice", IEEE Trans. Power Delivery, Vol. 10, pp. 1038-1051, April 1995.

27. M. Farzaneh and J. Kiernicki, "Flashover performance of IEEE standard insulators under icing conditions", IEEE Trans. Power Delivery, Vol. 12, pp. 1602-1613, October 1997.

28. T. Misaki and H. Tsuboi, "Computation of 3-Dimensional Eddy Current Problems by Using Boundary Element Method", IEEE Trans. Magnetics, Vol. MAG-21, No. 6, pp. 2227-2230, November 1985.

29. H. El-Kishky and R. S. Gorur, "Electric Potential and Field Computation along ac HV Insulators", IEEE Trans. Elect. Insul., Vol. 1, No. 6, pp. 982-990, December 1994.

30. S. Chakravorti and P. K. Mukherjee, "Power Frequency and Impulse Field Calculation around a HV Insulator with Uniform or Nonuniform Surface Pollution", IEEE Trans. Elect. Insul., Vol. 28, No. 1, pp. 43-53, February 1993.

31. E.S. Asenjo and N.O. Morales, "Low Frequency Complex Fields in Polluted Insulators", IEEE Trans. Elect. Insul., Vol. 17, No 3, pp. 262-268, June 1982.

32. E. Asenjo S., N. Morales O., and A. Valdenegro E, "Solution of Low Frequency Complex Fields in Polluted Insulators by Means of the Finite Element Method", IEEE Trans. Elect. Insul., Vol. 4, No. 1, pp. 10-16, February 1997.

33. CIGRE Task Force 33.04.09, "Influence of Ice and Snow on the Flashover Performance of outdoor insulators Part I: Effects of Ice", ELECTRA, No. 187, pp. 90-111, December 1999.

34. Victor F. Petrenko and Robert W. Whitworth, "Physics of Ice", Oxford University press, 1999.

35. P. V. Hobbs, "Ice Physics", Oxford University press, 1974.

36. G. P. Johari and S. J. Jones, "The orientation polarization in hexagonal ice parallel and perpendicular to the *c*-axis", Journal of Glaciology, 21, pp. 259-276, 1978.

37. G. P. Johari, "The dielectric properties of H_2O and D_2O ice Ih at MHz frequencies", Journal of Chemical Physics, 64, pp. 3998-4005, 1976.

38. S. R. Gough, "A low temperature dielectric cell and the permittivity of hexagonal ice to 2K", Canadian Journal of Chemistry, 50, pp. 3046-3051, 1972.

39. T. Matsuoka, S. Fujita, S. Morishima and S. Mae, "Precise measurement of dielectric anisotropy in ice Ih at 39 GHz", Journal of Applied Physics, 81, pp. 2344-2348, 1997.

40. G. P. Johari and E. Whalley, "The dielectric properties of ice Ih in the range 272-133 K", Journal of Chemical Physics, 75, pp. 1333-1340, 1981.

41. Vinay Jaiswal and M Joy Thomas, "Finite Element Modeling of Ionized Field Quantities around a Monopolar HVDC Transmission Line", Journal of Physics D: Applied Physics, Vol. 36, No 23, pp. 3089-3094, December 2003.

42. P.P. Silvester and R.L. Ferrari, "Finite elements for electrical engineers", Cambridge University Press, 1991.

43. R. Sundararajan and R. S. Gorur, "Dynamic Arc Modeling of Pollution Flashover of Insulators under dc Voltage", IEEE Trans. Elect. Insul., Vol. 28, No. 2, pp. 209-218, April 1993.

44. T. Guerrero, "Étude expérimentale du contournement des isolateurs recouverts de glace sous tensions de foudre et de manoeuvre", M.Eng. Thesis, UQAC, 2004.

45. C. Volat, "Modélisation physique et numérique par la méthode des éléments finis de frontière de la distribution du potentiel et du champ électrique le long d'un isolateur standard de poste 735 KV recouvert de glace", PhD Thesis, UQAC, 2002.

46. M. Farzaneh, J. Zhang and X. Chen, "Modeling of the AC Arc Discharge on Ice Surfaces", IEEE Trans. Power Delivery, Vol. 12, No. 1, pp. 325-338, January 1997.

47. E.M. Freeman and D.A. Lowther, "An Open Boundary Technique for Axisymmetric and Three Dimensional Magnetic and Electric Field Problems", IEEE T-MAG, MAG-25, pp. 4135-4137, September 1989.

48. D.A. Lowther and E.M. Freeman, "Further aspects of the Kelvin transformation method for dealing with open boundaries", IEEE T-MAG, Vol. 28, pp. 1667-1670, March 1992.

49. S. H. Wong and I. R. Ciric, "Method of Conformal Transformation for the Finite Element Solution of Axisymmetric Exterior Field Problems", COMPEL, pp. 123-135, 4, 1985.

50. I. R. Ciric and S. H. Wong, "Inversion Transformations for Finite Element Solutions of Three Dimensional Exterior Field Problems", COMPEL, pp. 109-119, 5, 1986.

51. Morf Jean Jacques et Ianovici Mircea, "Compatibilité électromagnétique", Presses polytechniques romandes, Lausanne, 1985.

52. M. Farzaneh, C. Volat and A. Gakwaya, "Electric Field Calculation around Ice-covered Insulator Using Boundary Element Method", IEEE International Symposium on Electrical Insulation, Anaheim, California, pp. 349-355, April 2000.

53. C. Volat, M. Farzaneh and A. Gakwaya, "3-D Modelling of Potential and Electric Field Distributions around an Ice-covered Insulator", Proceedings of the 58th Annual Eastern Snow Conference, Ottawa, Ontario, May 2001.

54. IEEE Std 4-1995, "IEEE Standard Techniques for High-Voltage Testing", IEEE Power Engineering Society, March 1995.

55. J. F. Drapeau, M. Farzaneh and M. J. Roy, "An Exploratory Study of Various Solutions for Improving Ice Flashover Performance of Station Post Insulators", Proceedings of the Tenth International Workshop on Atmospheric Icing of Structures, Brno, Czech Republic, 17th-20th June 2002.

APPENDIX A

A.1 Error Analysis

A.1.1 Experimental Results

All the experiments were done under the mentioned conditions for both positive and negative impulse voltages and the results are compared and the trends of data are still similar hence it is assumed that the experimental error is minimum and acceptable for the comparison with simulation results.

A.1.2 Simulation Results

Each case of the insulator was solved with the different mesh and solver options until the results were converged and then all the parameters (mesh and solver options) were set up for the comparison in that case.

Consider a wet ice-covered insulator (second ice geometry) coated with a semi-conducting glaze of thickness 0.5 mm and of conductivity 2.2 S/m under a 320 KHz sinusoidal voltage.

Case 1

Mesh parameters (maximum element size)

Insulator: 0.03 m

Semi-conducting glaze: 0.0075 m

Solver options

Polynomial order: 2

Conjugate gradient (CG) tolerance: 0.001 %

The potential distribution along the insulator is shown in Figure A.1.

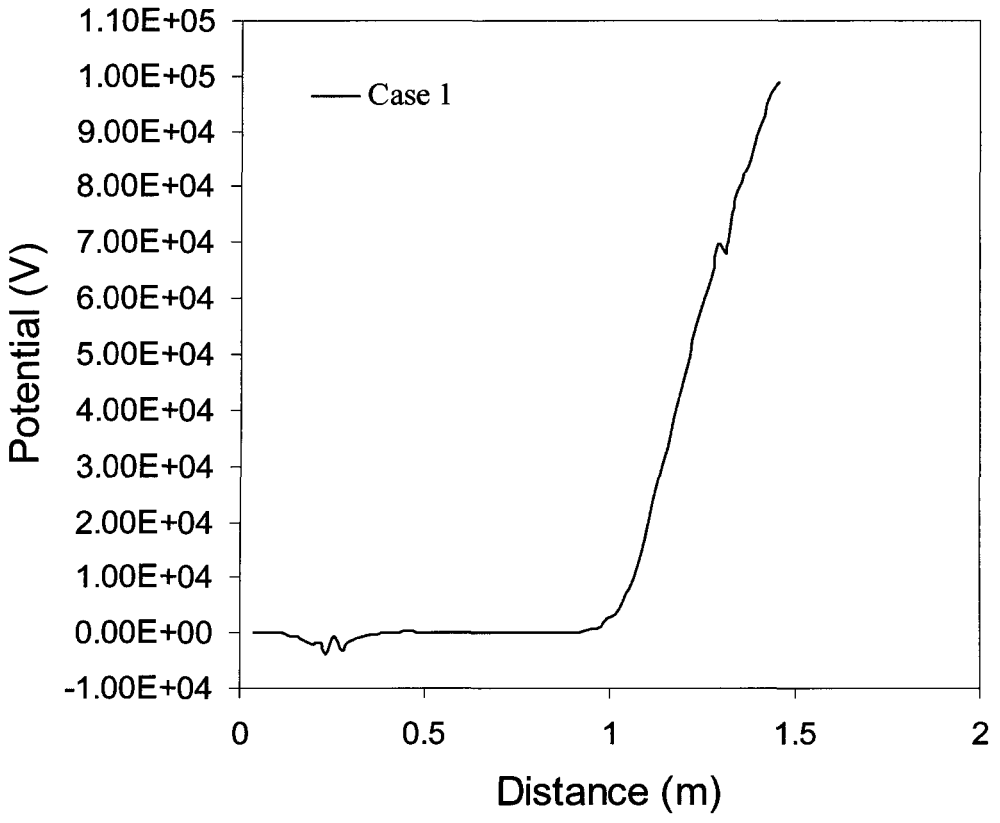

Figure A.1: The potential distribution along the insulator.

Case 2

Next the polynomial order is set to be 3 and all other parameters are same as Case 1. The results are shown in Figure A.2.

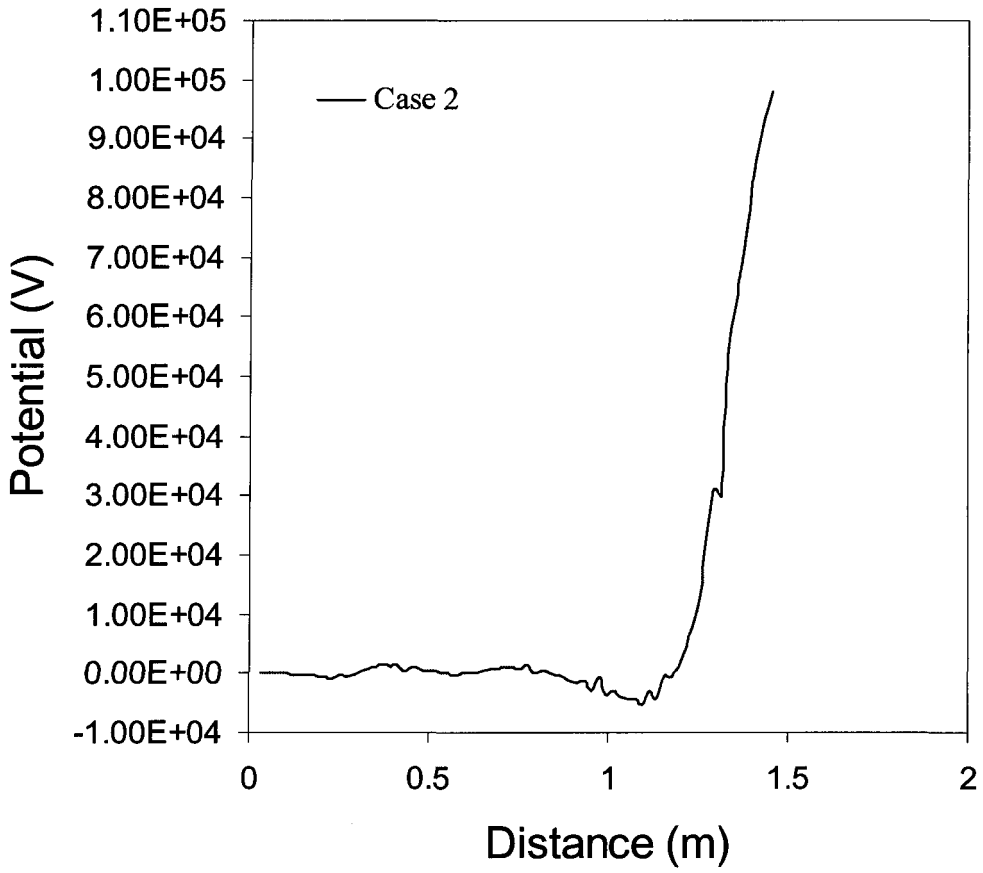

Figure A.2: The effects of polynomial order on the results.

Case 3

Next the CG tolerance is set to be 0.0001 % and all other parameters are identical to case 2. The potential distribution is shown in Figure A.3 and it can be seen that the results are now converged.

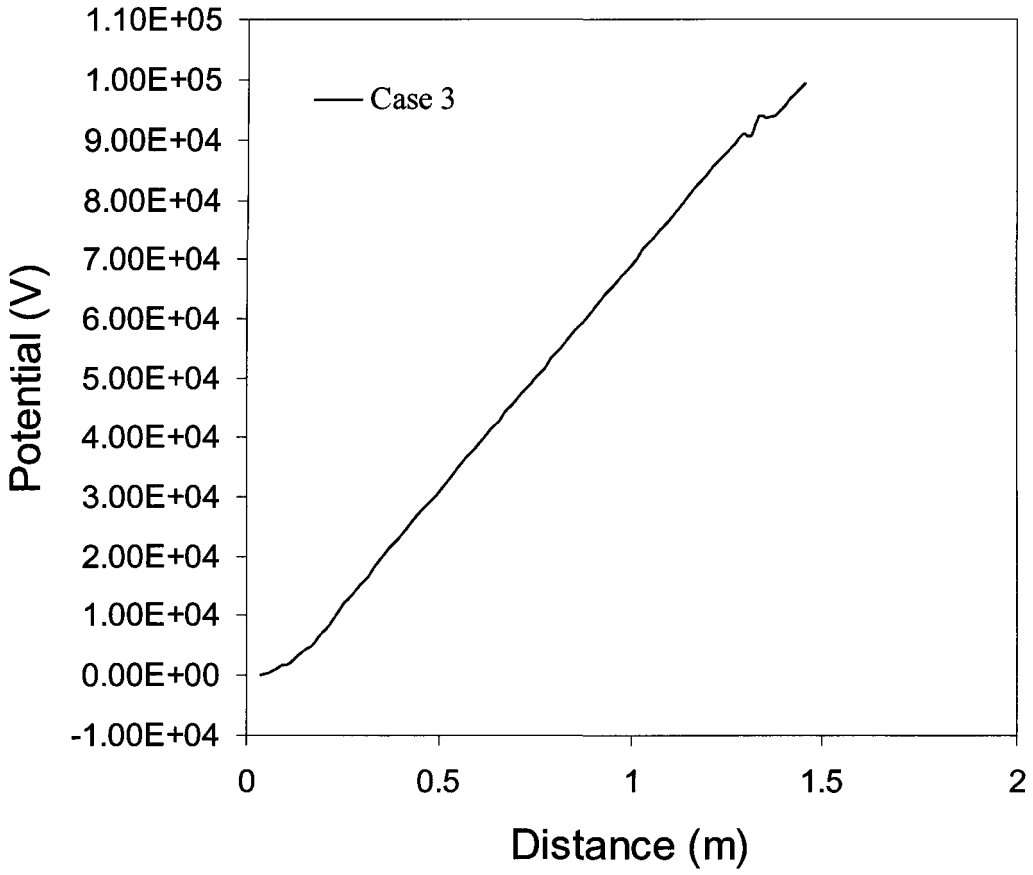

Figure A.3: The effects of the polynomial order and CG tolerance on the results (converged).

Case 4

Next the maximum element size of the insulator is set to be 0.003 m and all the other parameters are same as case 1. The results are shown in Figure A.4.

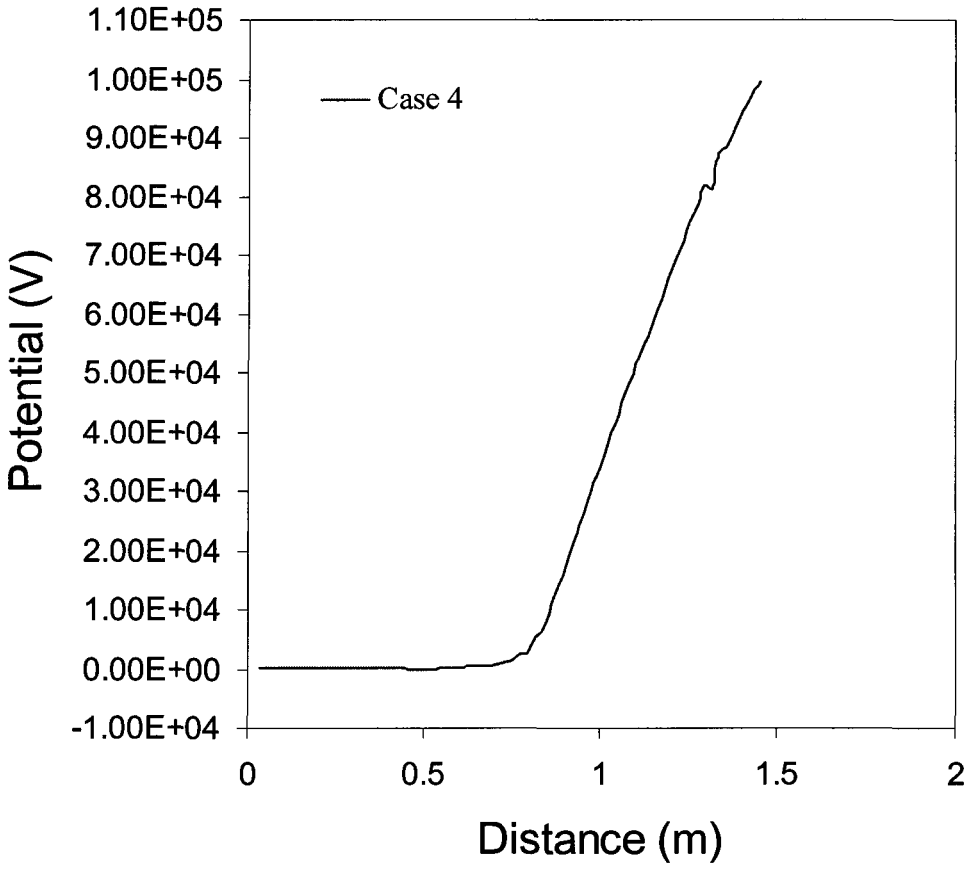

Figure A.4: The solutions generated with a different mesh.

Case 5

Now the maximum element size of the semi-conducting glaze is set to be 0.00075 m and all the other parameters are identical to case 4. The results are shown in Figure A.5.

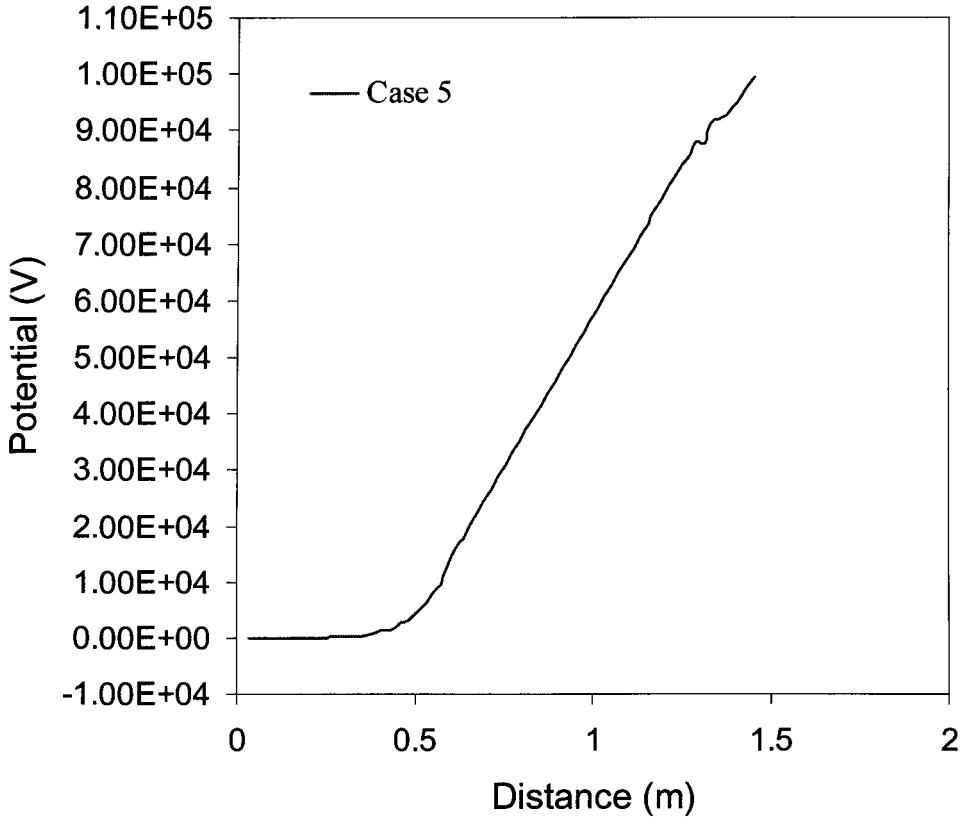

Figure A.5: The solutions generated with a very fine mesh and the polynomial order set to be 2.

Case 6

Next the polynomial order is set to be 3 and all other parameters are same as Case 5. The results are shown in Figure A.6.

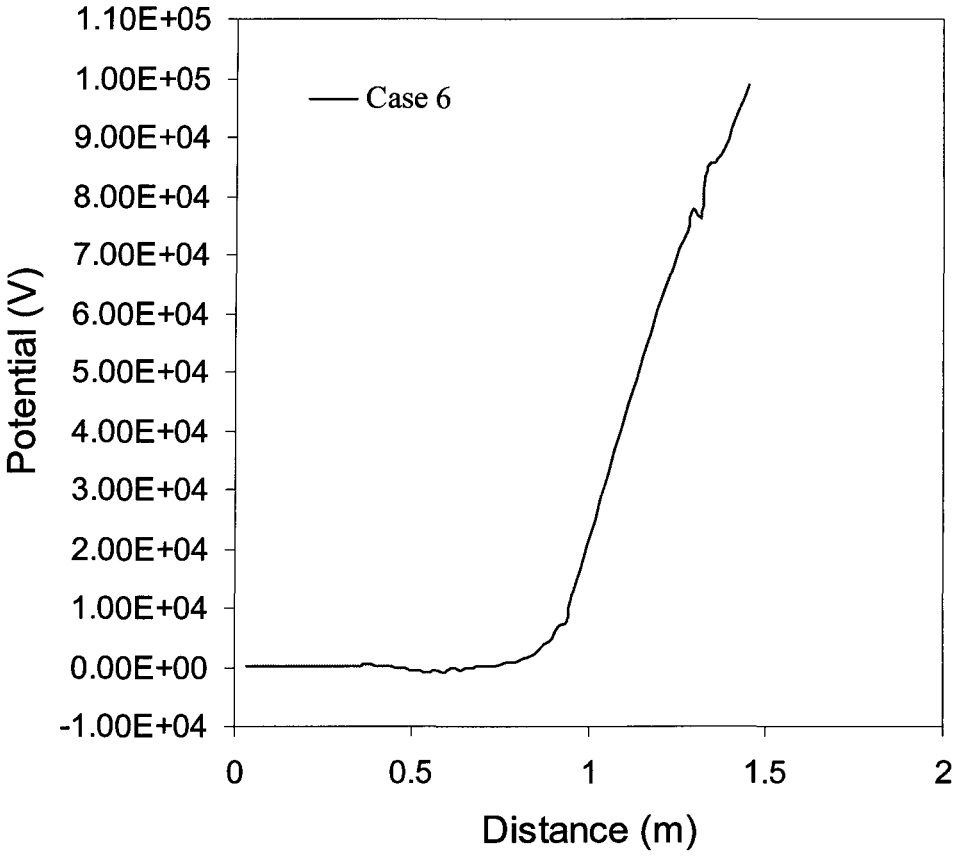

Figure A.6: The solutions generated with a very fine mesh and the polynomial order set to be 3.

Case 7

Now the polynomial order is set to be 4 and all other parameters are identical to case 5. The results are shown in Figure A.7.

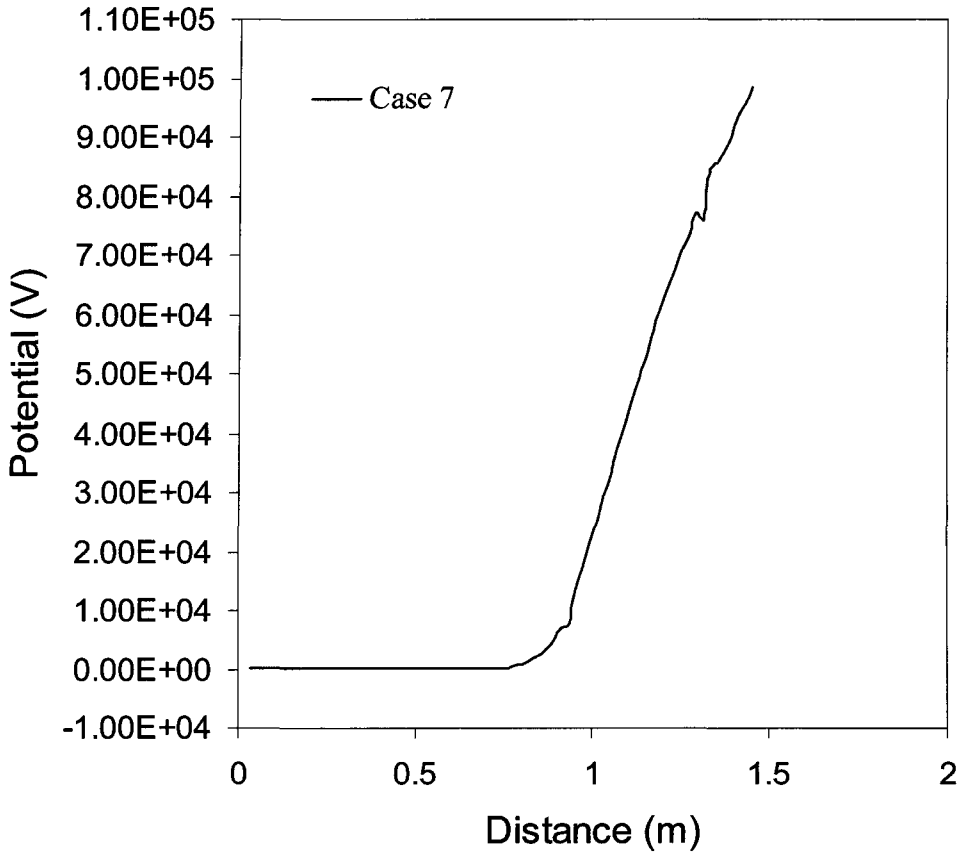

Figure A.7: The solutions generated with a very fine mesh and the polynomial order set to be 4.

Case 8

Next the CG tolerance is taken as 0.0001% and other parameters are same as Case 6. The solutions generated are shown in Figure A.8 and the results are now converged and similar to case 3.

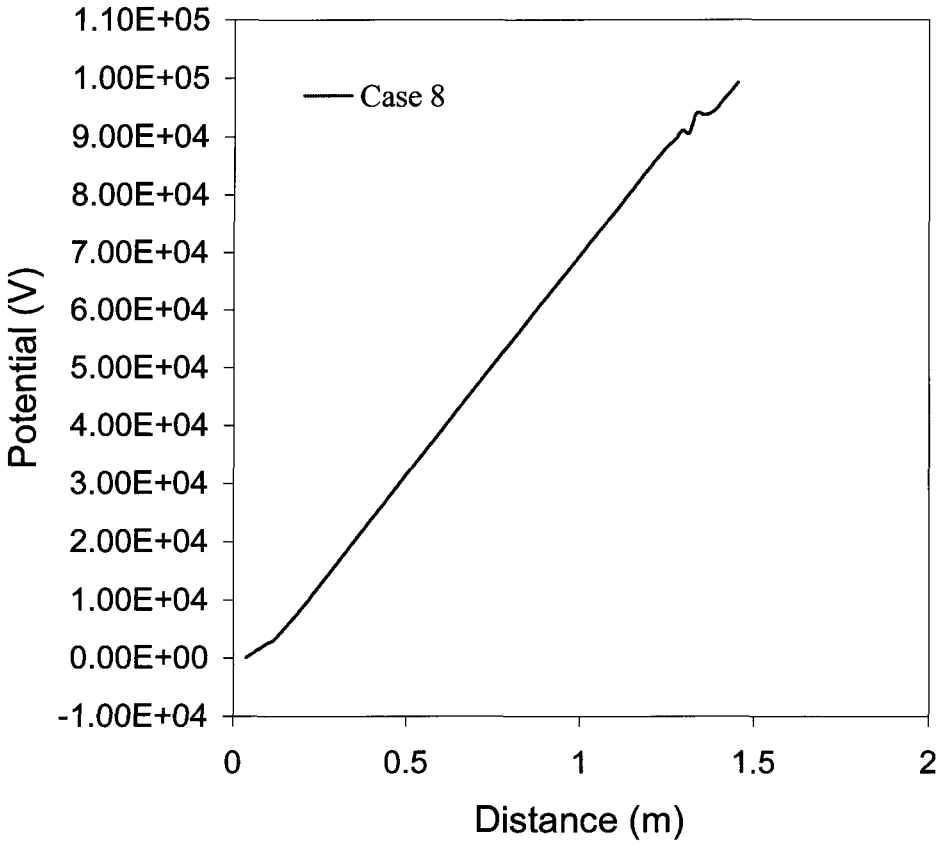

Figure A.8: The results (converged) generated with a very fine mesh and the CG tolerance set to be 0.0001%.

It can be seen from the figures that the mesh, polynomial order and CG tolerance have major effects on the results hence all the solutions in this research have been generated with a very fine mesh using fourth order polynomial approximations with adaptations and CG tolerance is taken as 1×10^{-6} at the expense of a very high computation time and also convergence of all the results have been verified in all the cases.

List of Publications from the Thesis:

Refereed Journal Paper:

1. Vinay Jaiswal, Masoud Farzaneh and David A. Lowther, "A Study of Impulse Flashover Performance of Semi-conducting Glazed Station Insulator under Icing Conditions based on Field Calculations", IEE Proceedings- Generation, Transmission and Distribution. (in press)

Refereed Conference Papers:

1. V. Jaiswal, M. Farzaneh and D. A. Lowther, "Effects of Semi-conducting Glaze Coating on the Electrical Performance of a HV Station Post Insulator Covered with Ice", Proceedings of the XIIIth International Symposium on High Voltage Engineering (ISH-2003), Delft, The Netherlands, 25th- 29th August 2003.

2. V. Jaiswal, M. Farzaneh and D. A. Lowther, "A Study of Potential Distribution along Semi-conducting Glazed Standard Post Insulator under Icing Conditions", Proceedings of the 60th Annual Eastern Snow Conference (ESC-2003), Sherbrooke, Quebec, Canada, 4th-7th June 2003.

3. V. Jaiswal, M. Farzaneh and D. A. Lowther, "Calculation of Potential Distributions along Semi-conducting Glazed Insulator for Impulse Voltages under Icing Conditions", Proceedings of the IEEE Canadian Conference on Electrical and Computer Engineering (CCECE-2003), Montreal, Canada, 4th-7th May 2003.

4. V. Jaiswal, M. Farzaneh and D. A. Lowther, "Finite Element Method Modeling of Electric Field Calculations around an Ice-Covered Insulator", Proceedings of The Tenth International Workshop on Atmospheric Icing of Structures (IWAIS-2002), Brno, Czech Republic, 17th –20th June 2002.

5. V. Jaiswal and M. Farzaneh, "Impulse Flashover Performance of a Post Station Insulator under Icing Conditions based on the Electric Field Distribution", Accepted for publication in the proceedings of the XIVth International Symposium on High Voltage Engineering (ISH-2005), Beijing, China, 25th- 29th August 2005.

6. V. Jaiswal and M. Farzaneh, "Flashover Performance of Station Post Insulators under Icing Conditions based on Electric Field Distribution", Proceedings of The 11th International Workshop on Atmospheric Icing of Structures (IWAIS-2005), Montreal, Quebec, Canada, 12th –16th June 2005.